FABRICATION OF ASYMMETRIC PORES FOR BIOSENSORS AND TRANSPORT STUDIES

By

JOHN EDWARDSON WHARTON

A DISSERTATION PRESENTED TO THE GRADUATE SCHOOL
OF THE UNIVERSITY OF FLORIDA IN PARTIAL FULFILLMENT
OF THE REQUIREMENTS FOR THE DEGREE OF
DOCTOR OF PHILOSOPHY

UNIVERSITY OF FLORIDA

2007

To my family, for their continued support and love

ACKNOWLEDGMENTS

I wish to acknowledge the many people who have given me advice, help, and encouragement during my years in graduate school.

I would like to thank Prof. Dr. Charles R. Martin and the entire Martin group for the opportunity to work with them over the years. Prof. Martin was continuously supportive and always willing and ready to discuss some of our new ideas for research. I appreciate the level of independence that Prof. Martin allowed all of his students. Undoubtedly, this created an atmosphere of confidence among the students where creativity flourished.

I would like to thank Drs. Punit Kohli, Zuzanna Siwy, and Lane Baker for their patience and expert advice along the way. I wish to thank Fan Xu, Lindsay Sexton, Pu Jin, Lloyd Horne, Stefanie Sherrill, and Warren Mino for very important contributions to some of my projects; these great students have been very patient with me and are always willing to help with very high interest and good spirits.

Finally, I would like to thank my family and friends for showing confidence in me and for giving their love and support throughout the years.

TABLE OF CONTENTS

page

LIST OF FIGURES

Abstract of Dissertation Presented to the Graduate School
of the University of Florida in Partial Fulfillment of the
Requirements for the Degree of Doctor of Philosophy

FABRICATION OF ASYMMETRIC PORES FOR BIOSENSORS AND TRANSPORT STUDIES

By

John Edwardson Wharton

May 2007

Chair: Charles R. Martin
Major: Chemistry

The goals of this research are to develop asymmetric nanopores and nanotubes (single and multipore) in polymers and mica membranes by the track-etch method, and an extension of this technology, for sensing, nanostructure fabrication, and to investigate the transport properties of conical pores. The first part of this work describes an extension of the track-etch method to make conical pores in a reproducible fashion. We have demonstrated here that we can, not only reproducibly prepare track-etched based conical nanopore sensor elements, but that we can predict from the experimental parameters used during the second etch, what the diameter of the all-important nanopore tip will be. For these reasons, we believe that the track-etch method will prove to be the technology of choice for taking artificial-nanopore resistive-pulse sensors from the bench top to the practical prototype-device stage of the R&D effort.

The second part of this work describes a method to make asymmetric pores in tracked muscovite mica films using an etch-refill-etch approach. Tracks in the films were initially etched away with hydrofluoric acid to form nanoporous membranes. These nanopores were then refilled with silver nanowires or "metal tracks" using an electroless plating method. One face of the membrane was then exposed to a solution of hydrofluoric acid and nitric acid, which etched the bulk material and the nanowires respectively, at two different rates. By controlling the

concentration ratio of hydrofluoric acid to nitric acid, tapered pores with diamond shaped cross-section were obtained. Replicas of the asymmetric pores were accomplished by carbon vapor deposition, and scanning electron microscopy was used to give evidence of the resulting nanotubes. In this study, excellent control over tip size and cone angle was demonstrated.

In the third section, electroless gold plating properties on the surface and pore walls of track-etched Kapton polyimide nanoporous membranes were studied. Scanning electron microscopy (SEM), atomic force microscopy (AFM), and ion current measurements were used to characterize the surfaces and dimensions of the pores in the membrane. Nanoporous Kapton polyimide membranes were electroless gold plated over different times and the pore diameter characterized using SEM. Ion current measurements were used to measure the diameter of very small pores. AFM images show that after electroless gold plating, the gold surface layers are smooth compared to a similarly structured polycarbonate membrane. Electroless plating the membranes for 12 hours produced Au wires in the pores. Removing the membrane by oxygen plasma revealed that the plating in the walls is also relatively smooth.

The final part of this work describes asymmetric diffusional transport of neutral molecular species through nanoporous polymer membranes. Membranes containing conical nanopores from polyimide (Kapton HN Dupont) foils were prepared by the track-etching technique, based on irradiation of the polymer with swift heavy ions and subsequent etching of the latent tracks. The transport properties (e.g., flux) of these membranes were investigated using UV-Vis spectroscopy. Transport experiments were performed with bare polymer membranes without any modification. We report the preferential direction of the flow of molecules through conical nanopores and spatial or concentration dependence of diffusion coefficient for a particular flow direction.

CHAPTER 1
INTRODUCTION AND BACKGROUND

Nanopore fabrication technology has produced nanoporous materials that are potential candidates for applications in various fiels, such as bionanotechnology,[1, 2] gas separation,[3] catalysts[4] and micro-electronics[2, 5] In particular, the track-etch method has become an indispensable technology for the production of nano- and microstructured materials.[6] This technology can be applied directly to most polymers and – via the replication technique- to a wide variety of materials, including metals.[6] Track-etch membranes were first marketed three decades ago and remain the best product for a number of biological, medical, analytical and scientific applications.[6]

Recently, there has been a surge of interest in developing abiotic analogues of biological nanopores as sensing elements for chemicals and biological sensors.[7] We have explored the fabrication of such synthetic nanopores using the track-etch method. Particular interest is in the fabrication of synthetic conical pores for resistive-pulse sensing. Resistive-pulse sensing using conical nanopores is in its infancy. Studies in this area could prove beneficial for future applications of conical pores for science and technology.

Membranes and porous materials have found various applications in filtration and separation processes.[8, 9, 10] Modern biotechnology has posed new challenges in the application of such membranes, and requires pores with diameters similar to those of molecules under study,[11] (e.g., as small as several nanometers). The nanometer scale of such pores is necessary in both achieving optimal control of the flow of biomolecules, as well as in developing sensors for their detection. The transport properties of such nanometer scale pores are not well understood yet. The hint that nanopores behave differently from micropores, comes from Mother Nature.[12]

Biological channels and pores have diameter of ~ 1 nm and are critical for functioning of living organisms.

This chapter is divided into six sections which provide the background information for this research. Section 1 reviews the track-etch method, first discovered by Price and Walker, for preparation of pores in dielectric materials. The track-etch method is used in the preparation of conical pores described in Chapters 2, 3, 4 and 5. Section 2 reviews membrane-based template synthesis. This method, pioneered by the Martin group, is used in preparation of nanostructured materials described in Chapters 2 and 3. Section 3 review resistive-pulse sensing; which is the focus of the application of Chapter 2 and 3. Section 4 describes plasma based etching; a procedure necessary for the liberation of carbon tube in mica templates in Chapter 2. In Section 5, an introduction of Asymmetric Diffusion is given. Asymmetric diffusion is the topic of Chapter 5. Finally, Section 6 is the dissertation overview.

Ion Track-Etch Method

Track Formation

When dielectric materials, such as polymers, ceramics and minerals, are bombarded by swift ions, latent tracks are formed along the path of the ions (Figure 1-1).[13, 14] Ion track materials can be divided into two categories: (a) single-tracked and (b) multiple-tracked materials. Single-tracked materials can be produced by controlling the beam optics and fluence of the heavy ion beam.[15] Commonly tracked materials are Makrofol-KG, Kapton-H, PVDF, mica films, cellulose nitrate, CR-39 and Lexan polycarbonate. Swift ion beams are produced by cyclotrons or linear accelerator and the radiation is characterized by extremely high linear energy transfer.[6] The conventional ionization radiation sources, such as radioactive isotopes or electron accelerators,[16] are less sophisticated and less expensive and are mostly used in the industrial

processes.[6] Present-day heavy ion accelerators provide beams with ion energies in the order of 10MeV/u and even 100MeV/u which expands the treatment dept up to millimeters.[6]

Acceleration and Irradiation Facilities

About a half dozen heavy ion accelerators employed for irradiation of materials on the industrial scale exist. The Tanden Van de Graaff accelerators at Brookheaven National Laboratory are used to bombard materials with ions for manufacturing and testing purposes.[6] At the Grand Accelerator National d'Ions Lours, France, ions are produced in an electron cyclotron resonance(ECR) source.[6] The cyclotron of Louvain la Neuve is a multiparticle , variable energy, cyclotron capable of accelerating protons, alpha particles and heavy ions. The RFQ + cyclotron combination at the Hahn-Meitner Institute in Berlin, delivers intense beams of ion species such as Kr or Xe with energies from approximately 1.5-6 MeV/u[17] At the Flerov Laboratory of Nuclear Reactions(Dubna) a beam line connected at the U-400 cyclotron is equipped with scanning systems which allows one to obtain a homogeneous distribution of ion tracks on the target up to 60 cm in width and 6 cm in height.[6] Additionally, a liner accelerator at GSI (Darmstadt),[6] the AVF cyclotron at TRCRE JAERI (Takasaki)[6] and some others are used in experiments on polymer modification.[6]

Chemical Etching of Ion Tracks

After irradiation, the materials are subject to chemical etching which preferentially removes the latent ion track (Figure 1-2)[16] This etching process results in pore formation in the material.[16] Etching is the pore-size-determining and pore-shape-determining stage of the technology. In a homogeneous isotropic medium, mainly two influential parameter describe the etch process–the bulk etch rate V_B and the track etch rate V_T (Figure 1-3).[6] The ratio of track etch rate to the bulk etch rate is called the track-etch-ratio. When V_T is >> V_B, pores turn out to be cylindrical as opposed to conical. In other words, high track-etch-ratio yields cylindrical pores,

where as low track-etch-ratio yields conical pores. The arctangent of the inverse track-etch-ratio (V_B/V_T) yields the half cone angle of the pore. The bulk etch rate depends on the material, on the etchant composition and on the temperature.[14] The track etch rate depends on the sensitivity of the material, irradiation conditions, post-irradiation conditions and etching conditions.[6, 14]

The Effect of Storage of Tracked Material

The most important storage factors are the atmosphere in which the material is stored, the temperature and the illumination conditions during storage. In the presence of oxygen the latent ion tracks becomes susceptible to track etching. This is due to the oxidation of the radicals formed during irradiation. When polymers are stored at temperatures close their glass transition temperature, rearrangement on a molecular scale can take place which may lead to annealing of the ion tracks. Storing under illumination may lead to photo oxidation and is able to increase the track etch ratio by orders of magnitude. It is reported that tracks in poly(ethylene terephthalate) (PET) may be sensitized by uv radiation of 310 to 400 nm. Soaking in weak solvents, such as dimethyl formamide or water-soluble gass can sensitize ion tracks in PET.[6]

Effect of Etch Promoters

Etch promoters are organic solvents that accelerate the etch process when added to the etch bath. It has been observed that track etch ratios in polycarbonate (PC) can be above ten thousand. On the other hand, track etch ratio can be dramatically decreased down to 2 to 4 in PET by the addition of solvents such as methanol, ethanol or propanol, leading to wide cone angles. These organic solvents help to dissolve large fragments ready to move into the liquid phase by disengaging them from their neighbors.[6] Figure 1-4 shows an example of etch promotion using ethanol in PET.[18]

Etch Properties of Selected Polymers

In PET ($OOC\text{-}C_6H_4\text{-}COO\text{-}CH_2CH_2$), the main points of etch attack are the partially charged –COO- ester groups, which are hydrolyzed by alkalis. During alkaline etching the ordinary bond between carbon and oxygen is broken which produces $–COO^-$ and HO- at the ends of the formed fragments.

For polycarbonate ($OOC\text{-}O\text{-}C_6H_4\text{-}C(CH_3)_2\text{-}C_6H_4$), the main point of etch attack is the carbonate group –O-COO-. During the alkaline etching, chemical bonds are ruptured on both sides of the carbonate group, leading to the formation of carbonate ions, CO_3^{2-}. The other product is diphenylol $HO\text{-}C_6H_4\text{-}C(CH_3)_2\_C_6H_4\text{-}OH$.

In Polyimide ($C_6H_4\text{-}O\text{-}C_6H_4$), the preferential point of etch attack is the oxygen. At high pH the imide group will be hydrolyzed. The etching mechanism is complex because of the simultaneous factors of oxidation and alkalinity. The chemical reaction responsible for etching different polyimide can be different because they are made up of monomer units. [19]

Effect of Thermal Annealing

By increasing the temperature of the tracked material, ion tracks can be thermally annealed. For polymers, heating above the glass transition temperature mobilizes the polymer fragments formed along the ion path. These fragments are sucked into the voids of the neighboring pristine material, wiping out the latent ion track.[14]

The Effect of Temperature during Etching

Etch rates usually increase with temperature. Therefore, to obtain high throughput makes it necessary to work at high temperatures. It is found that by alternating the temperature during etching, high aspect ratio pores with large diameters can be obtained. At room temperature diffusion processes can be faster than chemical reactions of the etchant within the polymer. [14]

From this basis, the technique to make pores with large cone angles were develop by soaking at low temperature and etching at high temperature.[20]

Effect of Detergents

Amphiphilic detergents may increase the track-etch-ratio. These detergents have been shown to produce nanopores with cigar-like shapes and very small entrance openings. It is thought that amphiphilic detergents attach to the hydrophilic surface layer, rendering it less permeable to the etchant.[21]

Etch Properties in Muscovite Mica

Damage tracks are form in single crystal muscovite mica ($KAl_2(AlSiO_3O_{10})(OH)_2$ from ion irradiation along the (001) direction. Because the etching rate along the tracks is much faster than both the lateral and bulb etch rate, when the tracks are etched through, nanopores with small cross-section and small taper angle (0.02°) are created.[22] In muscovite mica, all the pores are diamond-shaped with inner angles very close to 60° and 120° (Figure 1-5). All the pores in a given sample have the same size and orientation.[22] By correlating the results of scanning electron microscopy and X-ray diffraction on etched mica crystals, it was found that the orientation of the diamonds is exactly the same as that of the mica unit cell. The four sides of the diamonds are parallel to the four oxygen-terminated planes within the unit cell. These facts points out that the diamond–shaped pores have their origin in the mica crystal structure. Also, this shows that the uniform diamond shape arises because the oxygen-terminated planes are those with the slowest etch rate, and the pores are aligned because the template are single crystals.[22]

Template Synthesis

The Martin group has pioneered a general method for the preparation of nanostructured materials called template synthesis[23-25] Template synthesis method entails depositing a desired

material of interest into a porous solid. The size and shape of the nanomaterial depend on the dimentions of the nanocavities within the porous template material. Depending on the membrane and synthetic material used, nanostructures such as solid nanofibers or nanotubes can be obtained. The method is termed "general" because nearly any chemical synthesis method used to prepare bulk materials can be adapted to synthesize materials. There are reports of metals,[10, 26-32] polymers,[33-36] carbons[37-39] and semiconductors[40, 41] prepared by the template synthesis method. More advance material preparation include composite nanostructured material, both concentric and tubular[42, 43] and segmented composites nanowires.[44]

Template Synthesis Strategies

Three commonly used templates are; porous polymers, alumina and mica membranes (Figure 1-6). Some of the more common synthetic strategies used to prepare nanomaterials include chemical vapor deposition,[38, 45, 46] electrochemical[47-49] and electroless deposition,[50, 51] chemical[52] and electrochemical polymerization,[53] and sol-gel chemistry.[40, 54] Special attentions will be devoted to the electroless deposition inside polymers and mica, and chemical vapor deposition in mica since these are the methods used for preparing templates in chapters 2, 3, and 4 respectively.

Electroless Deposition

The electroless deposition method involves the use of a chemical reducing agent to plate a metal from a solution onto a surface. Unlike electrochemical deposition, a conductive surface is not necessary. The key requirement of electroless deposition is arrangement of the chemistry such that the kinetics of the homogenous electron transfer from the reducing agent to the metal ions is slow. This is essential because the metal ions would simply be reduced in the bulk solution for fast electron transfer. In electroless deposition, a catalyst needs to be coated onto the pore walls so that reduction of the metal ion only occurs at the pore surfaces. Figure 1-7 shows

the schematic representation that was used to prepare silver and gold nanowires and nanotubes within PET, Kapton and Mica track-etched membranes. The membranes were first exposed to a sensitizer (Sn^{2+}). This is accomplished by simply immersing the membrane for 45 minutes in a solution that is 0.026 M in $SnCl_2$ and 0.07 M in trifluoroacitic acid in 50/50 methanol/water. The tin sensitizer binds to the pore walls and membrane surfaces via complexation with the amine, carbonyl and hydroxyl groups. [63] After sensitization, the membrane is rinsed thoroughly with methanol and immersed into an aqueous solution of ammoniac silver nitrate (0.029 M Ag $(NH_3)_2^+$) for 5 minutes. A redox reation occours in which the surface bound tin (II) is oxidized to tin (IV) and the Ag^+ is reduced to elemental Ag. As a result, the pore walls and the membrane surface become coated with nanoscopic silver particles. The membrane is again thoroughly rinsed with methanol. The silver coated membrane is then immersed into a gold plating bath that is 7.9 x 10^{-3} M in $Na_3Au\ (SO_3)_2$, 0.127 M Na_2SO_3, and 0.625 M in formaldehyde at 4°C. The Au galvanically displaces the Ag particles because the reduction potential of Au is more positive than that of Ag. As a result, the pore walls and surfaces become coated with Au particles. These particles are excellent catalytic sites for the oxidation of formaldehyde and the concurrent reduction of Au (I) to Au (0).[63] Without a catalyst, the kinetics of the electron transfer from the reducing agent (formaldehyde) to Au (I) is slow; therefore, the gold plating continues on gold particles instead of in the bulk solution. The reaction can be represented as follows:

$$2Au\ (I) + HCHO + 3OH \rightarrow HCOO^- + 2H_2O + 2Au\ (0) \qquad (1\text{-}1)$$

This method yields the Au nanowires or nanotubes within pores plus Au surface layers on both face of the membrane. These structures run through the entire thickness of the template membrane (Figure 1-8). By controlling the plating time, the inside diameter of the tubes can be varied because the thickness of both the Au surface films and nanotube wall increase with

plating time. By controlling the plating time, the inside diameter of the nanotubes can be varied, even as low as 1 nm in diameter.[28] As a result, these membranes can be used in a simple membrane permeation experiment to cleanly separate small molecules on the basis of molecular size.[28] Also, by chemisorbing appropriate thiols to the Au nanotube wall based on well known gold-thiol chemistry, the Au nanotube membrane can be made to preferentially transport cations vs. anions and hydrophobic vs. hydrophilic molecules.[10, 27, 31, 55] In addition, Au nanotube membranes are electronically conductive and can be charged electrostatically in an electrolyte solution.[27] This introduces ion transport selectivity, allowing the Au nanotube membranes to be electromodulated between ideal-cation and idea-anion transport states.[27] Thus these Au nanotube memebranes are ideal model systems for studying how pore size, chemistry, and charge affect the transport selectivity at the nanometer scale.

Chemical Vapor Deposition (CVD)

CVD is commonly used to prepare carbon nanomaterials. We[38, 56] and others[57, 58] have synthesized carbon nanotubes within the porous alumina membranes using CVD. This involves placing an alumina membrane in a high-temperature furnace (ca. 700°C) and passing a gas such as ethane, propene or ethylene through the membrane. Thermal decomposition of the gas occurs on the pore walls, resulting in the deposition of carbon nanotubes within the pores. High surface area microporous carbon with long-range order has been synthesized by using zeolite Y as a template with propylene CVD.[59] Besides carbon nanostructures, other nanomaterials have been obtained by CVD. For example, the martin group has used a CVD method to coat an ensemble of gold nanotubes with concentric TiS_2 outer nanotubes.[43]

Resistive-Pulse Sensing

Resistive-pulse[60] sensors for molecular and macromolecules analytes[60-77] use a nanopore in a synthetic or biological membrane as the sensor element. This method, which when applied to

such analytes is sometimes called stochastic sensing,[60, 69] entails mounting the membrane containing the nanopore between two electrolyte solutions, applying a transmembrane potential difference, and measuring the resulting ion current flowing through the electrolyte-filled nanopore. In simplest terms, when the analyte enters and translocates the nanopore, it transiently blocks the ion current, resulting in a downward current pulse (Figure 1-9). The frequency of such analyte-induced current pulses is proportional to the concentration of the analyte, and the identity of the analyte is encoded in the magnitude and duration of the current pulse.[60-77]

The majority of such resistive-pulse biosensing data has been obtained using a biological nanopore, α-hemolysin (α-HL), embedded in a supported lipid-bilayer membrane as the sensor element (Figure 1-10).[60-69] This biological nanopore sensor has two key advantages. First, it can be made analyte selective by using chemical or genetic-engineering methods to attach molecular-recognition agents to the nanopore. As a result numerous different analyte types including metal ions,[64] DNA,[65, 66] proteins,[67] and small molecules[68] have been selectively detected with the α-HL nanopore. Second, the biological nanopore can be reproducibly prepared from the commercially available α-HL protein, which is obviously of great importance if practical, real-world, sensing devices are ultimately to be derived from this technology.[78] There is however a key impediment to developing practical sensors based on the biological nanopore. This problem concerns the fragility of the supported bilayer membrane that houses the nanopore. Such membranes typically survive for periods of only hours before rupture, much too short of a time to make a practical sensing device.[69]

One approach for solving this problem is to replace the biological nanopore, and bilayer membrane, with an artificial nanopore embedded in a mechanically and chemically robust synthetic membrane.[69-77, 79, 80] Such artificial nanopores are often prepared by modern

microlithographic methods, using for example a focused ion[71] or electron[72] beam to bore the nanopore into a silicon or Si3N3 membrane. We and others are exploring an alternative technology, called the track-etch method,[16, 19, 81, 82] for preparing nanopores for resistive-pulse sensors.[70, 75-77, 79, 80] Analytes detected with prototype track-etched nanopore sensors include small molecules,[70] DNA,[75, 76] proteins[77] and nanoparticles.[79] Furthermore, there are older reports of developing virus sensors based on track-etched nanopores.[80]

The sensor elements we evaluated were conically shaped nanopores[70, 75-77, 79, 81] prepared by the track-etch method in polyethylene terephthalate (PET) membranes. Such conical nanopores have two openings - the large-diameter (base) opening at one face of the membrane and the small-diameter (tip) opening at the opposite face (Figure 1-11). Fabrication methods to prepare these conically shaped nanopores for resistive pulse sensing, is addressed in chapters 1.

Plasma-Based Etching

Plasma etching, a dry etching process, has become a very useful means of removing small quantities of material from a variety of substrates quickly and efficiently.[83] Plasma processes have been used in many highly sensitive integrated applications to precisely remove specific materials from sample surfaces. To generate plasma, a pair of electrode is needed; one is connected to a radio frequency (RF) voltage and the other is grounded. RF energy is applied to the electrodes which accelerates electrons to increase their kinetic energy. The electrons collide with a neutral gas to form a collection of gaseous species including ions, free radicals, electrons, photons and neutrals.[83] The gaseous species can react with the surface to be etched such that reaction product is volatile and can be pumped away. There are several types of plasma etching-physical etching (anisotropic), chemical etching (isotropic) and reactive ion (combination of physical etching and chemical etching). Usually in plasma based etching, both chemical etching and physical etching occur.[83]

There are many applications for plasma etching such as photoresist removal, glass-like compound etching (e.g., SiO_2) and polymer etching to produce microstructures and nanostructures. For example, large-area, well-ordered, periodic nanopillar arrays with lateral dimensions as small as 40 nm have been developed based on a combination of colloidal lithography and plasma etching techniques.[84, 85] The etching mask on silicon substrates were prepared using the close-packed structures formed by monodisperse polystyrene beads.[84, 85] Polymer surfaces can also be modified by plasma treatment, for example, to improve wetting properties and to enhance the adhesion of plasma-deposited coatings.[86]

Plasma etching technique is described in Chapter 2 to remove carbon surface layers from mica tracked etched membrane that was previously exposed to CVD. This was necessary to expose the underlying mica surface for dissolution with HF so that the carbon nanotube can be revealed.

Asymmetric Diffusion

In some systems, diffusive transport through membranes may in some circumstances pass more readily in one direction than the other. This phenomenon is known as asymmetric diffusion, and is known in the context of transport across membranes,[87-89] and in the context of osmosis.[90, 91] The above asymmetric phenomena is explained either by the binding of particles at intra-pore sites or other electrostatic interaction with the pore surface. In this research, we show that asymmetric diffusion can occur with no binding or electrostatic interaction of particle with the pore surface. It is demonstrated in Chapter 5 that asymmetric diffusion can take place by purely geometric constraints. Here, conical nanopores, with tip diameter comparable to that of the diffusion molecule, are the used for asymmetric diffusion of neutral molecules.

Dissertation Overview

The goal of this research is to develop conical nanopores and nanotube (single and multipore) in polymers and mica membranes by the track-etch method and extension of this technology for sensing and other applications, and to investigate the transport properties of these conical pores. The previous part of Chapter 1 has reviewed background information for this dissertation including the ion track-etch method, membrane based template synthesis, electroless metal deposition, chemical vapor deposition, resistive-pulse sensing, plasma based etching and asymmetric diffusion.

In Chapter 2, an extension of the track-etch method to make conical pores in a reproducible fashion is demonstrated. We have shown here that we can not only reproducibly prepare track-etched based conical nanopore sensor elements, but that we can predict from the experimental parameters used during the second etch, what the diameter of the all-important nanopore tip will be. For these reasons, we believe that the track-etch method will prove to be the technology of choice for taking artificial-nanopore resistive-pulse sensors from the bench top to the practical prototype-device stage of the R&D effort.

Chapter 3 describes a method to make asymmetric pores in tracked muscovite mica films using an etch-refill-etch approach. Tracks in the films were initially etched away with hydrofluoric acid to form nanoporous membranes. These nanopores were then refilled with silver nanowires or "metal tracks" using an electroless plating method. One face of the membrane was then exposed to a solution of hydrofluoric acid and nitric acid, which etched the bulk material and the nanowires respectively, at two different rates. By controlling the concentration ratio of hydrofluoric acid to nitric acid, tapered pores with diamond shaped cross-section were obtained. Replicas of the asymmetric pores were accomplished by carbon vapor

deposition, and scanning electron microscopy was used to give evidence of the resulting nanotubes. In this study, excellent control over tip size and cone angle was demonstrated.

In Chapter 4, electroless gold plating properties on the surface and pore walls of track-etched Kapton polyimide nanoporous membranes were studied. Scanning electron microscopy (SEM), atomic force microscopy (AFM), and ion current measurements were used to characterize the surfaces and pore dimensions of the membrane. Nanoporous Kapton polyimide membranes were electroless gold plated over different times and the pore diameter characterized using SEM. Ion current measurements were used to measure the diameter of very small pores. AFM images show that after electroless gold plating, the gold surface layers are smooth compared to a similarly structured polycarbonate membrane. Electroless plating the membranes for 12 hours produced Au wires in the pores. Removing the membrane by oxygen plasma revealed that the plating in the walls is also relatively smooth.

Finally, Chapter 5 describes asymmetric diffusional transport of neutral molecular species through nanoporous polymer membranes. Membranes containing conical nanopores from polyimide (Kapton HN Dupont) foils were prepared by the track-etching technique, based on irradiation of the polymer with swift heavy ions and subsequent etching of the latent tracks. The transport properties (e.g, flux) of these membranes were investigated using UV-Vis spectroscopy. Transport experiments were performed with bare polymer membranes without any modification. We report the preferential direction of the flow of molecules through conical nanopores and spatial or concentration dependence of diffusion coefficient for a particular flow direction.

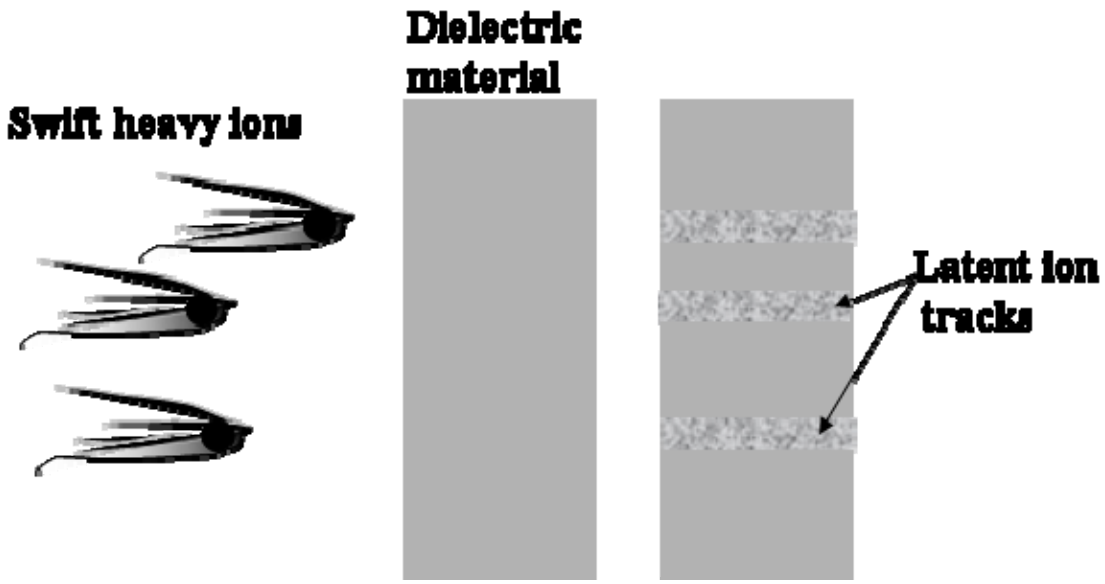

Figure 1-1. Swift heavy ions impinge on a dielectric material creating damaged ion tracks.

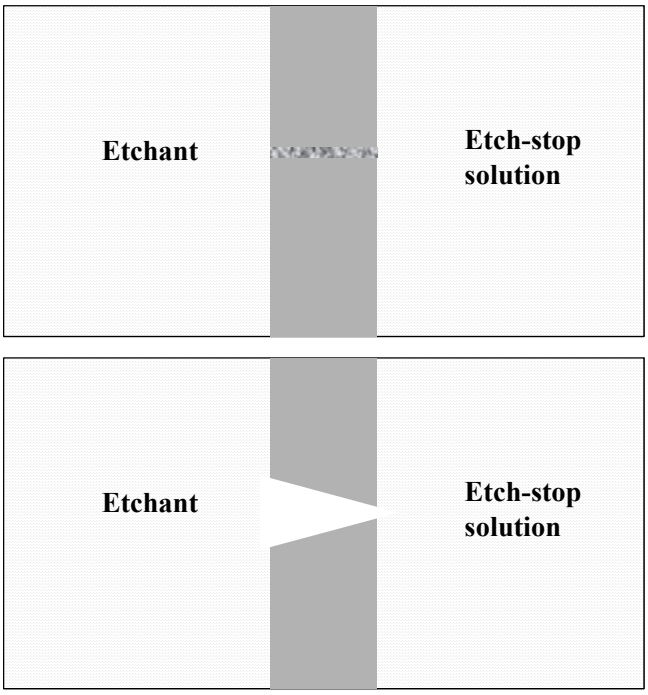

Figure 1-2. After irradiation, the materials are subject to chemical etching which preferentially removes the latent ion track.

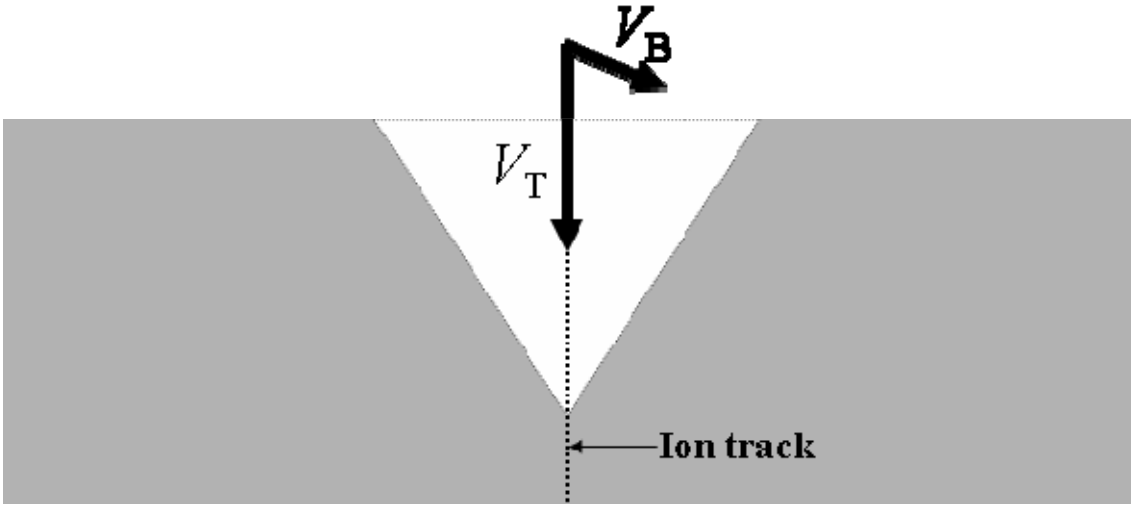

Figure 1-3. Etched pore geometry in a homogeneous isotropic medium to a first approximation, showing track etch rate, V_T, and bulk at rate, V_B.

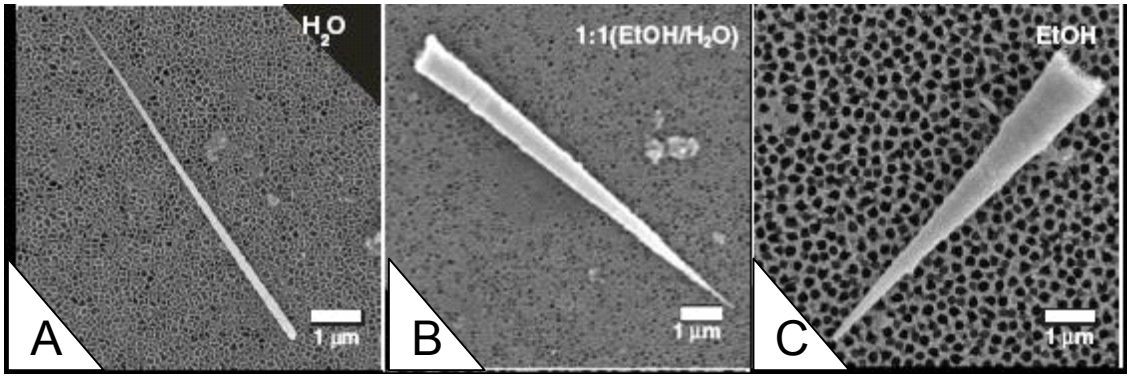

Figure 1-4. Scanning electron micrographs of Au nanocones replicas of PET conical pores. Increasing fraction of ethanol in the etch solution results in greater cone angle (A-C).[Adapted from Scopece, P.; Baker, L. A.; Ugo, P.; Martin, C. R. *Nanotechnology* **2006**, *17*, 3951-3956.]

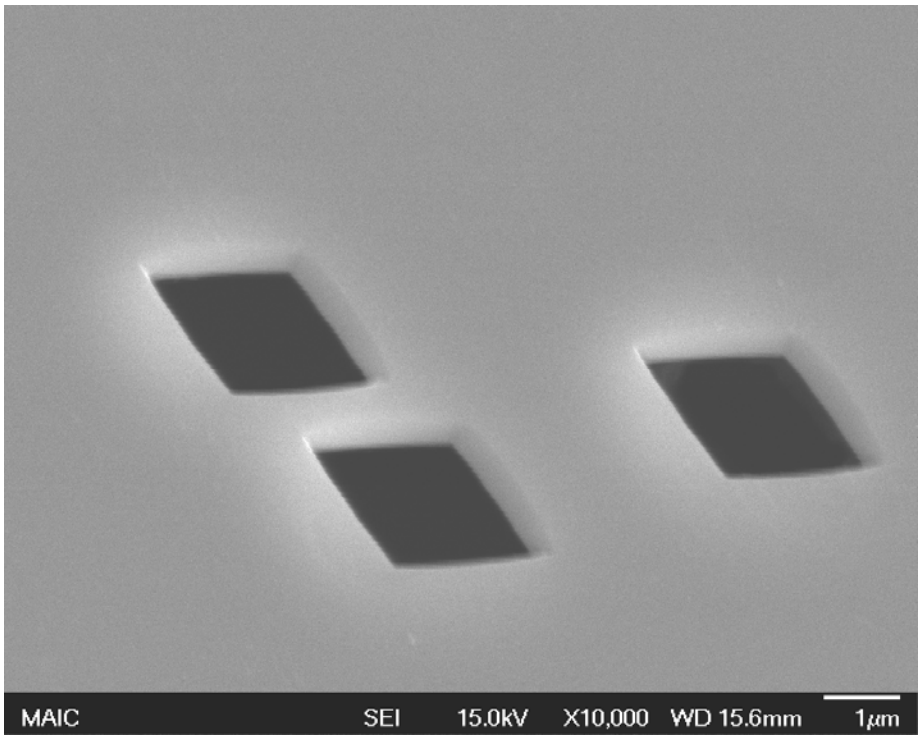

Figure 1-5. Scanning electron micrographs of etched particle tracks in single-crystal mica

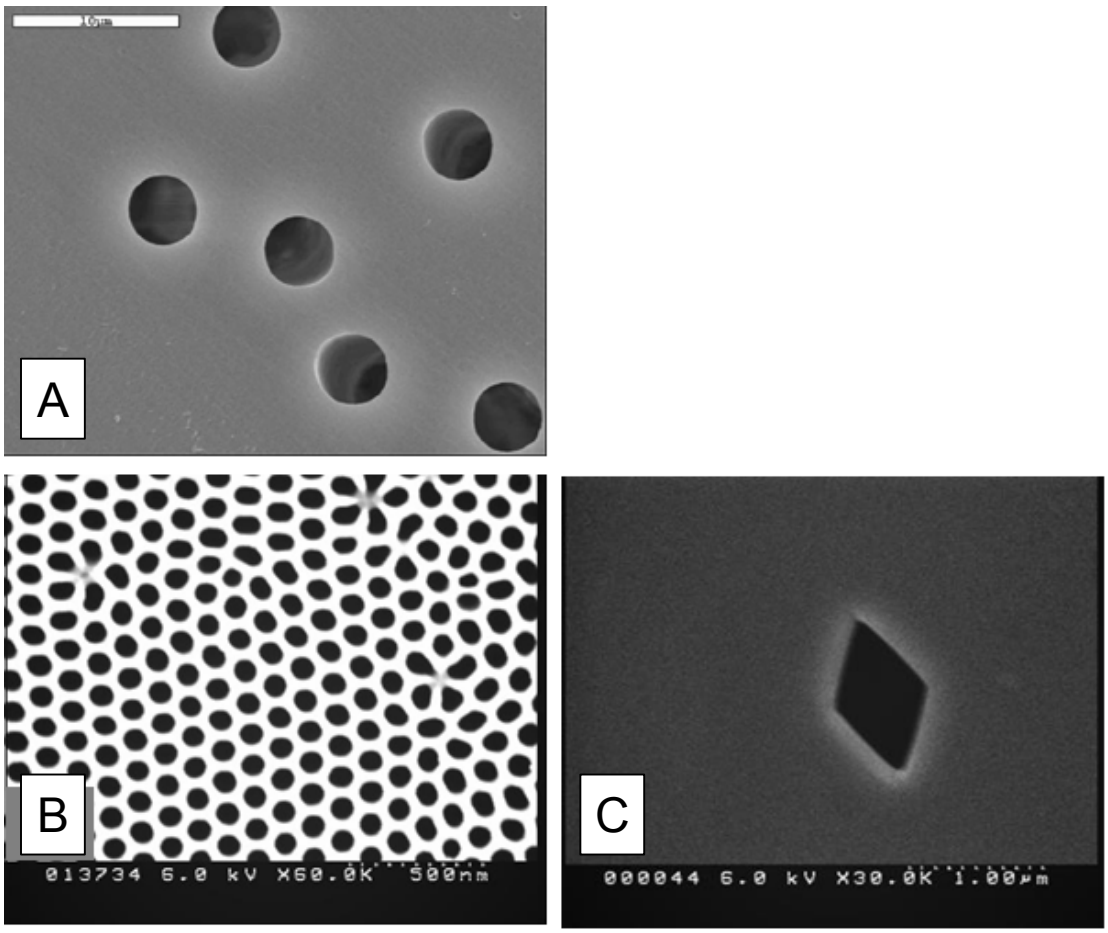

Figure 1-6. Scanning electron micrographs of a porous polycarbonate, alumina and mica membranes used for template synthesis (A-C, respectively).

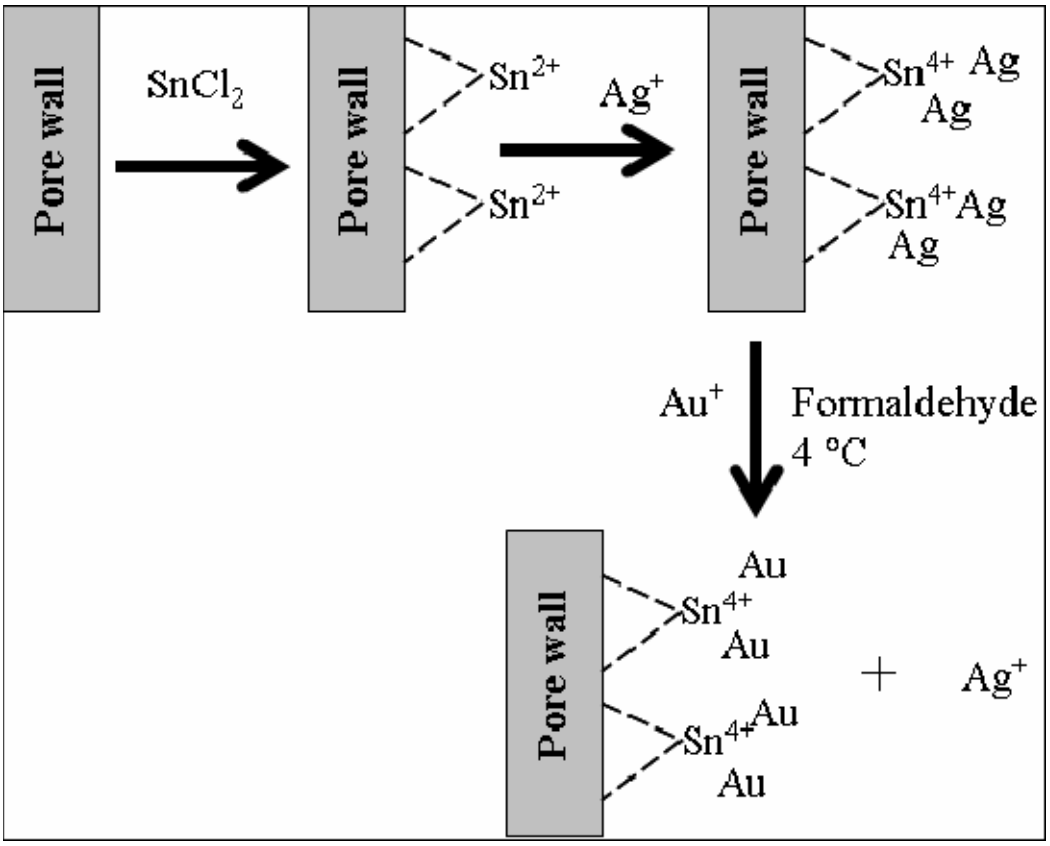

Figure 1-7. Schematic diagram of Au electroless plating procedure

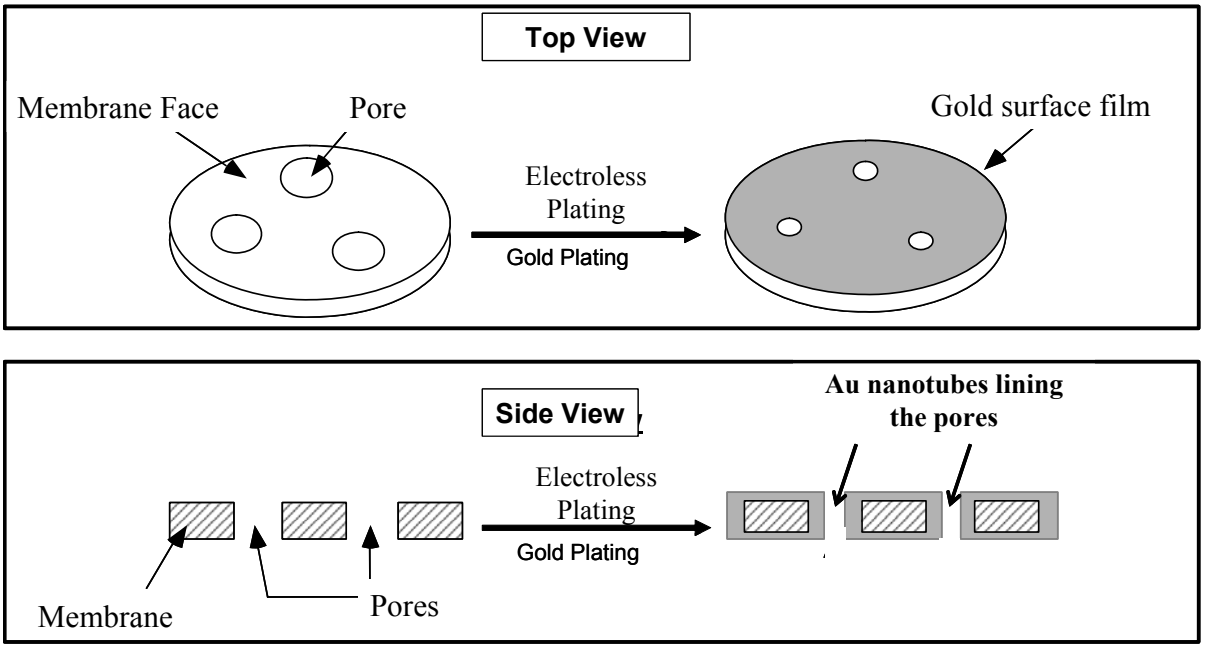

Figure 1-8. Schematic illustration of Au nanotubes obtained from electroless gold deposition

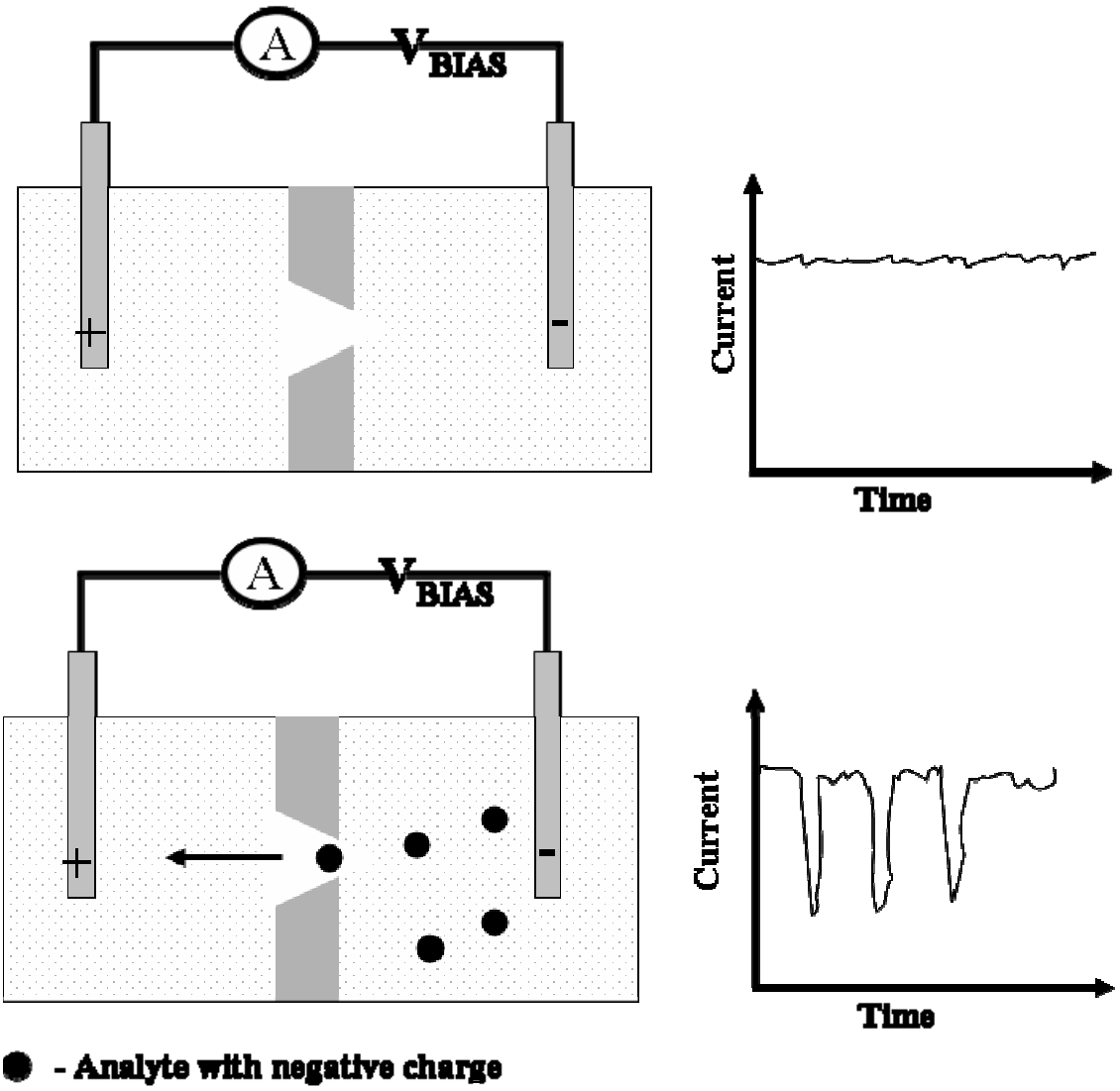

Figure 1-9. Schematic illustration of resistive-pulse sensing

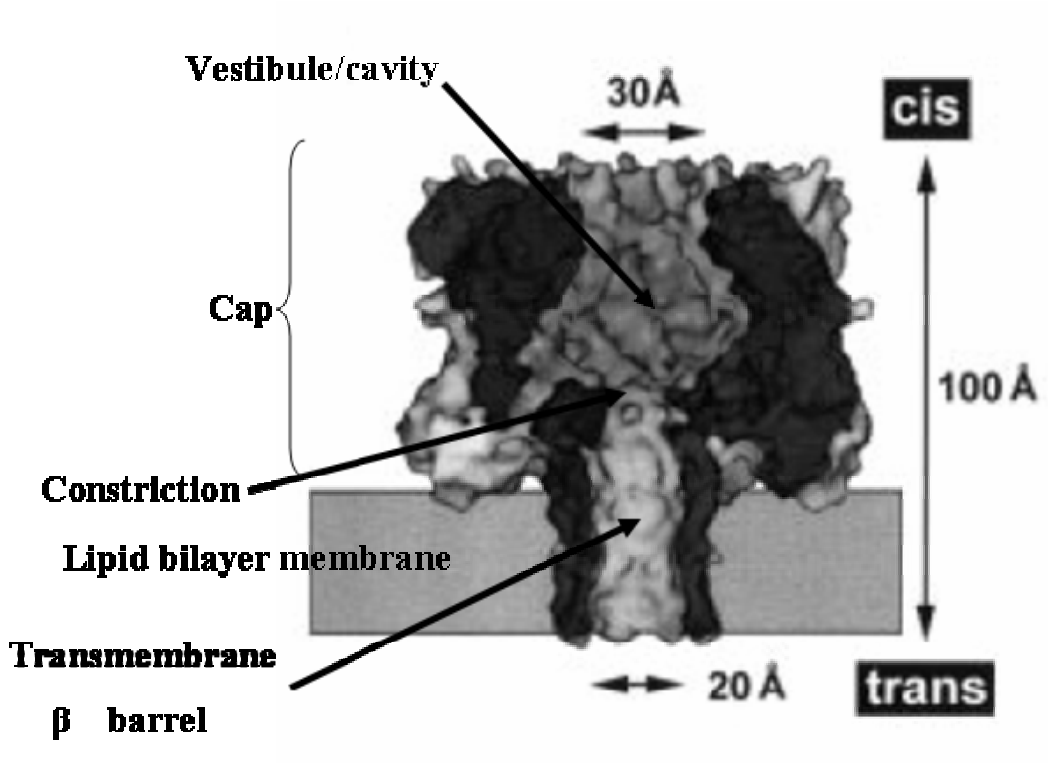

Figure 1-10. Essential features of the staphylococcal α –hemolysin pore shown in a cross-section based on the crystal structure.[Adapted from Bayley, H.; Martin, C. R. *Chemical Reviews (Washington, D. C.)* **2000**, *100*, 2575-2594.]

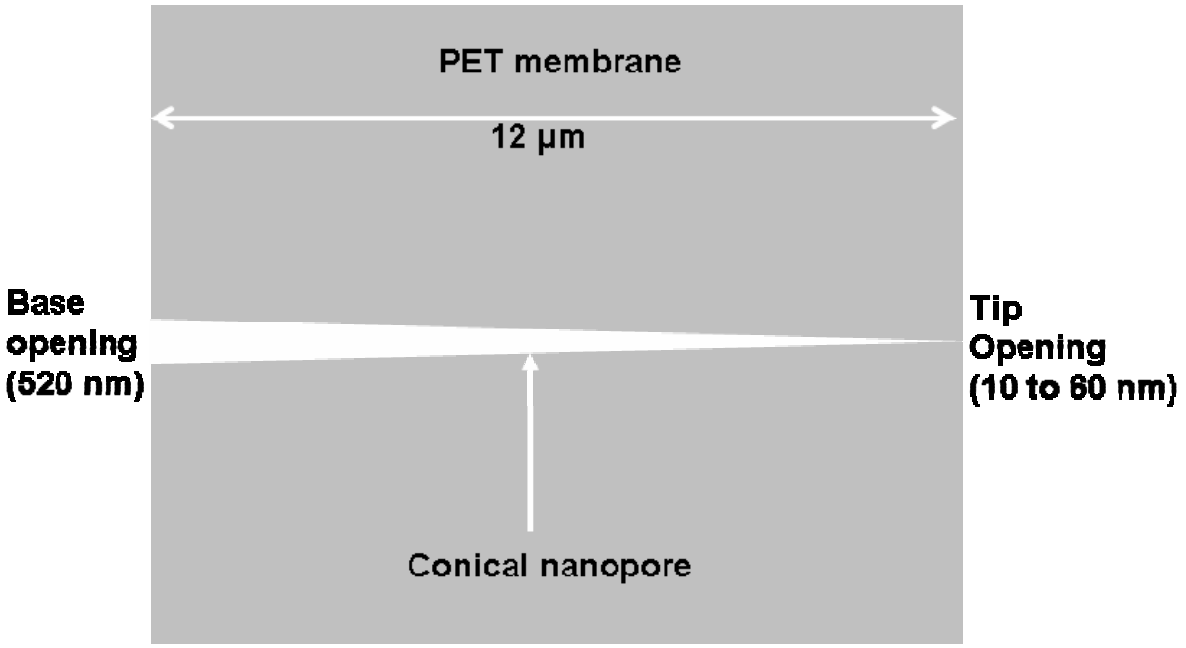

Figure 1-11. Schematic of a conical nanopore sensor element showing the base diameter and range of tip diameters used in these studies (drawing to scale)

CHAPTER 2
A METHOD FOR REPRODUCIBLY PREPARING SYNTHETIC NANOPORES FOR RESISTIVE-PULSE BIOSENSORS

Introduction

Resistive-pulse[60] sensors for molecular and macromolecules analytes[60-77] use a nanopore in a synthetic or biological membrane as the sensor element. This method, which when applied to such analytes is sometimes called stochastic sensing,[60-69] entails mounting the membrane containing the nanopore between two electrolyte solutions, applying a transmembrane potential difference, and measuring the resulting ion current flowing through the electrolyte-filled nanopore. In simplest terms, when the analyte enters and translocates the nanopore, it transiently blocks the ion current, resulting in a downward current pulse. The frequency of such analyte-induced current pulses is proportional to the concentration of the analyte, and the identity of the analyte is encoded in the magnitude and duration of the current pulse.[60-77]

The majority of such resistive-pulse biosensing data has been obtained using a biological nanopore, α-hemolysin (α-HL), embedded in a supported lipid-bilayer membrane as the sensor element.[60-69] A key advantage of this biological-nanopore sensor element is that it can be reproducibly prepared from the commercially available α-HL protein. This is of great importance if practical, real-world, sensing devices are ultimately to be derived from this technology.[78] There is, however, a key impediment to developing practical sensors based on the biological nanopore. This problem concerns the fragility of the supported bilayer membrane that houses the nanopore. Such membranes typically survive for periods of only hours before rupture, much too short of a time to make a practical sensing device.[69]

One approach for solving this problem is to replace the biological nanopore, and bilayer membrane, with an artificial nanopore embedded in a mechanically and chemically robust synthetic membrane.[69-77, 79, 80] Such artificial nanopores are often prepared by microlithographic

methods, using for example a focused ion[71] or electron[72] beam to bore the nanopore into a silicon or Si_3N_3 membrane. We and others are exploring an alternative technology, called the track-etch method,[16, 19, 81, 82] for preparing nanopores for resistive-pulse sensors.[70, 75-77, 79, 80] Analytes detected with prototype track-etched nanopore sensors include small molecules,[70] DNA,[75, 76] proteins[77] and nanoparticles.[79] Furthermore, there are older reports of developing virus sensors based on track-etched nanopores.[80]

This field of artificial-nanopore resistive-pulse sensing is currently in its infancy. A key question that must be addressed before practical sensors can be developed is - can the nanopore sensor element be prepared reproducibly, as the biological nanopore can? We address this critically important issue here.

The sensor elements we evaluated were conically shaped nanopores[70, 75-77, 79, 81] prepared by the track-etch method in polyethylene terephthalate (PET) membranes. Such conical nanopores have two openings - the large-diameter (base) opening at one face of the membrane and the small-diameter (tip) opening at the opposite face (Figure 2-1a). We have found that the diameters of both of these opening can be controlled with good reproducibility using a new two-step pore-etching procedure. Furthermore, we have developed a simple mathematical model that allows us to predict the diameter of the tip opening from the parameters used during pore etching. Good agreement was obtained between the predicted and experimentally measured tip diameters.

Experimental

First Etch Step

The tracked PET membrane (from GSI) was mounted in cell shown in Figure 2-1b, and the etch solution (9 M NaOH) was placed in one half cell and the stop solution (1M formic acid plus 1 M KCl) in the other. A platinum wire electrode was placed in each solution and a Keithley

6487 was used to apply a transmembrane potential difference of 1V during etching, with polarity such that the anode was in the etch solution. The electrochemical reactions occurring at the anode and cathode are discussed in the Supplementary Materials. Etching was terminated after two hours by replacing the contents of the etch half-cell with stop-etch solution. The membrane was then rinsed with purified water (Barnstead D4641, E-pure filters).

Determination of the Diameter of the Base Opening

Multi-track membranes (10^6 cm^{-2}) were subjected to the same first etch step as used for the single-track membranes, and the base openings were imaged *via* FESEM (JEOL JSM-6335F). The average base diameter obtained (520$\pm$45 nm) is associated with measurements of 50 pores in five different multi-track membrane samples.

Electrochemical Measurement of the Tip Diameter

The membrane was mounted in the cell, and the half cells were filled with 100 mM phosphate-buffered saline, pH = 7.0 that was also 1 M in KCl. The specific conductivity of this solution was measured using a conductometer (YSI 3200) at 25° C; a conductivity of 0.107 S cm^{-1} was obtained. A Ag/AgCl electrode immersed into each solution was used in conjunction with the Kiethly 6487 to obtain the current-voltage curve for the nanopore (Figure 2-2). We have validated this electrochemical method by comparing diameters obtained via this method with diameters for the same pores measured by electron microscopy.[92, 93]

Second Etch Step

The etch solution in this case was 1 M NaOH, and its conductivity was measured at 0.160 S cm^{-1} (25° C). The membrane was mounted in the cell, and the half cells were filled with this etch solution. A platinum electrode was immersed into each half-cell solution, and the Keithley 6487 was used to apply a transmembrane potential difference of 1V and measure the nanopore ion current as a function of time. Etching was terminated at specified current values (Figure 2-3,

Figure 2-4) by replacing the etch solution in both half cells with the stop-etch solution. The membrane remained in the stop etch for at least 30 min and was then rinsed with purified water.

Bovine Serum Albumin (BSA) Resistive-Pulse Sensing

Conical nanopores sensors having two different tip diameters, 58 nm and 44 nm, were prepared; the base diameter for both sensors was 520 nm. After etching the pore walls were coated with gold nanotubes using the electroless plating method described previously.[28] After electroless plating the tip diameters of the resulting gold nanotubes were measured using the electrochemical method discussed above; tip diameters of 32 nm and 23 nm were obtained. The Au-coated nanopore walls were then functionalized with a thiolated PEG (MW 5000 Da, Nektar Therapeutics) to prevent non-specific protein adsorption.[94] This was accomplished by immersing the nanotube-containing membrane in a 0.1 mM solution of the PEG at 4 ^{o}C for ~15 hours. The membrane was then immersed in purified water for 1.5 hours to remove any unbound PEG. The tip diameters were then re-measured; values of 27 nm and 17 nm were obtained.

The BSA (Sigma) was dissolved in 10 mM phosphate-buffered saline that was also 100 mM in KCl (pH 7.4). The concentration of BSA was 100 nM, and the BSA solution was placed on the tip side of the membrane. Buffer was placed on the base side and a transmembrane potential of 1000 mV was used to drive the protein through the nanopore (tip to base) by electrophoresis.

Results and Discussion

Conical Shaped Nanopores are Ideal Resistive-Pulse Sensor Elements

Resistive-pulse sensing entails mounting the nanopore membrane between the two halves of an electrolyte-filled cell (Figure 2-1 (b)) and passing an ionic current through the electrolyte-flooded nanopore. In a conically shaped nanopore the voltage drop caused by this ion current is focused to the electrolyte solution in the tip opening of the nanopore.[79] Indeed, the field strength

in the solution within the nanopore tip can be greater than 10^6 V m^{-1}, when the total voltage drop across the nanopore membrane is only 1 V.[79] A consequence of this focusing effect is that the nanopore ion current is extremely sensitive to analyte species present in the nanopore tip. That is, there is an analyte "sensing zone" just inside the tip, which makes conically shaped nanopores ideally suited for the resistive-pulse sensing application. This has been demonstrated with prototype conical-nanopore sensors for analyte species ranging in size from small molecules, to proteins, to nanoparticles.[70, 75-77, 79]

The Core Technology: The Track-Etch Method

The track-etch method has been practiced commercially for decades to make polymeric nanopore membranes for filtration applications.[16, 19, 81, 82] It entails passing high energy particles through the membrane, to create damage tracks, followed by chemical etching to convert these damage tracks into pores. While the commercial process yields membranes that contain high pore densities, a method for preparing *single-damage-track membranes* was developed at the Gellsellschaft fur Schwerionenforschung (GSI).[19] We purchased such single-track PET membranes from GSI for these studies. *This is an important point with regard to the overall sensor-fabrication technology - the key precursor material, the tracked membrane, can be obtained commercially.*

The First Etch Step

Both etch steps used the cell shown in Figure 2-1b. Step 1 entails placing a solution that etches the damage track on one side of the membrane and a solution that neutralizes this etchant on the other side.[81] For PET the etchant is NaOH, and the etch-stop is formic acid. This yields a conically shaped pore (Figure 2-1a) with the base opening facing the etch solution and the tip opening facing the etch-stop solution. To determine when the etchant has broken through to the etch-stop solution, and a contiguous pore has been obtained, an electrode is placed in each

solution, and a potential difference is applied across the membrane. Before breakthrough, the transmembrane ion current is zero, and breakthrough is signaled by a sudden rise in the current.[81]

We previously showed that the diameter of the base opening could be controlled by varying the potential applied across the membrane during this first etch step.[92] An applied transmembrane potential of 1.0 V was used in the first etch step for all of the nanopores investigated here. To obtain a measure of the reproducibility of the base diameter obtained after the first etch step, we subjected multi-track membranes (10^6 tracks cm^{-2}) to the same first etch as used for the single-track membranes, and imaged the base openings using field emission scanning electron microscopy (FESEM, Figure 2-4). We used multi-track membranes for this study because it is difficult to locate the base opening in electron micrographs of a single-nanopore membrane. We have previously shown that the pore diameter obtained for tracked-etch membranes is independent of track density.[95] A base diameter of 520±45 nm was obtained, indicating good reproducibility in base diameter after the first etch step.

However, the tip diameter varied between 1 and 7 nm and could not be reproduced from etch to etch. We reasoned that this is an inherent feature of this "anisotropic" etch process. This is because the etch and etch-stop solutions are mixing (and neutralizing each other) in the nascent tip, which makes it difficult to control the etch rate in this critically important region of the nanopore.

Measuring the Diameter of the Tip Opening after the First Etch

Because the tips after the first etch are so small, they are very difficult to find and image via electron microscopy. Therefore, an electrochemical method described previously[70, 76, 81, 92] was used to measure the diameter of the tip. This entailed mounting the membrane sample in the cell (Figure 2-1b), filling both half cells with an electrolyte solution of known ionic conductivity,

and obtaining a current-voltage (I-V) curve associated with ion-transport through the nanopore (Figure 2-2).

The experimental slope of this linear I-V curve is the ionic conductance, G_1, (in Siemens, S) of the nanopore, which is given by[81]

$$G_1 = (\sigma_{KCl} \pi d_b d_t) / 4 L \quad (2\text{-}1)$$

where σ_{KCl} is the experimentally measured conductivity of the KCl-based electrolyte used (S cm-1), L is the length of the nanopore (membrane thickness), db is the experimentally measured diameter of the base opening, and d_t is the diameter of the tip opening. Because all of the other parameters in Equation 1 are known, d_t can be calculated.

The Second Etch Step

In the second step NaOH etch solution is placed on both sides of the membrane. Again, a transmembrane potential is applied, and the ion current flowing through the nanopore is measured as a function of time during this etch. Our key innovation is that the second etch is stopped at a prescribed value of this nanopore ion current rather than at some prescribed time after starting the second etch (e.g., Figure 2-3). We adopted this approach because of the variability in tip diameter obtained after the first etch step. The consequence of this variability is that if we stopped the second etch at a prescribed time, we would obtain a corresponding variability in the tip diameters obtained after the second etch step. In contrast, as we will see below, there is an exact mathematically relationship between the ion current flowing through the nanopore when the second etch is stopped (I_f) and the diameter of tip opening.

To prove that the pores obtained after the second etch truly are conically shaped, we used an electroless plating method[28] to deposit correspondingly conically shaped gold nanotubes within the pores of the multipore membranes described above. The PET membrane was then

dissolved and the conical nanopores collected by filtration and imaged by FESEM.[18] These images show that a nearly ideal conically shaped pore is obtained (Figure 2-5).

Measuring the Diameter of the Tip Opening after the Second Etch

The same electrochemical method was used, but the mathematics is slightly different. We define the diameters of the base and tip openings after the first etch step as d_{b1} and d_{t1} and the diameters after the second etch as d_{bf} and d_{tf}. These diameters are related via

$$d_{bf} = (d_{b1} + \Delta x) \tag{2-2}$$

$$d_{tf} = (d_{t1} + \Delta x) \tag{2-3}$$

where Δx is the change in diameter during the second etch. Substituting Equations 2-2 and 3-3 for d_b and d_t in Equation 2-1 yields

$$G_2 = (\sigma_{KCl}\, \pi\, (d_{b1} + \Delta x)(d_{t1} + \Delta x)) / 4\, L \tag{2-4}$$

where G_2 is the slope of the current-voltage curve used to determine the tip diameter after the second etch, d_{b1} and d_{t1} are the experimentally determined base and tip diameters, respectively, after the first etch, σ_{KCl} is the experimentally measured conductivity of the electrolyte used (100 mM phosphate-buffered saline, pH 7, that was also 1 M in KCl; $\sigma = 0.107$ S cm^{-1}), L is the membrane thickness, and Δx is the change in diameter between the first and second etch steps.

We define the parameter M as

$$M = \frac{\sigma_{KCl}\, \pi}{4L} \tag{2-5}$$

which allows us to write, after some simple algebraic manipulation,

$$\frac{G_2}{M} = d_{b1}d_{t1} + (d_{b1} + d_{t1})\Delta x + \Delta x^2 \tag{2-6}$$

Substituting $(d_{tf} - d_{t1})$ for Δx (where d_{tf} is the diameter of the tip opening after the second etch), and again applying some simple algebraic manipulations, yield

$$d_{tf}^2 + (d_{b1} + d_{t1})d_{tf} - \frac{G_2}{M} = 0 \tag{2-7}$$

This is a quadratic equation in d_{tf} for which the solution is

$$d_{tf} = \frac{-(d_{b1} - d_{t1}) + \sqrt{(d_{b1} - d_{t1})^2 + 4G_2 / M}}{2} \tag{2-8}$$

Note that the quadratic formula has two roots; *i.e.,* there should be a $\pm$ instead of a + between the two terms in the numerator of Equation 2-8. However, the root that results when subtraction is used yields a negative value for the tip diameter.

Because all of the parameters on the RHS of Equation 2-8 are known, d_{tf} can be calculated. Furthermore, because the base diameter at the start of the second etch is large (520 nm), the change in base diameter during the second etch (Δx in Equation 2-2) is negligibly small for all but the very largest tip investigated here (60 nm, Figure 2-6).

Reproducibly Varying the Tip Diameter

Figure 2-6 shows a plot of nanopore tip diameter, measured after the second etch step (Eq. 2-5), vs. the nanopore ion current at which this etch was stopped (I_f). We see that the tip diameter can be reproducibly varied over the range from 10 to 60 nm (data points in Figure 2-6). This is important because this is exactly the range in tip diameters we used in our prototype protein,[77] DNA,[76] and nanoparticles[79] sensors. The lower limit (10 nm) is determined by the tip diameter obtained after the first etch which, again, was in the range of 1 to 7 nm. However, we have shown that the walls of such nanopores can be lined with gold nanotubes,[77] and that the diameter of these tubes can be controlled at will down to 1 nm.[96] Hence, if tip diameters smaller than 10 nm are needed, a pore with a 10 nm tip can be gold plated to reduce the tip to any desired value. Furthermore, tips larger than the 60 nm maximum shown in Figure 2-6 can be easily prepared by simply stopping the second etch at larger values of I_f.

The Mathematical Model

We begin by defining a new conductance, G_{etch}, which is the ion current at which the second etch is stopped (I_f) divided by the transmembrane potential applied during the second etch (E_{ap}). With this definition, Equation 4 can be rewritten as

$$I_f = E_{ap} (\sigma_{etch} \pi (d_{b1} + \Delta x)(d_{t1} + \Delta x)) / 4 L \quad (2\text{-}9)$$

where σ_{etch} is the experimentally measured conductivity of the NaOH solution used in the second etch. Equation 2-9 is again a quadratic Equation in d_{tf} for which the solution is

$$d_{tf} = \frac{-(d_{b1} - d_{t1}) + \sqrt{(d_{b1} - d_{t1})^2 + 4I_f / K}}{2} \quad (2\text{-}10)$$

where $K = E_{ap} \sigma_{etch} \pi/4L$ (see Derivation of Equation 2-5, below). Equation 2-10 allows us to calculate the value of the tip diameter after the second etch step (d_{tf}) for any value of I_f at which the second etch was stopped.

We noted above that the base diameter before and after the second etch is essentially the same for all but the largest tip in Figure 2-6. This allows us to simplify Equation 2-9 to

$$I_f = E_{ap} \sigma_{etch} \pi d_{b1} d_{tf} / 4 L \quad (2\text{-}11)$$

which can be rearranged to

$$d_{tf} = I_f 4 L/ (E_{ap} \sigma_{etch} \pi d_{b1}) \quad (2\text{-}12)$$

This obviously provides a much simpler relationship between d_{tf} and I_f.

Plots of d_{tf} vs. I_f calculated using the simplified equation (Equation 2-12) and the exact equation (Equation 2-10) are shown as the two solid lines in Figure 2-6. The tip diameters calculated by these two equations are identical for tips below ~20 nm. Furthermore, the agreement between the experimentally measured (Equation 2-8) and theoretically calculated (Equation 2-10) tip diameters is good, especially considering that there are no adjustable

parameters in the calculations. For example, at $I_f = 20$ nA the experimental and calculated tip diameters differ by less than 10%, and at 40 nA they are identical.

The calculated tip-diameter values are, in general, slightly smaller than the experimental values. This results from an interesting feature of the transport properties of conical nanopores - if there is charge on the pore wall and if the tip opening is small, such nanopores act as ion current rectifiers.[97] The consequence of this rectification phenomenon is that the ionic conductivity of an electrolyte solution within the tip of the nanopore can be lower than the value measured for a bulk sample of the same electrolyte. Since we used the bulk-solution conductivity in our calculations, the calculated values are in general low. Excellent agreement is obtained between the experimental and calculated diameters for the largest tip (Figure 2-6) because large-tip pores do not rectify the ion current.[98] We believe that procedures to obviate the small disagreement between the experimental and calculated tip diameters can be developed, and we are currently pursuing this issue.

To illustrate the importance of controlling the tip diameter in resistive-pulse sensing, we obtained current-pulse data for a prototype protein analyte, bovine serum albumin (BSA), with nanopore sensors having two different tip diameters. The sensors in this case were conical PET nanopores that had been lined with gold nanotubes[28, 77] and then coated with a poly(ethylene glycol thiol) (PEG) to prevent nonspecific protein adsorption.[94] The tip diameters, 17 nm and 27 nm, were measured after PEG functionalization.

Figure 2-7 shows current-pulse data obtained for BSA with these two different sensors. The current-pulse signature can be defined by the average duration and magnitude (ΔI) of the current pulses. The magnitude of the current pulse is important because if ΔI is not larger than the peak-to-peak noise in the background current, the current pulse will be undetectable. We

found that ΔI is larger for the nanopore sensor with the smaller tip opening (ΔI = 80±20 pA) than for the sensor with the larger tip opening (ΔI = 35±9 pA). This is because the roughly 4 nm x 4 nm x 14 nm[94] BSA molecule more effectively blocks the ion current as it translocates the smaller, 17 nm, tip.

Electrochemical Details

Pt electrodes were used to apply the transmembrane potential difference in both of the etch steps, and the applied potential was 1.0 V in both cases. The half reaction occurring at the Pt cathode was the reduction of the dissolved O_2 in the solution.

$$O_2 + 4H+ + 4\,e- \rightarrow 2H_20 \qquad (2\text{-}13)$$

The low (nA-level) currents, and the fact that the solutions were exposed to air during etching, insured that the O_2 was not depleted. The half reaction occurring at the Pt anode was the reverse of Equation 2-15.

Conclusions

In his review of nanowire-based chemical and biosensors, Lieber stresses the importance of being able to reproducibly prepare the nanowire sensing element.[78] The same is true for artificial nanopores to be used as resistive-pulse sensor elements. We have shown here that we can not only reproducibly prepare track-etched based conical nanopore sensor elements, but that we can predict from the experimental parameters used during the second etch, what the diameter of the all-important nanopore tip will be. For these reasons, we believe that the track-etch method will prove to be the technology of choice for taking artificial-nanopore resistive-pulse sensors from the bench top to the practical prototype-device stage of the R&D effort.

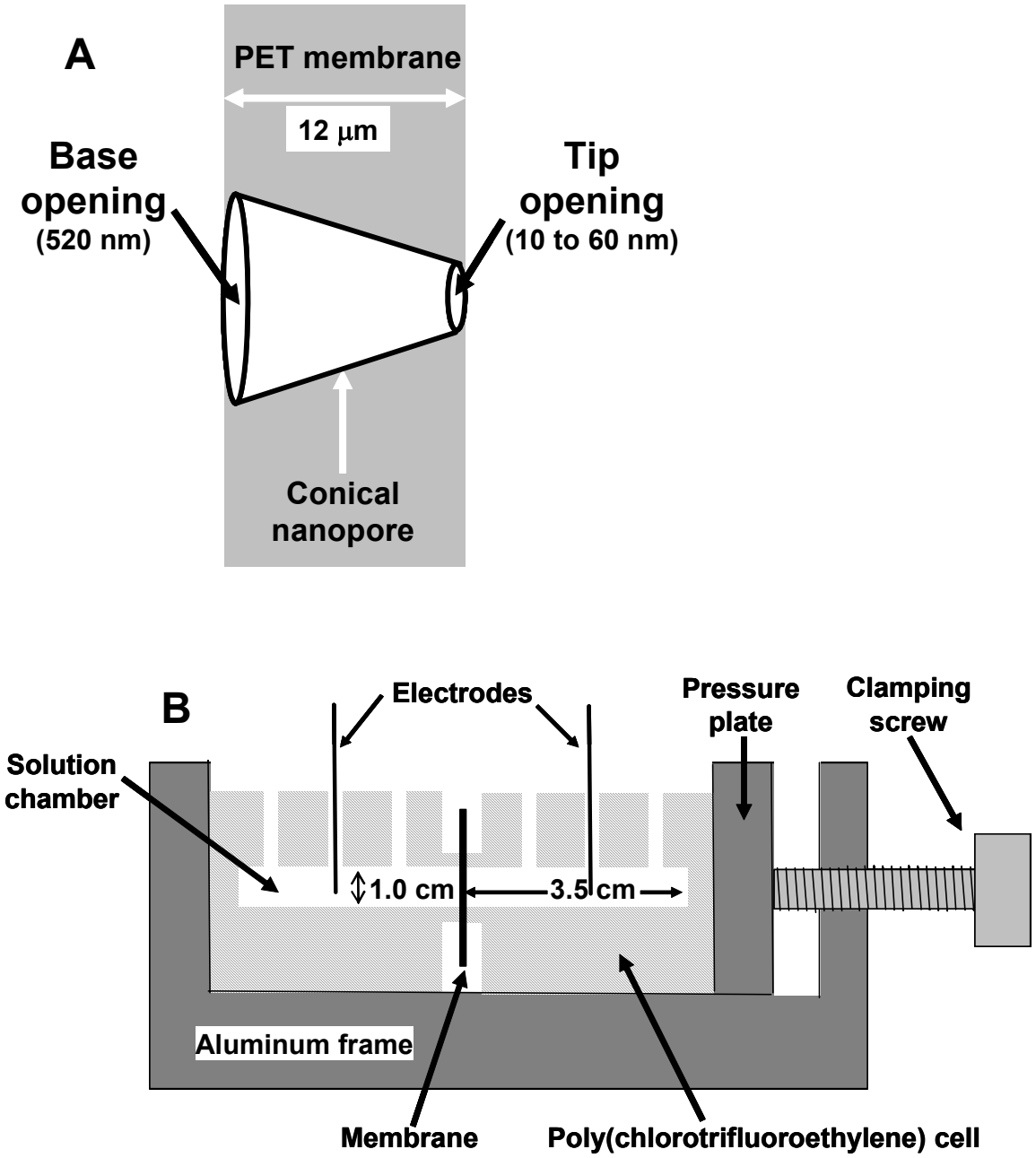

Figure 2-1. Schematic of a conical nanopore sensor element and etching cell. (A) The base diameter and range of tip diameters used in these studies (drawing not to scale). (B) Cell used to do the etching and to make all electrochemical measurements.

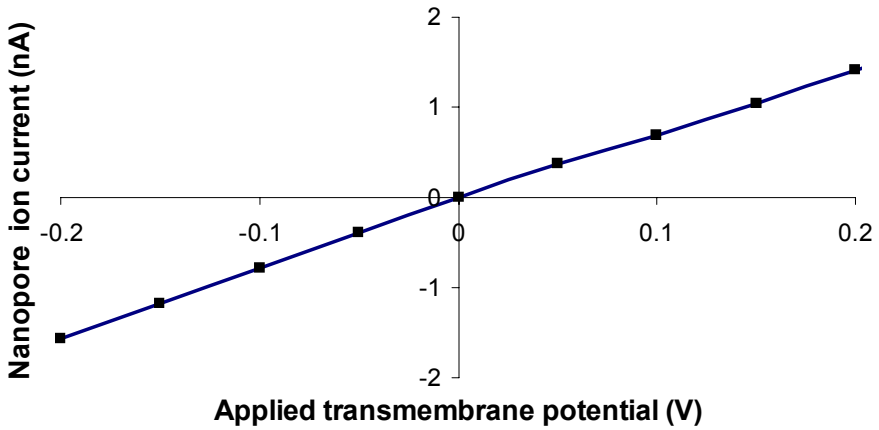

Figure 2-2. A typical current-voltage curve used to measure the tip diameter of the conical nanopore.

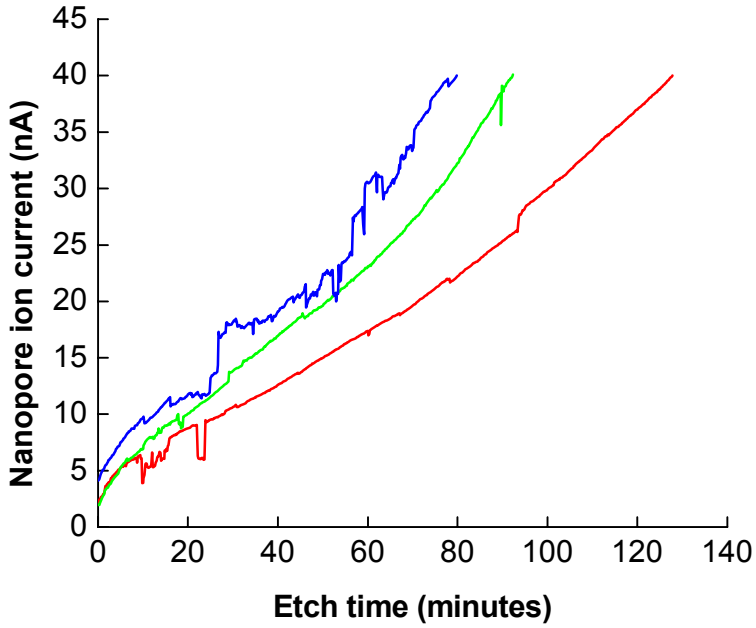

Figure 2-3. Current-time transients obtained during the second etch step for three membranes that were subjected to the same first etch. The second etch was stopped in each case when a final nanopore ion current (I_f) of 40 nA was obtained.

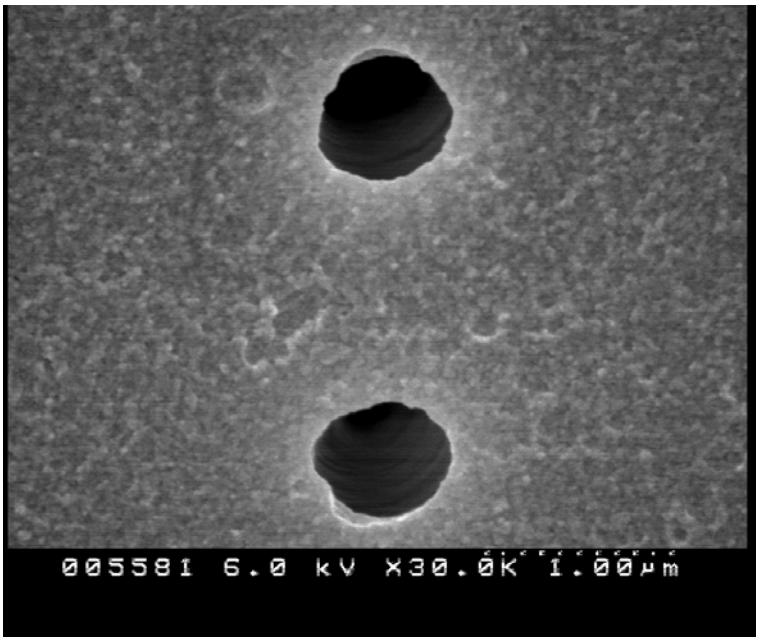

Figure 2-4. Scanning electron micrograph of the base openings of two conical nanopores in a multi-track PET membrane that had been etched (first etch step) as per the single-track membranes used in these studies.

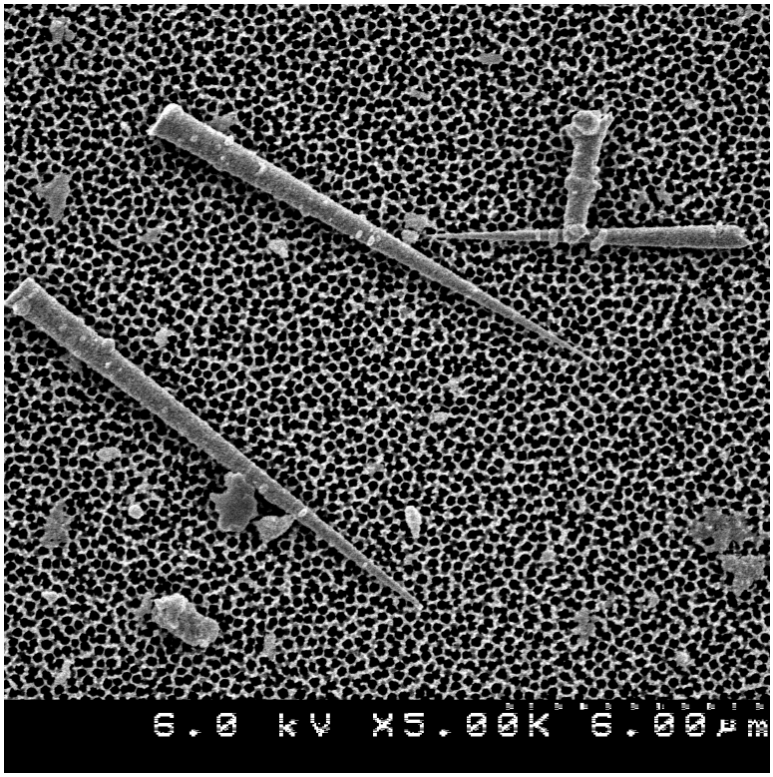

Figure 2-5. Scanning electron micrograph of conical gold nanotubes deposited in a conical nanopore membrane.

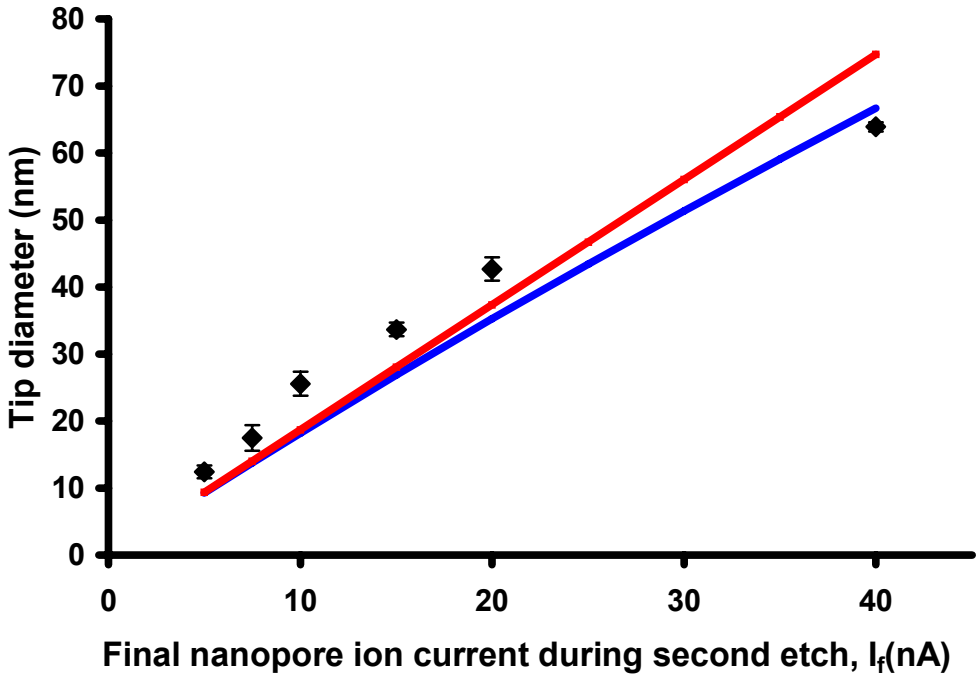

Figure 2-6. Plot of tip diameter measured after the second etch step vs. the final nanopore ion current (I_f) at which the second etch was stopped. The points are the experimentally measured tip diameters. The error bars are measurements on three different membrane samples prepared identically. The solid curves were calculated using the simplified equation (Equation 2-12, red curve) and the exact equation (Equation 2-10, blue curve).

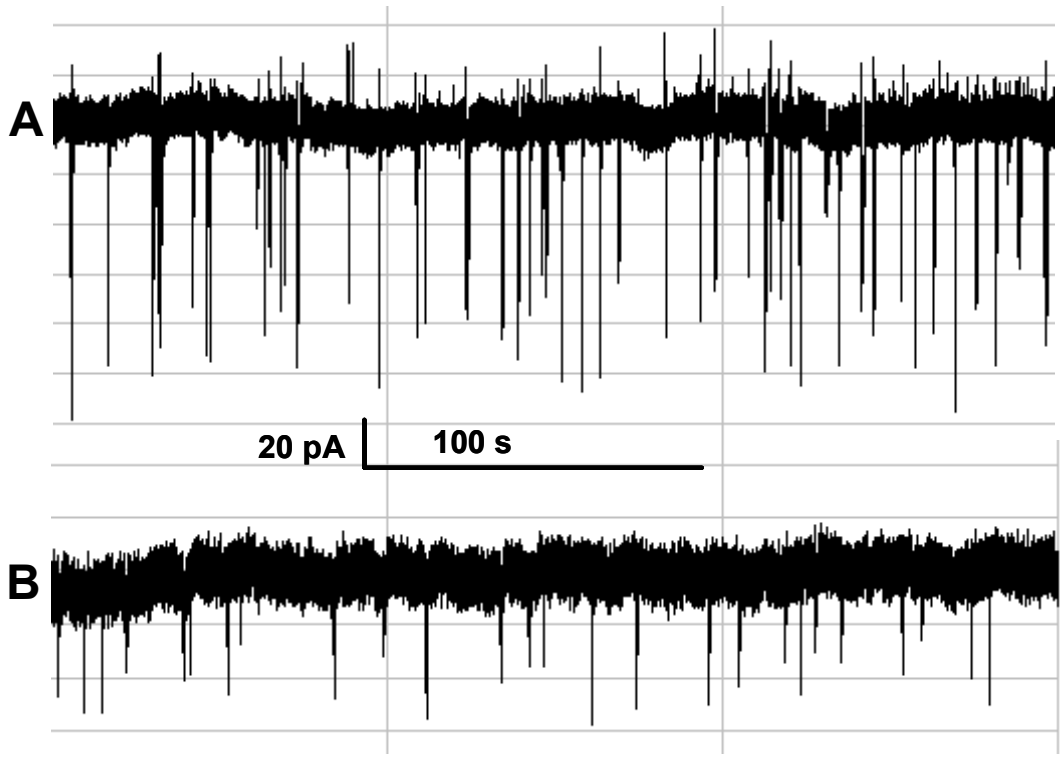

Figure 2-7. Current-pulse data obtained for a prototype protein analyte, bovine serum albumin (BSA) using PEG-modified conical nanotube sensors. (A) Tip diameters of 17 nm and (B) Tip diameters of 27 nm. BSA concentration = 100 nM. Applied transmembrane = 1000 mV.

CHAPTER 3
ETCH-FILL-ETCH METHOD FOR PREPARING TAPERED PORES IN ION TRACKED MICA FILMS

Introduction

The Martin research group and others have been investigating a general method for preparing nanomaterials known as template synthesis.[23, 96] This method entails the synthesis or deposition of a desired material within the pores of a nanopore membrane that serves as a template. These template membranes contain monodisperse pores that are typically cylindrical in geometry, and the pore diameter can be varied at will from tens of nanometers to tens of microns. Since typical pore geometries are cylindrical, correspondingly cylindrical nanostructures are usually synthesized via the template method; depending on the membrane and synthetic method used, these may be solid nanowires or hollow nanotubes. [99]

Recently, our research team and others have become interested in nanopores that have a conical pore shape and the correspondingly conical nanostructures synthesized via the template method within these pores. A number of applications can potentially benefit from conical pore geometry. For instance, it has been shown that such conically shaped nanopores can be used as the sensing element for new types of small molecule, [70] DNA, [75, 98, 100, 101] protein [77] and particle[79] sensors. Conically shaped gold nanotubes deposited within such pores can also act as mimics of voltage gated ion channels. [102] Membranes used for separations might also benefit from a highly asymmetric pore structure. Finally, in addition to sensing and separations platforms, conical nanostructures prepared by more conventional methods have been proposed for use as cathodes in field-emission displays. [103] To date, the vast majority of conical pores have been fabricated using tracked polymers. [81, 89, 93, 95, 97, 104, 105] However, we are interested in exploring materials other than polymers to use as conical pore templates because their different properties may prove potentially superior for certain applications, and other applications might

be realized that are not possible with polymers. One such material of interest is tracked muscovite mica.

Because mica is an inorganic crystalline material, it possesses some properties not present in polymers that might make it superior in some aspects for certain applications. For example, the surface of mica is molecularly flat, [106] and is a good candidate for platform for AFM imaging of DNA, [106] and support layer for lipid bilayers. [107] Also, mica is very chemically resistant and has high thermal and mechanical stability. [22, 108] Mica conical pores might prove much more stable for resistive pulse sensors than polymers. Furthermore, these properties make it possible for template synthesis of materials that require high temperatures. Additionally, nanostructures that demand special geometry that is difficult to obtain by conventional methods may be realized. For instance, tapered-shape carbon structure can provide mechanical stability yet provide very sharp tips, which may be useful for enhanced electron field emission. [109]

We and other have shown that the well-known track-etch method [16] can be used as a starting place for preparing such conical nanopores. [81, 89, 93, 95, 97, 104, 105] This method entails bombarding a thin film (5-20 μm) film of the material with a collimated beam of high-energy particles to create parallel damaged tracks through the film. To make cylindrical pores, the tracked membrane is simply immersed into a chemical etch bath, where preferential etching along the damaged track converts each track into a cylindrical pore. To make conical pores, the tracked membrane is mounted in an etching cell with an etch solution on one side of the tracked membrane and a stop solution on the other side.[81] This is shown schematically in Figure 3-1. Since the damaged track is etched at a longer duration time and faster at the face of the membrane exposed to the etch solution than at the face of the membrane exposed to the stop solution, conically shaped nanopores are obtained.

While this stop-etch approach has been successful in making conical nanopores in a variety of polymer materials, the method fails for the preparation of conical pores in mica membranes. The key impediment is due to the ratio of the track to bulk etching rate. The track etch rate is much faster than the bulk etch rate in mica (about 3000 time faster), [108] so that the etch solution traverses the entire membrane before any significant bulk etching takes place. This means that all parts of the membrane start etching almost at the same time in an isotropic fashion giving rise to uniform pores instead of asymmetrical pore shape. One approach to solve this problem is to replace the tracks of the mica films with a material that is more controllably etched, for instance metal nanowires. In this study, we developed a method to independently control the solution etch rate traversing the membrane, and also the etch rate of the surrounding bulk material, to give asymmetric pores. We prove this by using carbon vapor deposition to replicate the pores, dissolving the membrane to expose the tapered tubes, and imaging the nanotubes using scanning electron microscopy. The results of these investigations are reported here.

Experimental

Materials

Muscovite mica wafers (1.181X 0.0004 inches) were purchased from Spruce Pine Co. USA. Then these bare wafers were irradiated by swift heavy U^{25+} ions of 2.2GeV kinetic energy with fluence of 10^4 to10^7 cm^{-2} (GSI Darmstadt, Germany), which produced damage tracks through the mica membranes. Hydrofluoric acid (HF, 48~51% from ACROS), for etching and dissolving mica membranes, was used as received. Anhydrous tin (II) chloride 98% (Aldrich) and hydrochloric acid (ACROS) were used as received to sensitize the mica membranes for electroless plating. Ammonium hydroxide (Fisher), silver nitrate (Mallinckrodt), potassium sodium tartrate tetrahydrade (Aldrich), and magnesium sulfate (Fisher) were used as received to prepare silver plating solution. Ethylene (30% balanced with Helium, from Praxair) was used as

the CVD carbon precursor gas. Purified water was prepared by passing house-distilled water through a Millipore Milli-Q water purification system.

Initial Etching of Mica Tracks to Prepare Very Small Pores

Mica wafers, containing damaged tracks, were exposed to low concentration HF solution on both faces to create pores of about 10nm in diameter. The wafers were sandwiched between two half cells of a conductivity cell (Figure 3-2.) and 2% HF at 25° C were placed in each half cell for a period of 10 minutes. The etch process was terminated by quickly removing the etch solution and replacing it with water for 2 minutes. Fresh water was replaced several times for two minute intervals. Finally water was allowed to sit in the cell for another two hours.

Preparation of Tin Sensitizing Solution

Tin (II) chloride was used to sensitize the wafers so that electroless plating of silver can take place on the surfaces. Tin (II) chloride crystals (0.5 g) were placed in 100 mL water and stirred to give a cloudy appearance. 2 mL of 10 % hydrochloric acid was added using a pipette causing the mixture to become a clear tin (II) chloride sensitizing solution.

Preparation of Silver Plating Solution

Filling the pores in the wafer with silver wire was done to make a more controllably etched material. A two part electroless silver plating solution was made, where solution *A* contains the silver ions and solution *B* contains a reducing agent. Solution *A* was made by dissolving 45.4 g of silver nitrate to 450 mL of water and then adding ammonium hydroxide drop wise using a pipette until the solution goes from clear to dark brown and returns to clear. Solution *B* was made by dissolving 159 g of potassium sodium tartrate tetrahydrate and 11.4 g magnesium sulfate to 364 mL of water. Both solutions were stored away from light.

Filling the Pores with Silver Wires

The purpose of silver plating the nanopores in the mica membrane was to control the rate at which etch solution traverses the membrane relative to the lateral or bulk etch rate. First, the intended stop side of the membrane was exposed to tin by filling one half cell with the solution. The other half cell was left empty so that one face of the membrane was exposed to air. Tin solution remains in the cell for 45 minutes giving it time to properly wet and sensitize the inner walls of the pores. The membrane was then rinsed with water several times then was left to sit in water for at least one hour. After removal of water from the both half cells, the membrane was now ready for silver electroless plating. A dilute solution *A* (0.5 mL Solution *A* in 45 mL water) was cooled to 4°C and then 0.5 mL of solution *B* was added. This mixture was then placed in the half cell that was not exposed to tin solution (side to be etched). The conductivity cell containing the membrane was placed in a refrigerator, which was set at a temperature of 4°C, for one hour. Following electroless plating of silver, the remaining solution in the cell was removed and the cell was thoroughly rinsed with water. Figure 3-3 shows the schematic outline for this etch-fill-etch method.

Etching Silver Filled Mica to form Tapered Pores

The silver wire-containing mica membrane was exposed to HF/HNO_3 etch solutions on one face. This etch solution of HF (variable concentration) and HNO_3 (10%) etched mica and silver wire respectively at two different rates. After 3 hours the etch solution was removed and rinsed with water several times. The membrane was then left to sit in 10% HNO_3 for at least 3 hours to get rid of any residual silver. Finally, the membrane was rinsed in water several times followed by soaking for at least 3 hours.

Making Replicas of the Tapered Pores

Tapered carbon tubes were obtained using a chemical vapor deposition (CVD) method described in detail previously. [38, 110, 111] A piece of a porous mica membrane (preparation methods were described in the previous section) was placed vertically into a quartz tube (diameter: 4.5 cm, length: 48 cm). This tube was then inserted into a high-temperature tube furnace (Thermolyne 21100) and the furnace was heated to 670^{o}C under Ar flow. Once the temperature stabilized, the Ar gas was replaced with an ethylene gas (20 sccm), which thermally decomposed into carbon on the inner-wall and both faces of the mica template. After a desired deposition time, the heating was terminated, the ethylene gas was replaced by Ar flow, and the furnace was cooled down to room temperature. Unlike our previous CVD procedure with alumina templates, [111] heat pretreatment of the template in this experiment was skipped since the mica membranes we used can withstand temperatures above 900^{o}C without any physical deformation. The yielded carbon thickness can be controlled by varying the duration of deposition.

Preparation of the Carbon Tube Replicas for SEM Imaging

First, CVD carbon/mica membrane was put into 48~51% HF solution for 16 hr to dissolve away the mica template. Next, HF was then removed by pipette, leaving the liberated carbon nanoboxes (connected together by the carbon surface film) which were rinsed with methanol and suspended in methanol. The next preparation procedure entailed the removal of the carbon surface layer on one face of the CVD-treated mica membrane to expose the carbon tubes. This was accomplished by using an oxygen plasma etch procedure. A 1 cm x 1 cm hole was pre-made in one piece of aluminum foil. This hole defines the area of the membrane that is exposed to the oxygen plasma. The entire assembly, with the hole-containing Al foil facing up, was then placed in the center of vacuum chamber of a plasma reactive-ion etching system (Samco, model

RIE-1C). The following etch conditions were used: power = 100 W, O_2 pressure = 300 Pa, O_2 flow rate = 30 sccm. After etching away the carbon surface film (determined by measuring the conductivity of the membrane surface), the membrane was immersed into ~ 48-51 wt % HF solution to dissolve the mica template. This step does not result in free carbon tubes because they are held together by carbon surface film that was not exposed to oxygen plasma. Finally, the sample was rinsed with distilled water and air dried overnight. Sample imaging was conducted using JEOL 6335F field emission scanning electron microscope (FESEM). Prior to FESEM imaging, all samples were sputtered with Au/Pd using the Desk II Cold Sputter instrument (Denton Vacuum, LLC). The sputter current = 45 mA, Ar pressure = 75 mTorr, sputtering time = 60sec. The resulting Au/Pd film was ~ 16 nm.

Results and Discussion

During chemical etching of ion-tracked membranes, the damaged zone of the latent track is transformed into nanopores. [16] The simplest description of the etching process defines two parameters: the bulk etch rate (V_B) and the track etch rate (V_T). V_B depends on the material, etchant composition and temperature. V_T depends on additional parameters, such as sensitivity of the material to tracking, post-irradiation conditions and etching conditions. [14] When the tracked film is exposed to an etchant on one face as described above, the results give conical pores. In most ion-tracked materials, without exposure to extreme conditions (like exposure to high illumination) the V_B/V_T ratio defines the cone angle that is formed. [14] However, in mica V_T is 3000 times faster than V_B, [108] thus producing cone angles (0.02°)[108] that is almost zero, giving essentially pores with almost identical cross-sections along the membrane thickness. To improve the cone angle in polymeric materials, the V_B/V_T ratio is increased by a number of methods including increasing the etchant concentration, [108] applying a high transmembrane potential, [92]

and modifying the etch solution composition. [18] However, none of the above methods can work with mica since V_T is orders of magnitude greater than V_B. [108] To get around this problem, the etched ion tracks in mica was replaced with silver metal that can be independently etched with nitric acid to a wide variety of etch rates. Figure 3-4a is an SEM image of a membrane that was exposed on one face to 20% HF and10% nitric acid solution at 25° C for 3 hrs. Here, HF and HNO_3 solutions etch the bulk mica membrane and the metal track respectively. The base side clearly shows the tapered "cone" shape that resulted from this etch. The decreasing pores size is made quite evident from the progressive mica layers going down into the cone. The opposite face of the membrane (Figure 3-4b) shows the tip to be on the order of a magnitude smaller than the base.

The Martin group has been using conical pores for resistive pulse sensing of molecules. One important feature that make conical pores ideal for sensing is, that most of the resistance is focus in a short distant of the tip. As shown by Lee et al,[79] the electric field in conical pores is focused at the tip. The greater the half cone opening angle, the smaller the focus and hence a sensing zone for molecular translocation of the pore for resistive pulse sensing. Half cone opening angle depends on the V_L/V_T ratio, and we changed the concentration ratio of the etchants to achieve this. Because the concentration ratio of HF (the lateral etchant) to HNO_3 (the track etchant) is greater than used previously, the lateral to track etch rate increases V_L/V_T resulting in greater half cone opening angle (~ 21°). Figure 3-5 is an SEM image of a tapered mica pore that was etched with a higher percentage of HF solution than previously in Figure 3-4. We demonstrate here that the cone angle can be controlled at will, because we can independently control the solution etch rate traversing the membrane, and also the lateral etch rate, to give asymmetric pores. This implies that the effective pore length (the part of the pore where

resistance is focused), and hence the focus of electric field can be varied in these tapered mica pores. This is an important feature for resistive-pulse sensing that is likely responsible for pulse duration.

To indirectly capture the entire geometry of the tapered mica pores in the membrane, a replica was done using CVD method. Figure 3-6 clearly shows SEM images of carbon tapered nanotubes replicas of the mica pores. The angles are well defined and surface of the tube appears rather smooth at the magnification shown.

The half cone opening angle was calculated to be ~ 6°. This is a relatively large cone angle when compared to those of polymers that are etched without any promoters (Lane) or applied high potential (chad). The half cone opening angle can be calculated as

$$\beta = \arctan((d_b - d_t)/2L) \tag{3-1}$$

where L is the length of the pore, d_b and d_t are the large and small openings of the pore, respectively. For $d_b >> d_t$ the equation simplifies to:

$$\beta = \arctan(d_b/2L) \tag{3-2}$$

Figure 3-7 is a low magnification image of the carbon replicas of mica tapered pores indicating that we can indeed reproduce the tapered geometry mica pore uniformly.

Conclusion

This study described a method to make asymmetric pores in tracked muscovite mica films using an etch-fill-etch approach. Tracks in the films were initially etched away with hydrofluoric acid to form nanoporous membranes. We demonstrated that by controlling the concentration ratio of hydrofluoric acid to nitric acid during etching, tapered pores with diamond shaped cross-section can be obtained. Additionally, we have shown that the cone angle of the pores can be controlled be changing the concentration ratio of the bulk and metal etch solutions.

Replicas of the asymmetric pores were accomplished by carbon vapor deposition, and scanning electron microscopy was used to give evidence of the resulting nanotubes. These conical mica pores make prove more stable for resistive pulse sensing. Because it is so easy to tailor the cone angle, this might make these mica pores more suitable sensing devises. One potential capability that might be realized in resistive pulse sensing, is the tuning of the cone angle to control pulse duration.

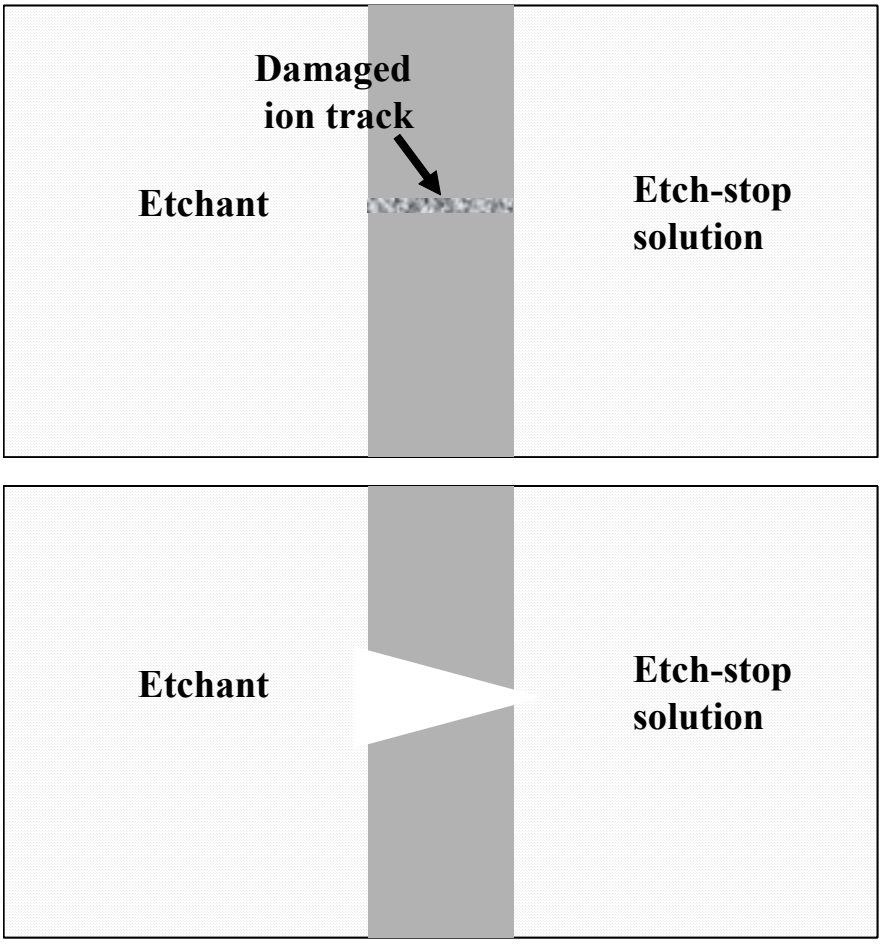

Figure 3-1. After irradiation, the materials are subject to chemical etching which preferentially removes the damaged ion track

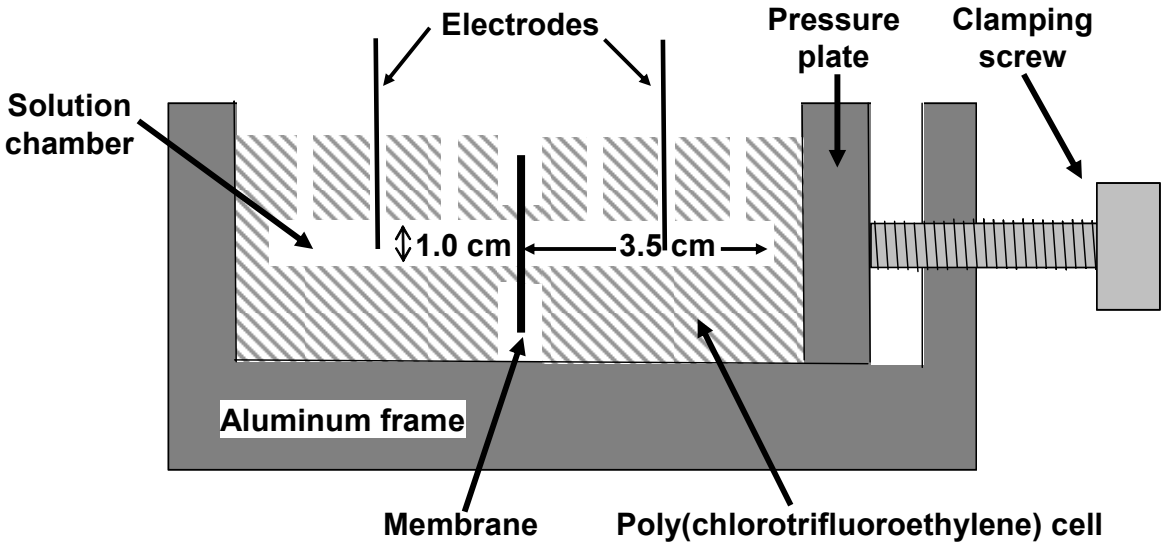

Figure 3-2. Schematic of cell used to do the etching and to make all electrochemical measurements.

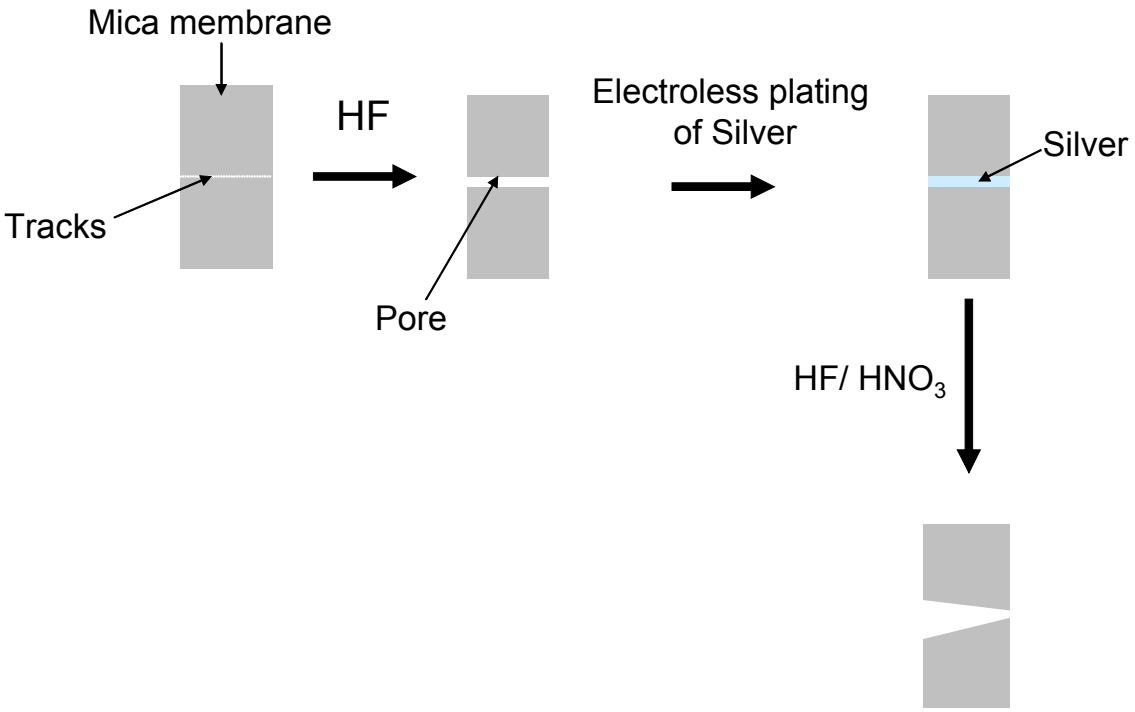

Figure 3-3. Schematic diagram of etch-fill-etch method

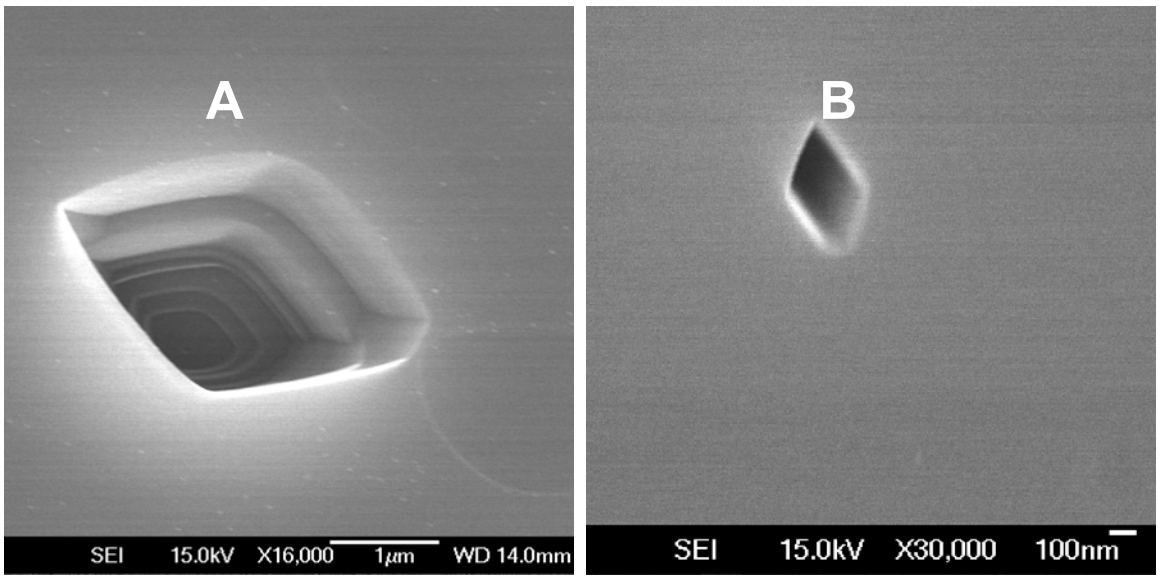

Figure 3-4. Scanning electron micrographs of mica membrane that was exposed on one face to 20% HF and10% nitric acid solution at 25°C for 3 hrs. (A) Side exposed to the etchant (the base). (B) Side exposed to water (the tip).

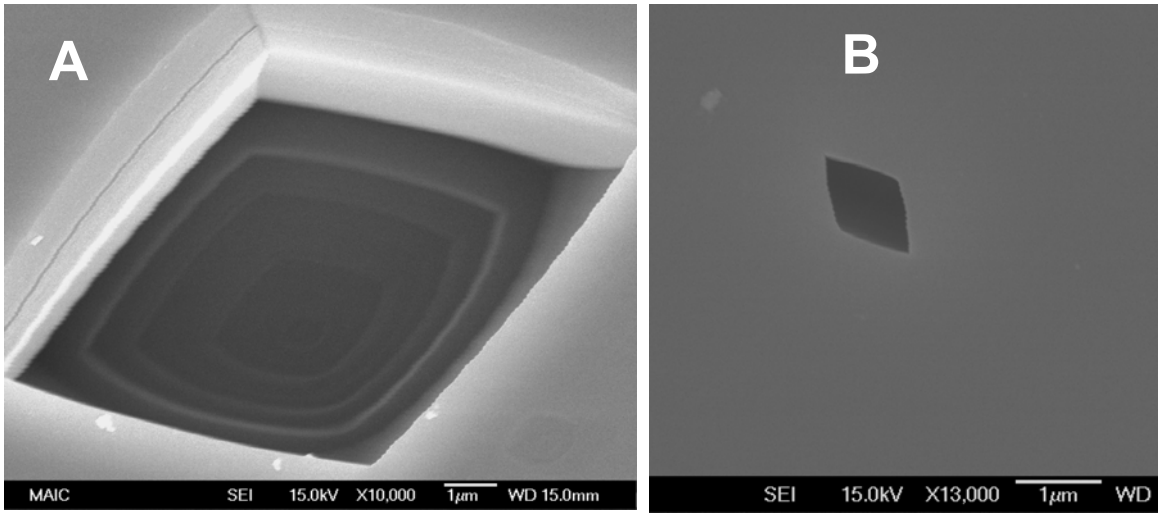

Figure 3-5. Scanning electron micrographs of mica membrane that was exposed on one face to 40% HF and10% nitric acid solution at 25°C for 3 hrs. (A) Side exposed to the etchant (the base). (B) Side exposed to water (the tip).

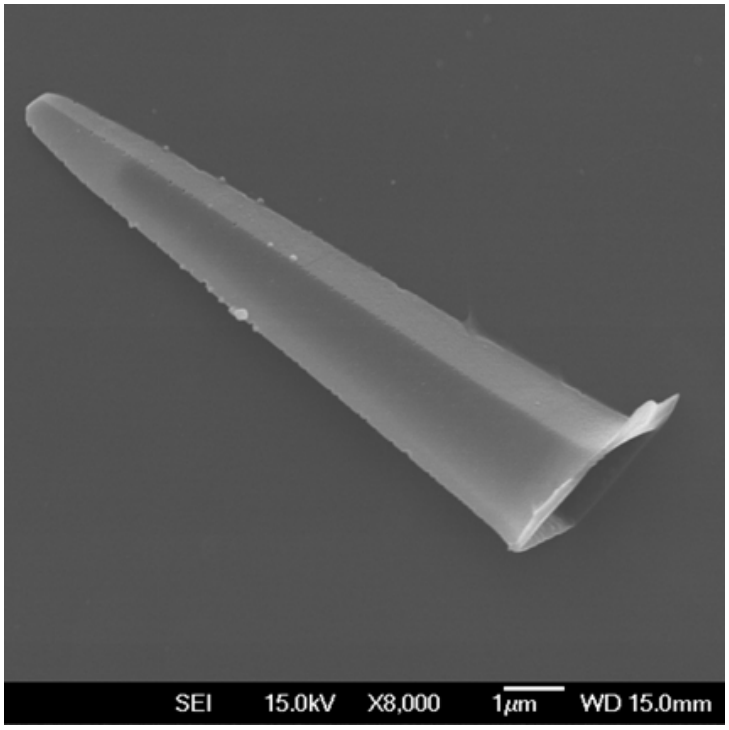

Figure 3-6. Scanning electron micrograph of carbon tapered nanotube replica of the mica tapered pore.

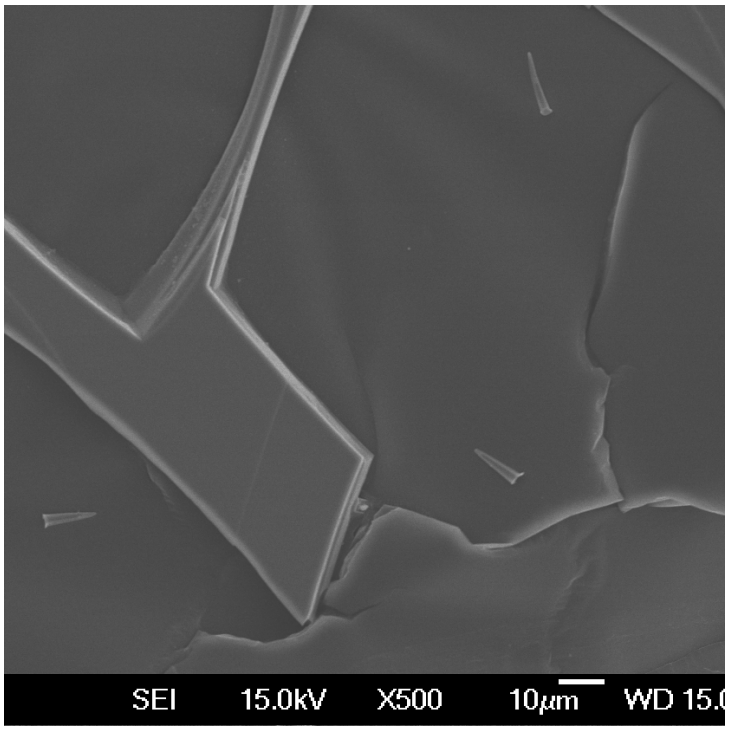

Figure 3-7. Low magnification SEM images of carbon tapered nanotube replicas of the mica tapered pore.

CHAPTER 4
ELECTROLESS AU PLATING OF TRACK-ETCHED KAPTON POLYIMIDE NANOPOROUS MEMBRANES

Introduction

Track-etched polymer membranes have found many applications in industry and research as filtration and separation materials. [6] Chemical modification of the inner walls of these membranes has made them more selective and sophisticated separation structures. [27, 28, 31] These chemical modifications have been made possible by first plating the inner walls of the pores of these membranes with gold, [23] then attaching a desired thiol terminated functional group. [31] For reproducible results of any analytical measurements done using the pores of these nanoporous membranes, it is crucial that the pores remain stable and have a well define internal diameter, particularly where the pore approaches the size of the analyte molecule. One of the problems faced when using some polymers such as polycarbonate (PC) and poly (ethylene terephthalate) (PET) membranes, is that very small pores tend to temporarily block during ion transport mesurement. [112] Another disadvantage discovered when using these membranes to measure ion current, is that possible dangling alkyl groups [113] render the pores from been well define and thus gives inconsistent results and lots of noise in the current measurement. [112] The polyimide Kapton on the other hand does not exhibit these disadvantages. [112]

Due to its abilities of maintaining excellent physical, electrical and mechanical properties at both low and high temperature extremes, Kapton is a very attractive polymer for use as a particle track-etch membrane for application in separation and filtration in industry and research. [16, 114, 115] It will be advantageous therefore, if like polycarbonate and PET, Kapton can similarly be electrolessly plated with gold to tailor pore diameter and, further, be modified with desired thiol terminated functional groups for selective separation.

The objective of this study was to determine if the polyimide Kapton, a very chemically resistant and stable polymer, can be electrolessly gold plated with similar or better quality compared to PC porous membranes. Additionally, investigate whether plating can be controlled-that is, tailor pore diameter of the membrane with plating time. It is interesting to note that to date; there is no known report of electroless plating of Kapton membranes.

Experimental

Materials

Kapton 50 HN foils (12.5 μm thick, 10^7 tracks per cm^2) were obtained from the linear accelerator laboratory UNILAC at the GSI (Darmstadt, Germany). Boric Acid was obtained from Fisher and used as received. NaOCl (13% active Cl), KI, $SnCl_2$, $AgNO_3$, $NaHCO_3$, were obtained from Aldrich and used as received. Trifluoroacetic acid, Na_2SO_3, NH4OH, formaldehyde and methanol were obtained from Mallinckrodt and used as received. Commercial gold-plating solution (Oromerse SO Part B) was obtained from Technic Inc. Milli Q water was used to prepare all solutions and to rinse the membranes.

Chemical Etching

Cylindrical pores were etched in the tracks of the Kapton foils using sodium hypochlorite solution as describes in detail elsewhere. [116] The shape and size of the pores can be tailored by the choice of etchant and the etching conditions. [116] To obtain cylindrical pores the etching rate along the track, the-so called track etch rate V_t has to be much faster than the non-specific etching of the polymer called the bulk etched rate V_b. [14, 81] The relation between V_t and V_b is explained in figure 4-1. [14, 81] Studies have shown that an efficient etching can be performed in sodium hypochlorite containing 13% active chlorine content. [116] Furthermore, it has been demonstrated that the shape of the pore can be regulated with an appropriate choice of pH. [116] When sodium hypochlorite is not buffered its pH ~ 12.6. At these conditions, and elevated

temperature of 50ºC, V_b of Kapton is high (~ 0.21 (μm / h) and the pores become strongly conical. Buffering the etchant with boric acid to pH ~9 enables one to obtain cylindrical pores. It is important to note that the etching works only at basic pH when the hydrolysis of imide bonds by OH^- is possible. The membrane was immersed in a Teflon container containing 400 ml of NaOCl solution at pH 9.8 and temperature of 50ºC. First, the container with the etchant solution is brought to 50ºC by placing it in a water bath controled by a water heater. The size of the pores increases with etching time. After etching, the membrane was rinsed with D. I. water and left to soak for two hours. The membrane was allowed to dry in air overnight.

Electroless Plating of Kapton

In order to better control the size and surface chemistry of Kapton, the membranes can be plated electrolessly with gold. [10] Tailoring of the pore size in polymer membranes by the time of performing the electroless plating with gold has been demonstrated previously. [28, 51] Since Kapton membranes possess carboxylate groups made available via imide hydrolysis by the etchant, it is expected that these would act as active sites for the bonding of tin (Π). Tin can then reduce silver ion which later acts as a nucleation site for the reduction of gold. The procedure followed the recipe for the electroless plating of polycarbonate. [28, 51]

Pore Diameter Measurement

Cylindrical pores were characterized by taking scanning electron microscopy (SEM) images of the membrane surfaces. Also, we have chosen to use an electrochemical technique based on measuring ion current to measure pore diameter. This entailed mounting the membrane sample in the cell (Figure 4-2), filling both half cells with an electrolyte solution of known ionic conductivity, and obtaining a current-voltage (I-V) curve associated with ion-transport through the nanopore. The experimental slope of this linear I-V curve is the ionic conductance, G, (in Siemens, S) of the nanopore, which is given by

$$G = (N A \sigma_{KCl} \pi d^2) / 4 L \quad (4\text{-}1)$$

where N is the pore density, A is the membrane area, σ_{KCl} is the experimentally measured conductivity of the KCl-based electrolyte used (S cm^{-1}), L is the length of the nanopore (membrane thickness), d is the pore diameter. Because all of the other parameters in Equation 4-1 are known, d can be calculated.

Results and Discussion

SEM and Ion Current Measurements

Figure 4-3 shows SEM images of Kapton porous membranes before and after electroless gold plating. Here we see that the pore diameter decreases with plating time. Figure 4-4 shows a plot of pore diameter as a function of Au plating time from 0 to 12 hours. The two methods of measuring pore diameter gave very similar results. This is important because only resistance measurements can be used for small pore diameter that cannot be resolved by SEM. This data indicate that one can tailor the pore diameter with plating time down to the nanometer scale. This capability is important for different transport studies and in sensor research where the size of the pore with respect to the analyte is important. [10, 28, 77, 96]

Atomic Force Microscope Images

Figure 4-5 shows the atomic force microscope images of the Kapton membranes before and after electroless plating. The membranes remain relatively smooth after gold plating compared to a similarly porous structured polycarbonate membrane after plating with gold.

Conclusion

Electroless gold plating properties on the surface and pore walls of track-etched Kapton polyimide nanoporous membranes were studied. SEM, AFM, and ion current measurements were used to characterize the surfaces and pore dimensions of the membrane. Nanoporous Kapton polyimide membranes were electroless gold plated over different times and the pore

diameter characterized using SEM. Ion current measurements were used to measure the diameter of very small pores. AFM images show that after electroless gold plating, the gold surface layers are smooth compared to a similarly structured polycarbonate membrane. Electroless plating the membranes for 12 hours produced Au wires in the pores. Etching away the membrane with sodium hypochlorite to expose gold tube replicas revealed that the plating in the walls is also smooth.

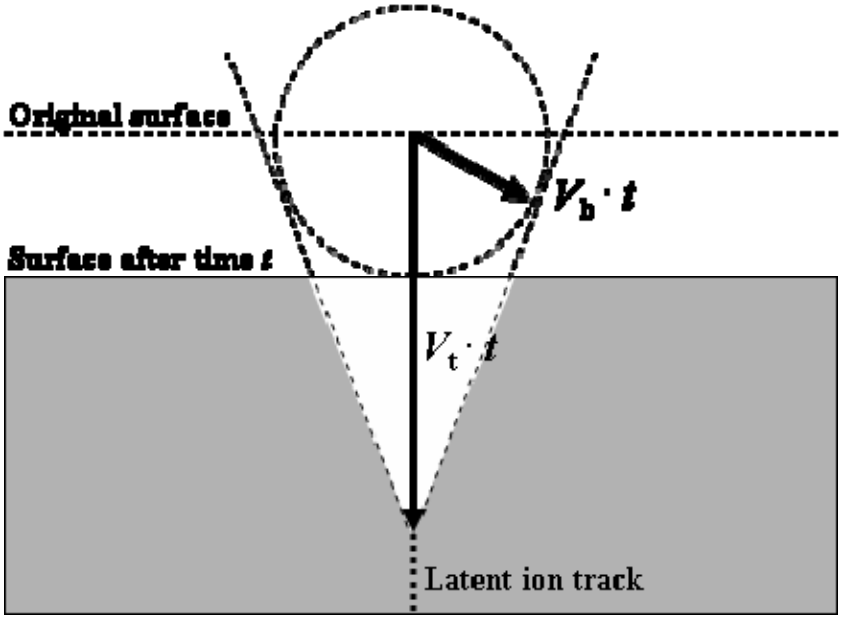

Figure 4-1. Definition of bulk etch rate V_b and track etch rate V_t.[Adapted from Apel, P. *Radiation Measurements* **2001**, *34*, 559-566.]

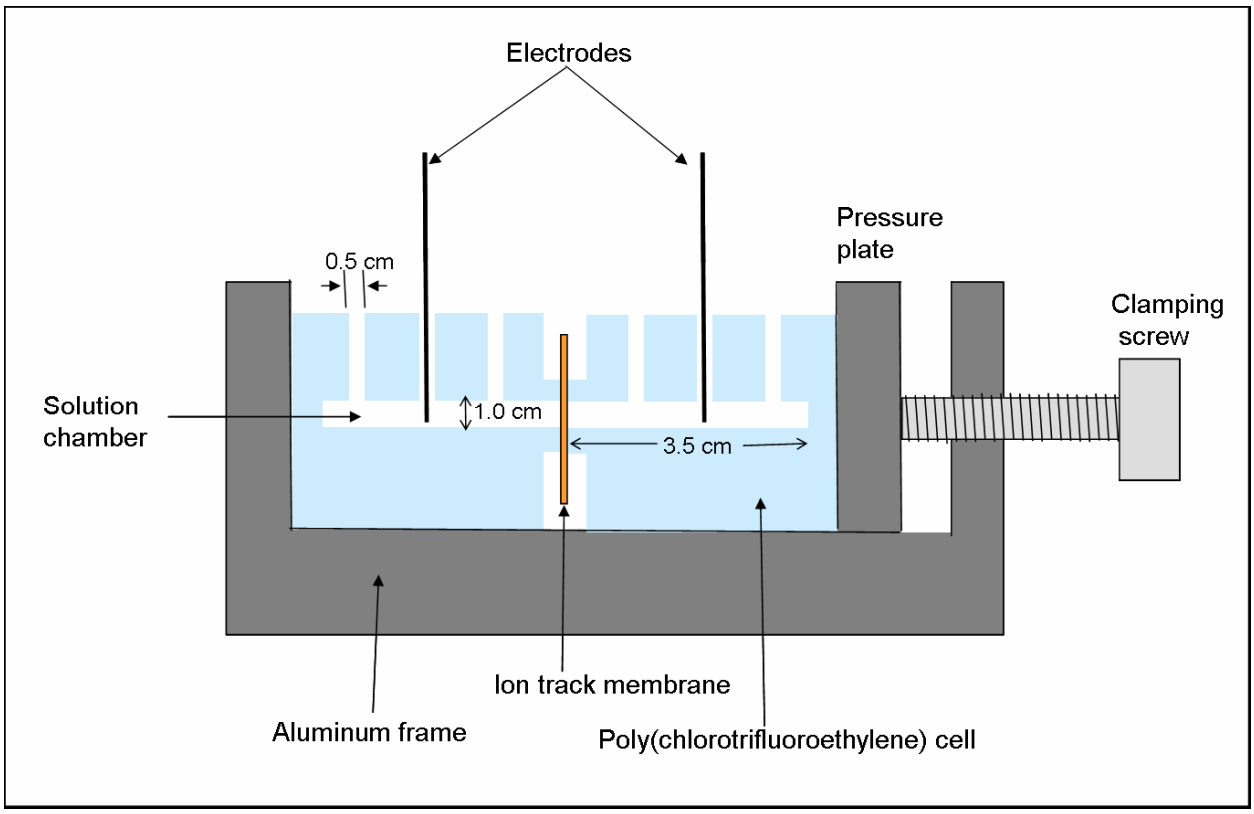

Figure 4-2. Schematic of cell used for electrochemical measurements.

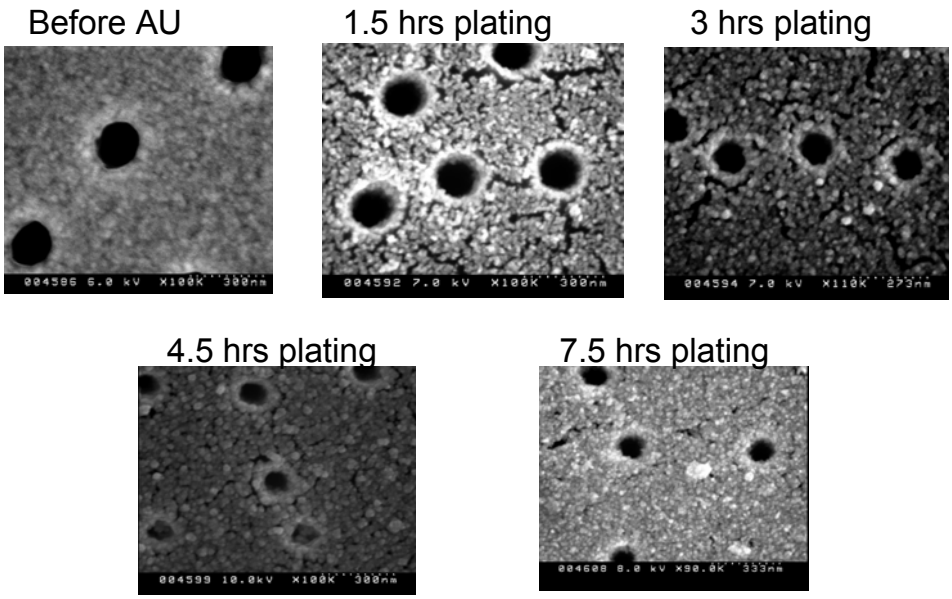

Figure 4-3. Pore diameters for different Au plating times.

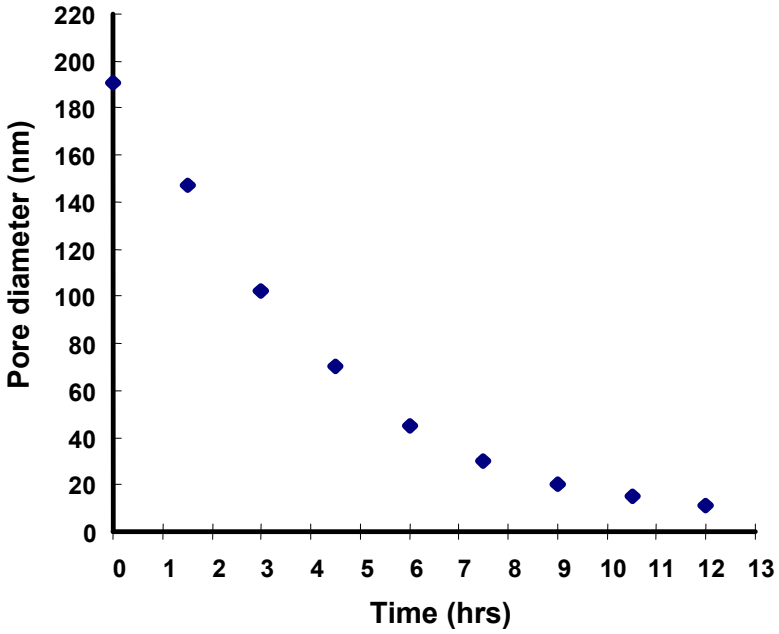

Figure 4-4. Pore diameter as a function of plating time with measurements taken from SEM image (0-7.5 hrs) and ion current resistance measurements (8-12 hrs).

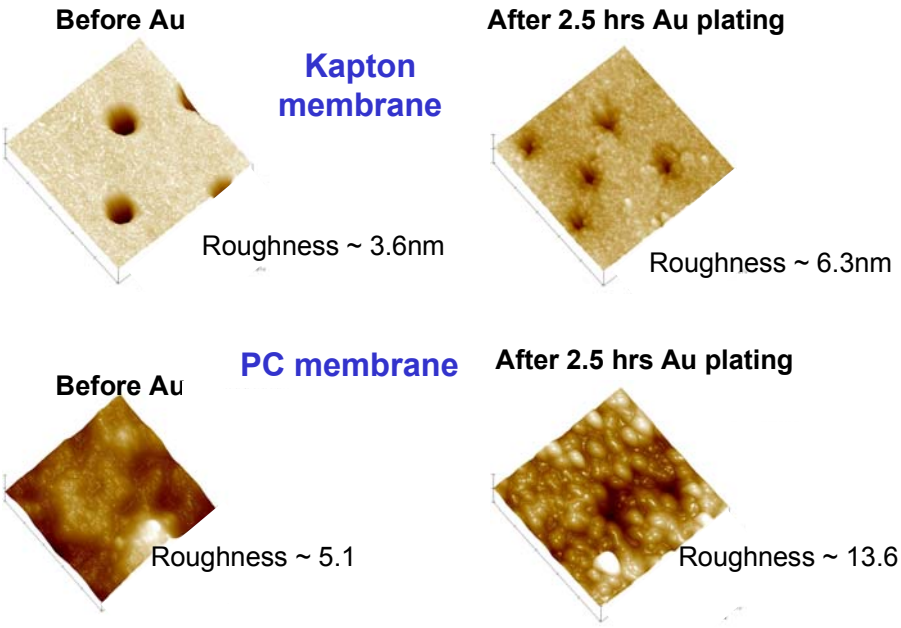

Figure 4-5. Atomic Force micrographs of Kapton and PC membranes before and after electroless Au plating

CHAPTER 5
ASYMMETRY IN DIFFUSIONAL TRANSPORT OF MOLECULES THROUGH KAPTON CONICAL NANOPORES

Introduction

Membranes and porous materials have found various applications in filtration and separation processes. [8-10] Modern biotechnology has posed new challenges in the application of such membranes, and requires pores with diameters similar to those of molecules under study [11] (e.g., as small as several nanometers). The nanometer scale of such pores is necessary in both achieving optimal control of the flow of biomolecules, as well as in developing sensors for their detection. The transport properties of such nanometer scale pores are not well understood yet. The hint that nanopores behave differently from micropores, comes from Mother Nature. [12] Biological channels and pores have diameter of ~ 1 nm and are critical for functioning of living organisms. Ion channels and pores exhibit transport properties not observed with larger pores, for example (i) selectivity for ions or molecules, (ii) rectification of ion current[117] (iii) ion current for constant voltages applied across the membrane[118] (iv) facilitated transport of molecules (v) transport of ions and molecules against their electro-chemical potential gradient. [119]

It has recently been demonstrated that asymmetric conical nanopores in polymer films can exhibit transport and rectification properties similar to biochannels. For example, conical nanopores in PET and Kapton membranes are cation selective and rectify ion current with a preferential direction of cation flow from the tip to the base of the cone. [81, 88, 105, 120, 121] However, unlike the above cases, in this investigation there is no applied transmembrane potential. Also, there are no electrostatic or binding interactions of the molecule with the pore surface. Since the molecule under study is neutral, transport through the membrane is by purely diffusional and geometrical constraints. Yet we found in our studies that the diffusion of molecules across these membranes, exhibit a rectification behaviour. It means that there was a

preferential direction of diffusion flow. This effect cannot be predicted by considering classical diffusion with constant diffusion coefficients. The rectification of conical nanopores is of tremendous significance for industrial filtration processes in which asymmetric membranes are often applied. One type of asymmetric membranes used in industry consists of a thin 'skin' of nanoporous material placed on a low resistance support, which assures high fluxes and good size separation. [122] Finding an optimal direction of concentration gradient will improve the filtration process. Asymmetric diffusion has been observed before with multi-membrane systems and membranes with two skins on two membrane faces of a membrane support. [123]

Diffusional Transport Described by Fick's Laws

Diffusional transport is described by Fick's two diffusion laws. For diffusion in one dimension, Fick's first law of diffusion describes the flux (the net number of moles of particles crossing per unit time, *t,* through a unit area perpendicular to the x-axis and located at *x*), stating that the flux of a molecule with diffusion coefficient, *D*, is directly proportional to the concentration gradient.

$$J(x,t) = -D\frac{\partial c(x,t)}{\partial x} \tag{5-1}$$

D normally is assumed constant, however there are known examples when *D* depends on position *x*, concentration *c* or even time *t*. [124, 125] The diffusion coefficient determines the time it takes a solute to diffuse a given distance in a medium. The diffusion coefficient depends on the physical characteristics of the solute as well as those of the medium. An approximate bulk diffusion coefficient (like that of molecules of similar masses) was used here, because, we are more concerned about emphasizing the preferential flux from one side of the membrane than the absolute flux values, themselves. The second of Fick's law expresses how the concentration of

the species depends on time. Here again, the general form of the law in one dimension, taking into account the possible forms of D is as follows:

$$\frac{\partial c}{\partial t} = \frac{\partial}{\partial x}\left(D \frac{\partial c}{\partial x} \right) \tag{5-2}$$

Hindered Diffusion in Cylindrical Pores

The effective diffusion coefficient of a solute within a pore of comparable size is lower than that of the bulk solution value. This phenomenon is called hindered diffusion and results from steric exclusion of the solute at pore opening and hydrodynamic or wall drag resistance due to the presence of the pore wall. For steady-state diffusion through a membrane with cylindrical pores that are comparable to the size of an uncharged solute, the effective diffusion coefficient can be expressed in terms of the solute-to-pore size ratio $\lambda (= a/r)$ by the Renking equation: [126, 127]

$$D / D_{\infty} \approx (1-\lambda)^2 (1 - 2.1044\lambda + 2.089\lambda^3 + 0.948\lambda^5) . \tag{5-3}$$

Here, restriction to diffusion due to steric hindrance at the entrance to the pores is given by the partition coefficient,

$$\Phi = (1-\lambda)^2 . \tag{5-4}$$

As established by Ferry,[128] a molecule must pass through the opening without striking the edge. Therefore the center of the solute particle cannot be located at a radius that exceeds (*r*-*a*) (Figure 5-1). The partition coefficient therefore, is equivalent to the fraction of the cross-sectional area of the pore that is accessible to the center of the molecule.

The second factor in the Renking equation, called the inverse enhanced drag,[127]

$$\mathrm{K}^{-1} = (1 - 2.1044\lambda + 2.089\lambda^3 + 0.948\lambda^5) \tag{5-5}$$

corrects for hydrodynamic or wall drag resistance, which is the friction between a molecule moving within a pore and its walls (Figure 5-2).

The total flux, J, through a membrane with cylindrical pores of length, L, and pore density, N, can then be given as:

$$J = \frac{\mathrm{N}\pi r^2 \Phi\ \mathrm{K}^{-1} D_\infty \Delta C}{L} \tag{5-6}$$

where D_∞ is the free diffusion coefficient of the solute in the bulk solution, ΔC is the concentration difference across the membrane, and $\mathrm{N}\pi r^2$ is the membrane porosity, ε.

Hindered Diffusion in Conical Pores

Equation 5-6 is for a membrane with cylindrical pores where r is constant. The pores used for this study are conical, and therefore r increases or decreases from one end of the membrane to the other, thus varying linearly with position. The porosity of conical pores is different from that of cylindrical pores, and is obtained by the product of the pore density and the geometric mean cross-sectional pore area:

$$\varepsilon = \frac{\mathrm{N}\pi d_b d_t}{4} \tag{5-7}$$

where d_b and d_t are the diameters of the large and small opening of the pores respectively. There are varying hindrance effects (steric and hydrodynamic) on diffusion over the length of the membrane. The average inverse enhanced drag, K^{-1}, is ~ 1 for conical pores because most of the wall drag resistance occurs in the region of the tip, which is a very small faction of the pore. For cylindrical pores, the partition coefficient determines the rate of entry of the molecules into the pores, and is equal to the ratio of the solute concentration in the pore to that of the bulk solution at equilibrium. However, unlike cylindrical pores, the partition coefficient that determines molecular entry into conical pores at steady state diffusion is not the same as the equilibrium partition coefficient. The partition coefficient, $\Phi(r(x))$, varies with r; which is a function of position, x, and therefore changes along the length of the pores. Hence it is expected that the

equilibrium concentration along a pore length is different. However, the partition coefficient and also the enhanced inverse drag within the pore, averages to be of negligible contribution to the flux since only a very small fraction of the pore approaches the size of the solute molecule. The value of these coefficients therefore approximates to 1. The asymmetry in diffusion, then, may be caused by the difference in steric hindrance at the entrance of either side of the pore. This will determine the amount of molecules that enter and leave the pore per unit time. The above arguments suggest that molecules entering from the large opening of a conical pore will have greater flux than those that enter from the smaller opening, provided that they can leave at the same rate. The limit to diffusion will be the partition coefficient at the tip. With these assumptions, the fluxes can be written for dilute solute concentrations as

$$J_b = \frac{\varepsilon\, \Phi_b\, \mathrm{K}^{-1}\, D_\infty\, \Delta C}{L} \tag{5-8}$$

$$J_t = \frac{\varepsilon\, \Phi_t\, \mathrm{K}^{-1}\, D_\infty\, \Delta C}{L} \tag{5-9}$$

where the subscripts *b* and *t* represents the directions of the net flux entering the large and small opening of the pores respectively, and K^{-1} is equal to 1.

We can also solve the diffusion problem with a constant *D*, through a conical nanopore with opening angle α, openings d_t and d_b, with solute concentraton c_0 at the tip, and zero concentration of solute at the base:

$$c(x) = c_0 \frac{d_t}{d_b}\left(\frac{L}{x} - 1\right),\ d_t \cdot \cot\alpha \le x \le L \tag{5-10}$$

valid for $d_t << d_b$.[129]

The diffusion problem with solute placed at the base side has the following form:

$$c(x) = c_0\left(1 - \frac{d_t}{d_b}\frac{L}{x}\right),\ d_t \cdot \cot\alpha \le x \le L \qquad (5\text{-}11)$$

When we calculate the fluxes (moles/s) in the two above mentioned conditions they are equal to each other:

$$j = D\frac{c_0 d_t}{d_b}\pi L \qquad (5\text{-}12)$$

These calculations indicated that 'classical' diffusion with constant D cannot describe our experiments, unless one takes into account the difference in boundary conditions due to the difference in the partition coefficient.

It was the purpose of this study to investigate the diffusion of neutral molecules from both ends of conical pores of the polyimide Kapton. Here the dimension of the tip of the conical pores approaches that of the molecules. To this end the diffusion of the water soluble neutral molecule phthalazine was studied.

Experimental

Materials

Kapton 50 HN foils (12.5 μm thick, 107 tracks cm^{-2}) were obtained from the linear accelerator laboratory UNILAC at the GSI (Darmstadt, Germany). Sodium hypochlorite (NaOCl, 13% active Cl) and potassium iodide (KI), were obtained from Aldrich and used as received. Phthalazine, sodium chloride, sodium phosphate dibasic, sodium phosphate monobasic, sodium azide was obtained from Fisher and used as received. Milli Q water was used to prepare all solutions and to rinse the membranes.

Kapton Polyimide Membrane

We used polyimide foils to prepare nanoporous membranes. Polyimide possesses a unique combination of properties that are ideal for a variety of applications in many different fields. The film maintains excellent physical, electrical, and mechanical properties over a wide temperature range. Polyimide also has very good chemical resistance and does not dissolve in organic solvents. We used 12.5 μm thick commercially available Kapton 50 HN, produced by DuPont.

Irradiation-Track Formation

For the preparation of membranes we used the-so called track etching technique. It is based on irradiating a dielectric film with swift heavy ions and subsequent chemical development (etching) of the damaged ion tracks. A unique feature of heavy ion irradiation is single-particle recording. That is to say, one swift heavy ion which penetrates the foil produces one damaged track. Therefore, counting the number of ions used for irradiation enables one to prepare membranes with tailored number of pores from the range 1 up to 10^{10} ions/cm^2. Kapton foils, which we used for these experiments, were irradiated with uranium ions of energy of 11.4 MeV/u, at the heavy ion accelerator UNILAC at the Institute for Heavy Ions Research, (GSI) Darmstadt, Germany. We used foils irradiated with the fluencies 10^7 and 10^8 ions/cm^2. The range of the ions is in all cases larger than the thickness of the polyimide membranes. The ions penetrate the membranes at normal incidence, creating damaged tracks, which is then followed by chemical etching to form pores (Figure 5-3).

Chemical Etching of Membrane Tracks

After irradiation of the Kapton foil with heavy ions, the latent tracks have to be chemically etched. The shape and size of the pores can be tailored by the choice of etchant and the etching conditions. To obtain cylindrical pores the etching rate along the track, the-so called track etch

rate V_t has to be much faster than the non-specific etching of the polymer called the bulk etched rate V_b. The relation between V_t and V_b is explained in Figure 5-4.

To obtain conical pores, one needs to choose etching conditions which assure high v_b. Preparation of conical pores is normally performed in a conductivity cell with etchant placed only on one side of the membrane. The other side of the membrane is in contact with a stopping medium, which neutralizes the etchant as soon as the pore is etched through. For example, if NaOH is used as an etchant, we use an acidic stopping medium. The chemical stopping is further supported by an electric stopping. The etching is performed under voltage with electrodes arranged in such a fashion that the anode is on the side of etchant, which retracts ions active in the etching process (e.g. OH^-) out from the pore (Figure5-5).

Etching with an applied voltage and measuring electric current affords a method to monitor the process. At the beginning of etching the current is zero, because the two chambers of the conductivity cell are not connected with one another. When the pore is etched through, the current value is finite and increases in time, indicating an increase of the pore diameter (Figure 5-6). Kapton is very resistant chemically, therefore, development of latent tracks has to be performed by a very aggressive etchant and at elevated temperatures. Previous studies have shown that an efficient etching can be performed in sodium hypochlorite containing 13% active chlorine content. Furthermore, it has been demonstrated that the shape of the pore can be regulated with an appropriate choice of pH. When sodium hypochlorite is not buffered its pH ~ 12.6. At these conditions, and elevated temperature of 50ºC, V_b of Kapton is high (~ 0.42 (μm / h) and the pores become strongly conical. Buffering the etchant with boric acid to pH ~9 enables one to obtain cylindrical pores. It is important to note that the etching works only at basic pH when the hydrolysis of imide bonds by OH^- is possible.

To obtain conical pores in Kapton, the irradiated samples were placed between two chambers of a conductivity cell and etched from one side in sodium hypochlorite. The other half of the cell is filled with 1 M potassium iodide (KI) solution as a stopping medium for the OCl^- ions of the etchant. As soon as the etchant completely penetrates the membrane, iodide ions reduce OCl^- to Cl^- ions: [112, 130]

$$OCl^- + 2H^+ + 2I^- \rightarrow I_2 + Cl^- + H_2O \qquad 5\text{-}13$$

Via this reaction, the etching process stops immediately after the breakthrough, allowing the preparation of extremely narrow pores.

Pore Diameter Measurement

SEM was used to characterize the opening diameters of conical pores, especially the big opening, which we call the 'base' (Figure 5-7). The small opening of conical pores, called the 'tip' is below resolution of SEM, therefore, we have to use another technique for its size estimation. We have chosen to use an electrochemical technique based on measuring ion current. The ionic conductance of a conical pore is related to its diameter by the following equation:

$$G = \frac{n \sigma \pi d_b d_t}{4L} \qquad 5\text{-}14$$

where n is the number of pores, σ is the conductivity of electrolyte, L is the length of the pore (or the equivalent membrane thickness), and d_b and d_t are the diameters at the base and tip of the cone respectively.

Transport Measurement

Measurements of neutral molecular transport through conical nanopores were performed using UV-Vis spectrometry (Agilent 8453). A U-cell set-up contained the permeate molecule solution on one side and a buffer, in our case PBS (in which the permeate was prepared) on the other side of the cell (Figure 5-8). The membrane was sandwiched between two transparent

tapes that have holes in the center that defined the transport area. This tape-membrane composite was clamped between the U-cell. The permeate solution was removed at certain time intervals and the permeate concentration was measured be UV-Vis spectrometry. Feed solution concentrations were varied in 4 ml PBS (pH 7.2), and the permeate side was only 4 ml PBS. The solution on both sides of the U-tube was stirred using stir bars and stir-plate set-up.

Viscosity Measurements

The viscosities of phthalazine and dextrose were measured using Cannon-Fenske viscometer No. 75 (model P200; Cannon Instruments)

Results and Discussion

Membrane Characterization

Figure 5-9 is an SEM image of the base side of a typical porous Kapton membrane used for the transport study. The average pore density, taken from approximately five hundred pores in five different locations of the image under low magnification, was $10^7/cm^2$. Figure 5-10 is an SEM image of the base showing a diameter of 1.68 μm. The size of the tip, which is below the resolution of SEM, was calculated from ionic conductance measurements (Figure 5-11) using equation 5-14. The average tip size used in this study was ~ 2 nm. The average diameter of the molecule for transport was ~ 0.7 nm.

Transport Measurements of Phthalazine

From equation 5-4, the partition coefficients at the base and tip approximate to 1 and 0.42 respectively. These values put the partition coefficient at the base about 2 times that at the tip. From the proposed equations, Figures 5-8 and 5-9 for base and tip fluxes, it is expected that at low concentrations the flux from base to tip should be about twice that in the opposite direction. Indeed, Figures 5-12 and 5-13 show that base fluxes are about twice that of tip fluxes for 1 and 3 mM solute concentrations. However, base fluxes approach those of tip fluxes as the

concentration of the solute increases, and both base and tip fluxes are similar at higher concentrations (Figures 5-14 and 5-15). Figure 5-16 shows this asymmetric behavior over a wider rage of concentrations.

The higher flux from base to tip direction can be explained by a lower access resistance of the solute to the pore. Figure 5-17 shows a comparison between the theoretical flux obtain from equation 5-9, and the experimental flux from tip to base. We see that these are in good agreement over the wide range of concentration used. The experimental flux from base to tip, on the other hand, deviates from theoretical values obtained from equation 5-8, particularly at higher concentrations. To determine whether the base flux or tip flux behaves in a classical way, a plot showing increase of flux through base and tip, respectively, with respect to the flux measured at 0.1 mM was generated (Figure 5-18). The straight line: Flux(c)/Flux(0.1mM) = c/0.1 obtained for the tip flux indicates that transport through tip behaves according to the Fick's law with a constant D. Transport through base is hindered for higher concentrations indicating that diffusion coefficient is concentration dependent.

The flux (mol/s) through an aperture of diameter d_t with boundary conditions c_0 is given by: $j_{\lim ited} = \pi d_t D c_0$. This value is smaller than the flux as given by eq. 5-12 . The flux through the tip is limited by the value of $j_{\lim ited}.$, while the flux through the base is not. The value of flux through a conical nanopore as given by eq. 5-12 can be easily obtained when the solute passes from base to tip.

The open question however remains, why the ratio of fluxes is concentration dependent. In order to answer this question, we examined behavior of the flux from base and tip side, respectively for different concentrations of the solute.

The Influence of Cosolute Concentration on Asymmetry

We investigated whether molecular crowding / jamming had any influence in the behavior of the base flux at higher concentrations. To do this, we used a constant concentration (5 mM) of phthalazine plus varying concentrations (0 to 100 mM) of the cosolute dextrose on the feed side of the cell. We then placed identical total concentrations on the permeate side of the transport cell using dextrose (Figure 5-19). This procedure was done to ensure that there was no osmotic influence on transport. Figure 5-20 is a calibration curve for phthalazine, and phthalazine with dextrose cosolute, generated from UV-visible absorption measurements. The two plots were placed together to show that the addition of dextrose as a cosolute to phthalazine does not affect the absorbance to any significant degree. Also, to address the issue of viscosity, kinematic viscosity measurements were done on phthalazine and dextrose over the concentration range used in this study. Figure 5-21 indicates that there is negligible change in viscosity over the range of concentrations (0 to 100 mM) used for this study. Figure 5-22 shows the influence of varying concentrations of the cosolute dextrose on the flux of phthalazine, which is kept at a constant concentration of 5 mM. The tip flux is not affected over the entire range of concentrations. However, the base flux is sharply decreased to that of the tip flux when dextrose is added to the feed solution. Even though phthalazine concentration was kept constant, base flux approached the tip flux in a very similar way when phthalazine concentrations were increased. The increase in total concentration on the base side of the membrane causes base flux to approach the limit of tip flux. Proper mathematical modeling of this effect is needed, taking into account dependence of diffusion coefficient on concentration of the solute and position in the channel. We would like to mention that theoretical studies were reported in which two sizes gas molecules were placed on the base side of conical pores, and one size molecule was too large to pass through the tip. In this situation a total jamming was found, causing the diffusion of the

small molecules to be zero over time. As expected, the rate of such jamming increased with concentration. On the other hand, when the molecules were placed on the tip side, no jamming occurred from that entrance. [131] We think that in our case, an increase in total concentration of the solutes might lead to similar partial molecular jamming of diffusion from base to tip. Decrease of the base flux provides evidence that it is the exit rate of the solute from the pore that limits the diffusion transport in the direction from base to tip.

Conclusions

Diffusion rates through a membrane can be asymmetric due to molecular binding, electrostatic interaction, and difference in osmotic potential. In this study we have demonstrated that asymmetric diffusion can also occur by purely geometric constrains of conical pores on the diffusing particles, where the tip of the cone is comparable to the dimension of the molecules. We show that asymmetric behavior of diffusion is concentration dependent and there appear to be some sort of partial jamming effect related to the increase in concentration of molecules from the large opening of the pores. To further shed more light on this interesting phenomenon, proper mathematical modeling of this effect is needed, taking into account dependence of diffusion coefficient on concentration of the solute and position in the channel.

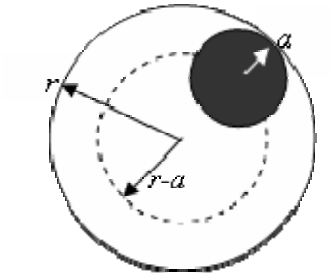

Figure 5-1. The partitioning of a spherical molecule of radius, *a*, in cylindrical pores of radius, *r*.[Adapted from Davidson, M. G.; Deen, W. M. *Macromolecules* **1988**, *21*, 3474-3481.]

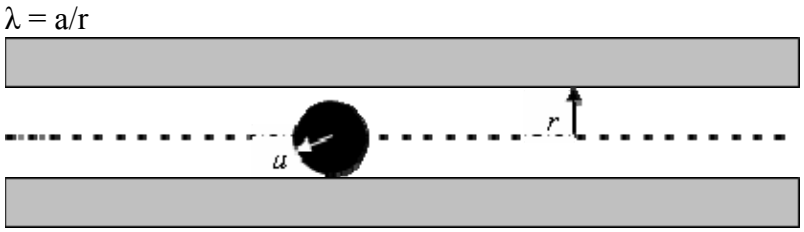

Figure 5-2. Spherical molecule of radius, a, moving within a cylindrical pore of radius, r.[Adapted from Davidson, M. G.; Deen, W. M. *Macromolecules* **1988**, *21*, 3474-3481.]

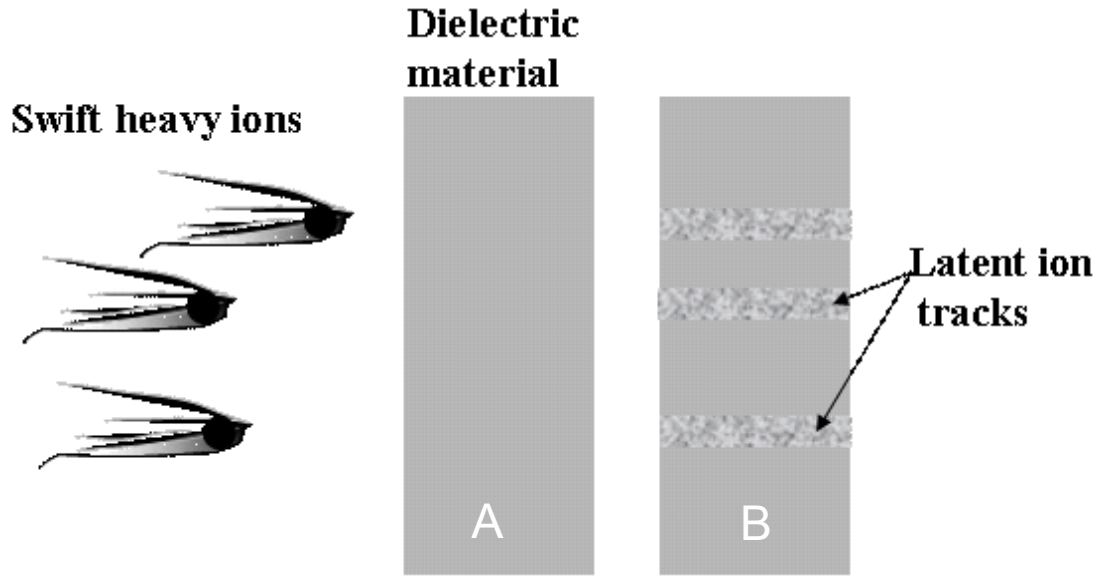

Figure 5-3. Swift heavy ions impinge on a dielectric solid leading to damaged ion tracks witch can be chemically etched to form pores(A and B, respectively)

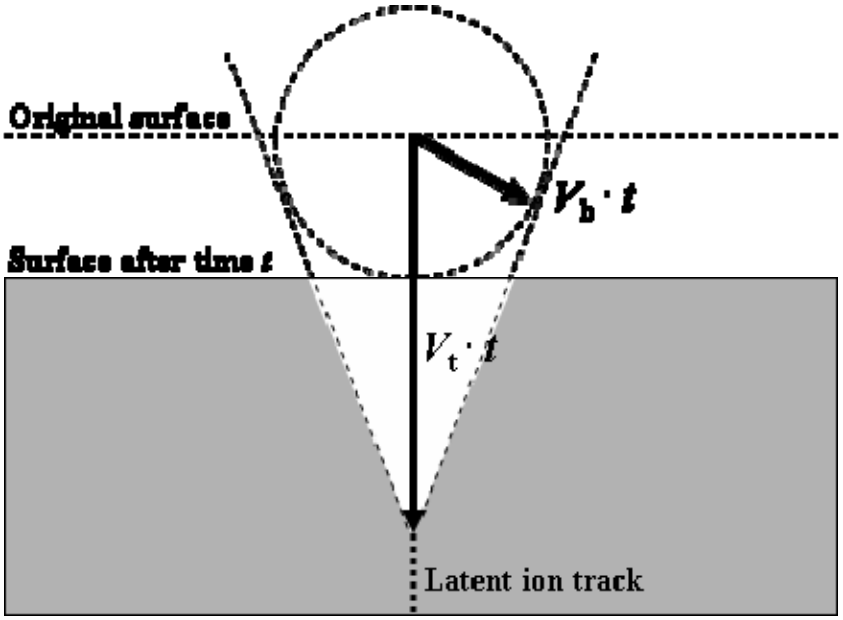

Figure 5-4. Definition of bulk etch rate V_b and track etch rate V_t.[Adapted from Apel, P. *Radiation Measurements* **2001**, *34*, 559-566.]

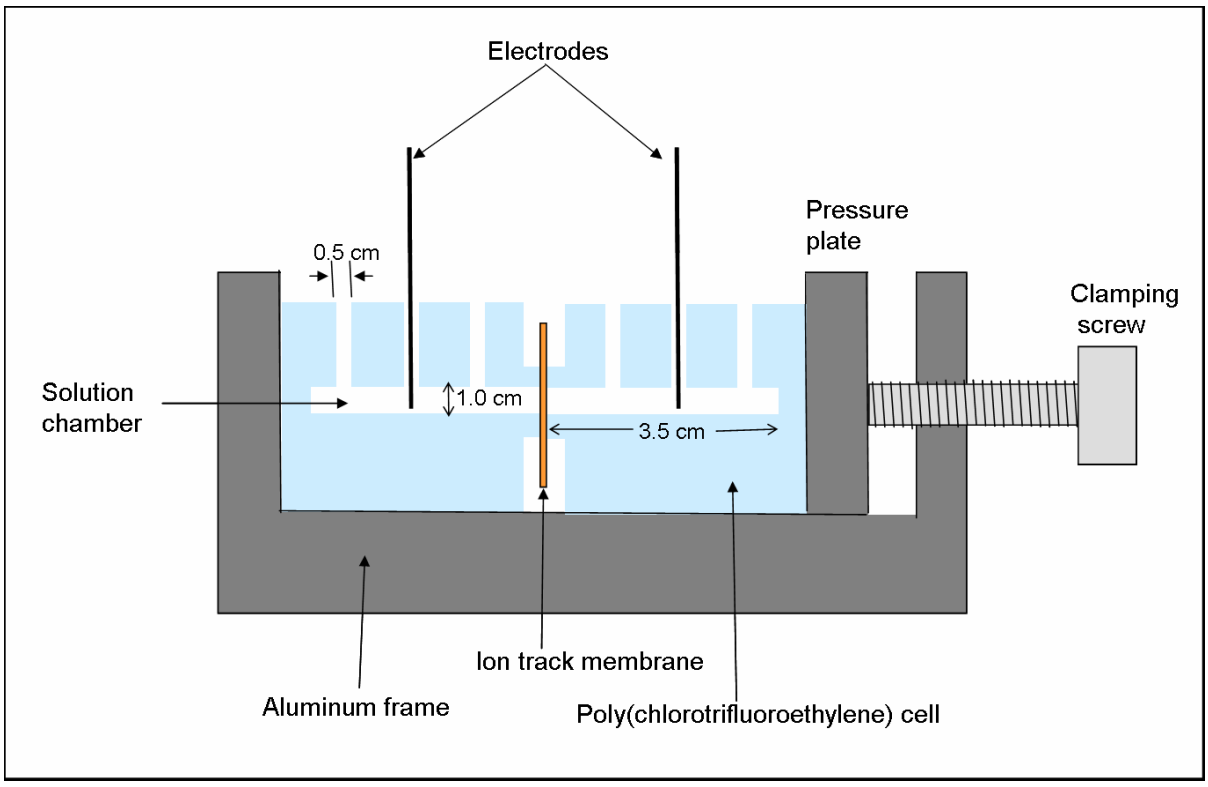

Figure 5-5. Conductivity cell used to prepare conical pores.

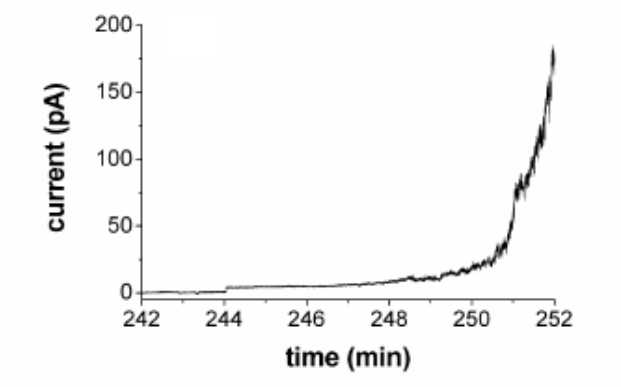

Figure 5-6. Etching curve showing moment of breakthrough with sharp increase in ion current.[Adapted from Siwy, Z.; Apel, P.; Dobrev, D.; Neumann, R.; Spohr, R.; Trautmann, C.; Voss, K. *Nuclear Instruments & Methods in Physics Research, Section B: Beam Interactions with Materials and Atoms* **2003**, *208*, 143-148.]

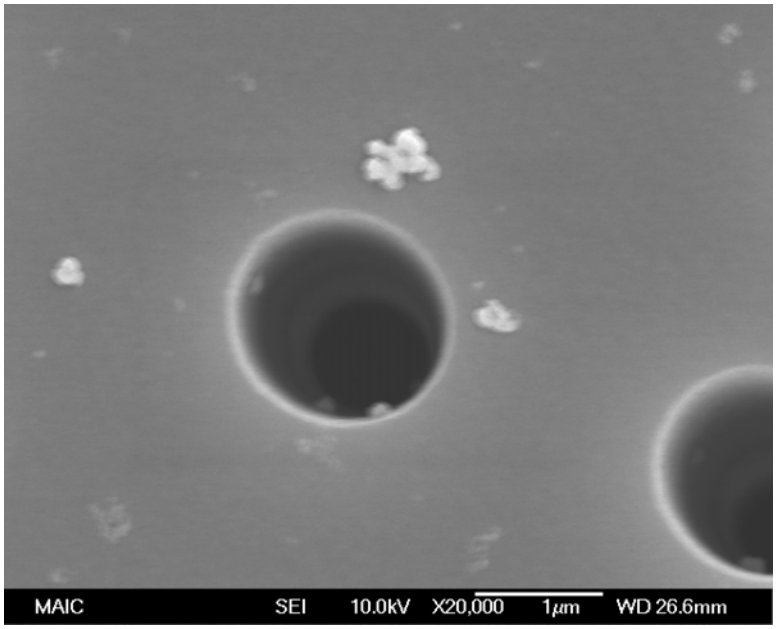

Figure 5-7. Kapton membran showing large opening (base) of conical pores

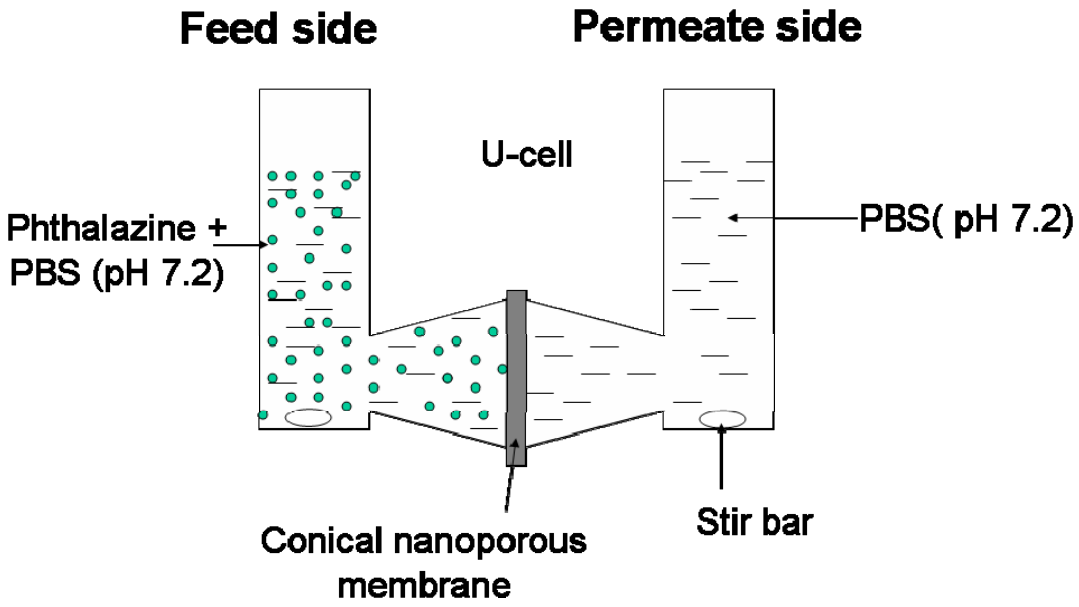

Figure 5-8. Experimental set-up for transport measurements

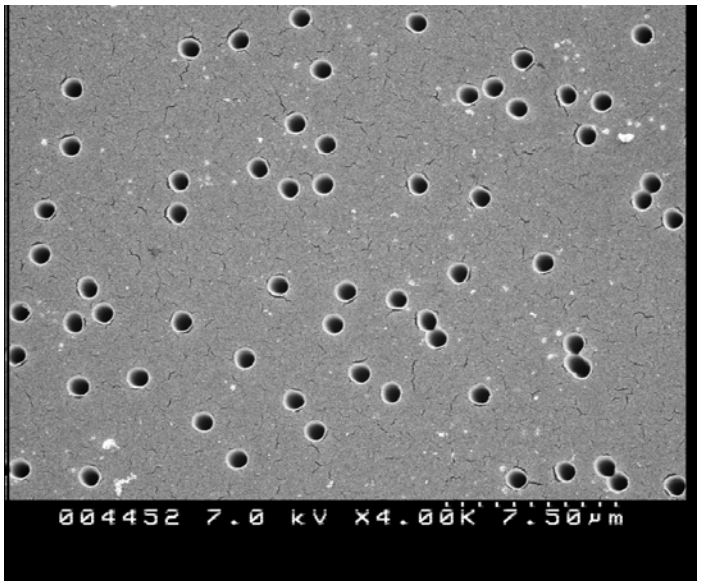

Figure 5-9. Scanning electron micrograph of base side showing pore density (10^7 pores/cm^2) of Kapton membrane.

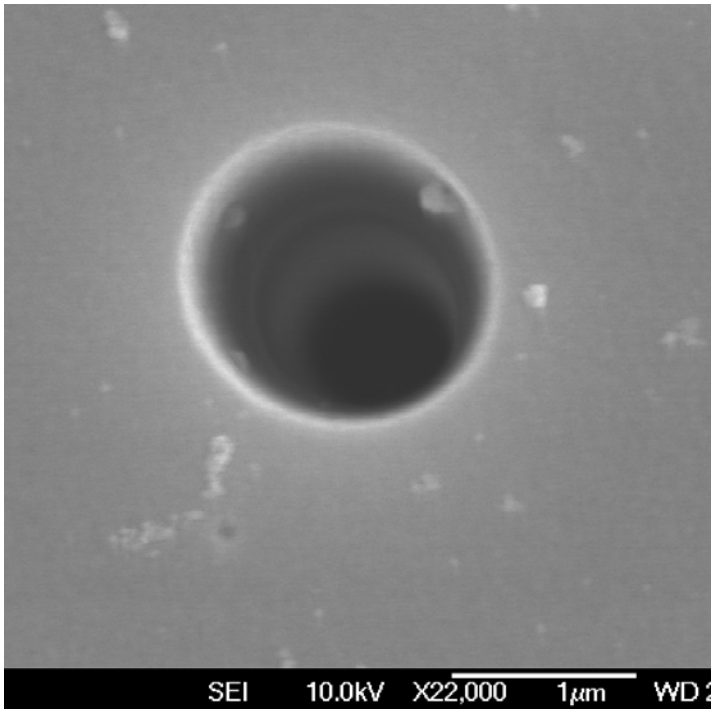

Figure 5-10. Scanning electron micrograph of the base showing diameter of 1.68 µm

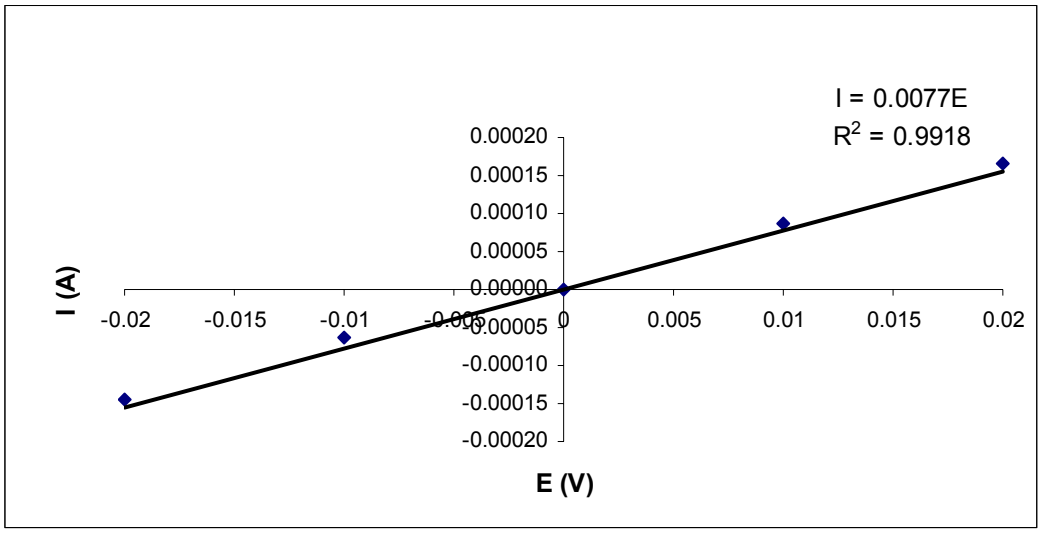

Figure 5-11. A typical current-voltage curve used to measure the tip diameter of the conical nanopores.

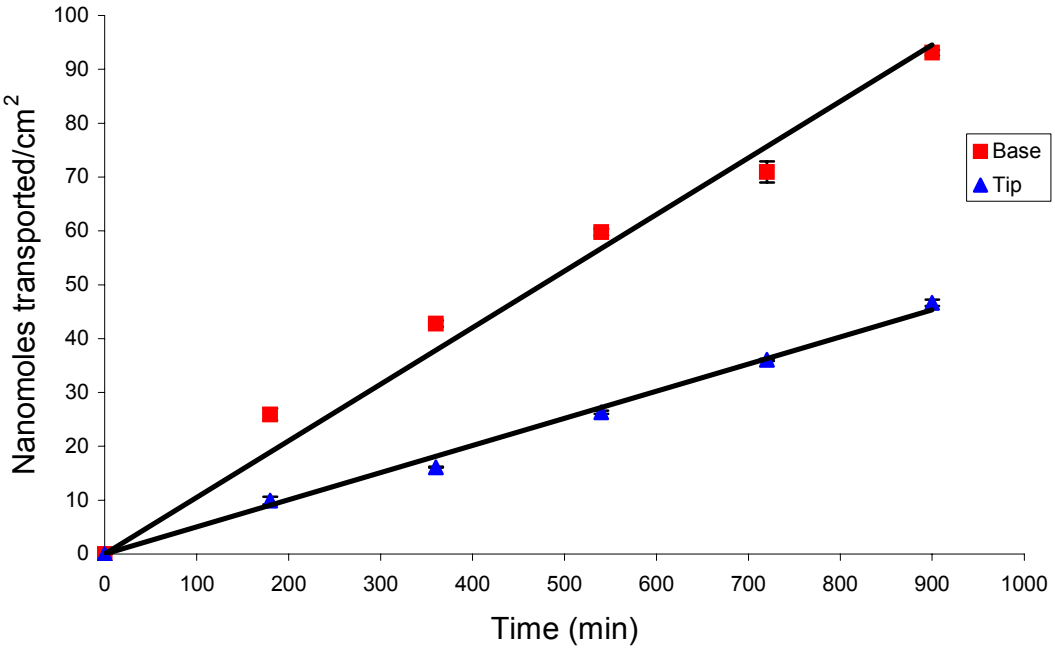

Figure 5-12. Base and tip fluxes for 1 mM phthalazine feed solution.

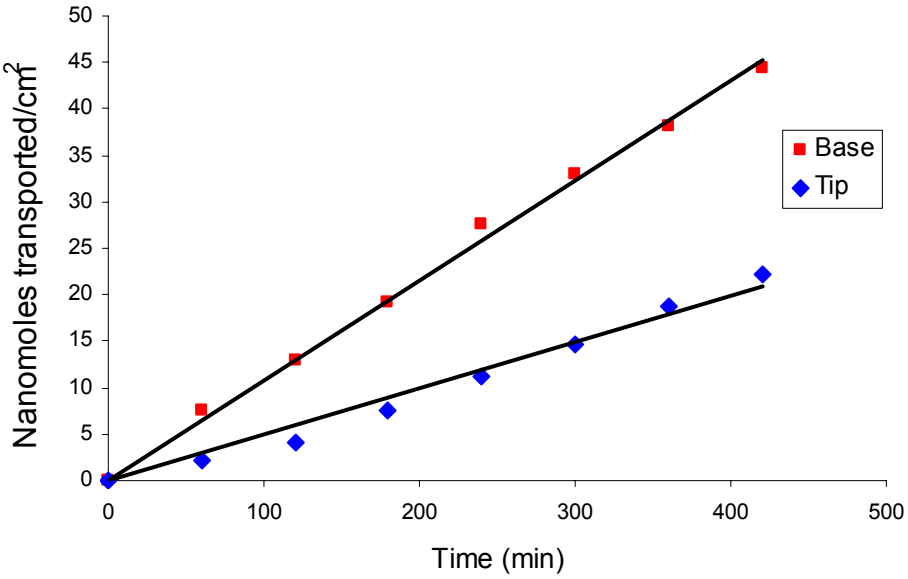

Figure 5-13. Base and tip fluxes for 3 mM phthalazine feed solution.

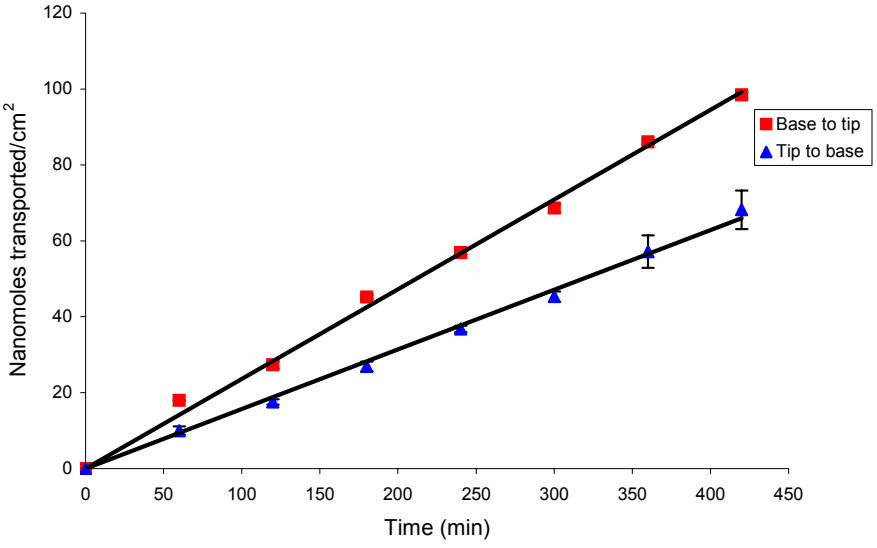

Figure 5-14. Base and tip fluxes for 10 mM phthalazine feed solution.

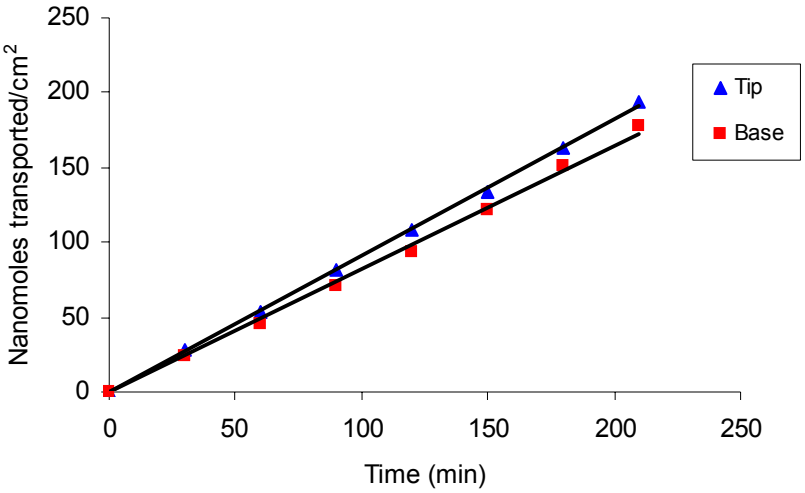

Figure 5-15. Base and tip fluxes for 50 mM phthalazine feed solution.

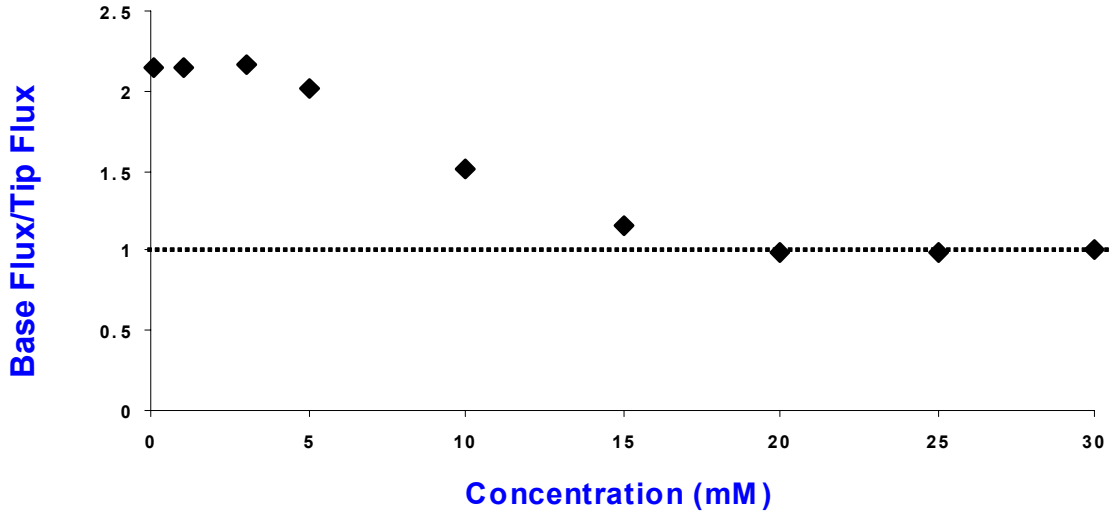

Figure 5-16. Asymmetric behavior of flux versus concentration.

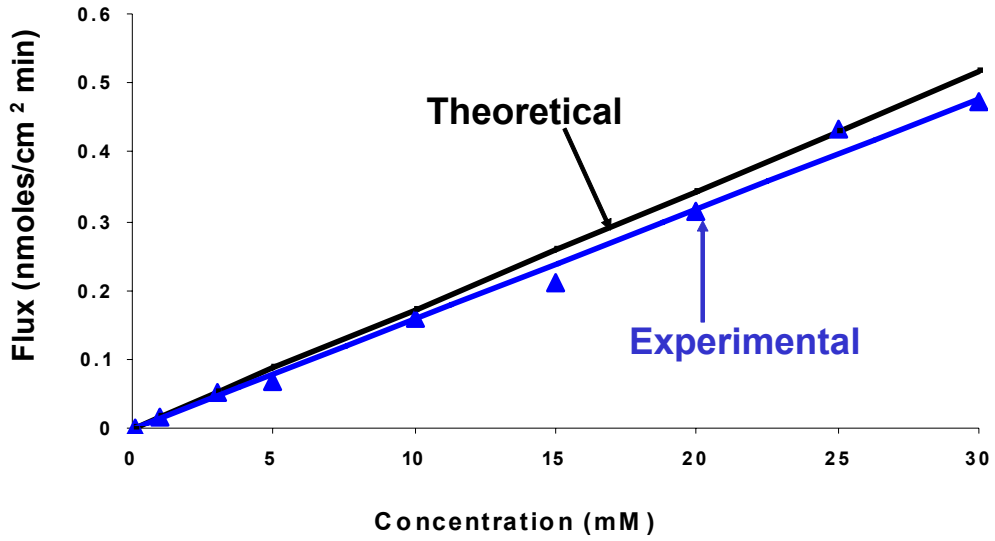

Figure 5-17. Theoretical and experimental tip flux vs concentration

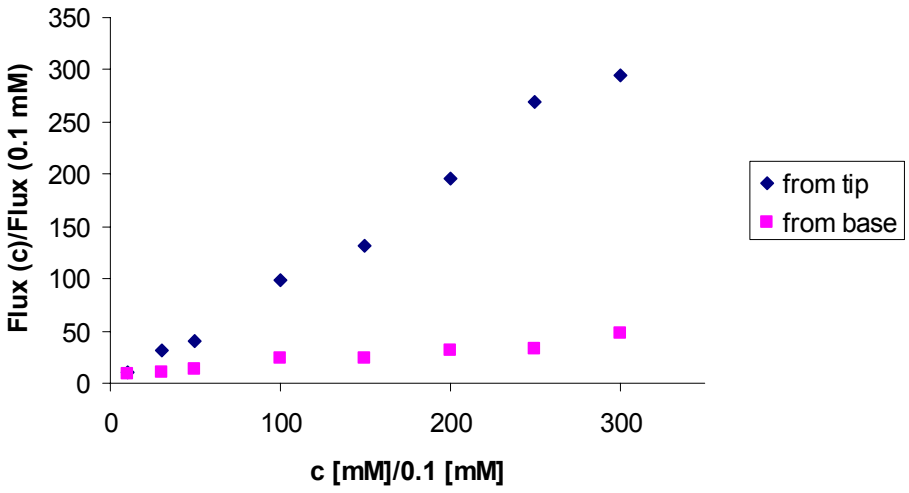

Figure 5-18. Increase of flux through base and tip, respectively, with respect to the flux measured at 0.1 mM.

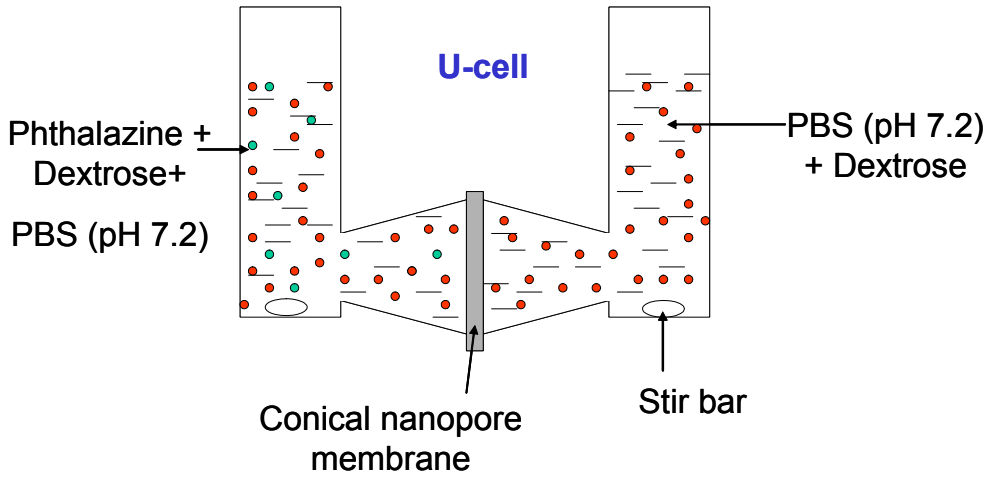

Figure 5-19. Experimental set-up for transport measurements of phthalazine with cosolute dextrose

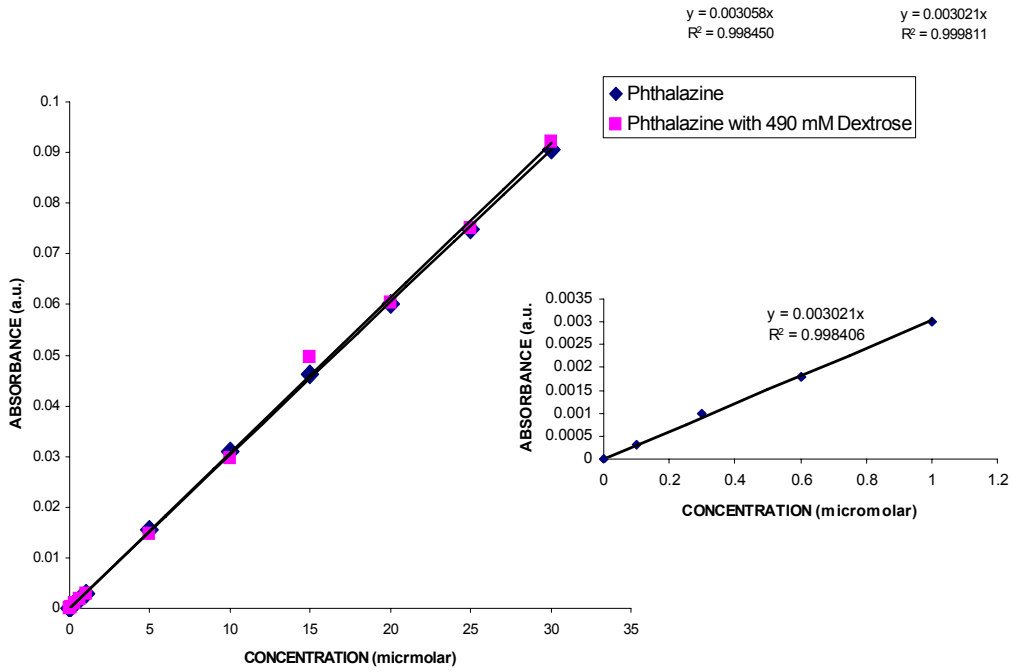

Figure 5-20. Calibration curve of phthalazine, and phthalazine with the highest concentration of dextrose cosolute used

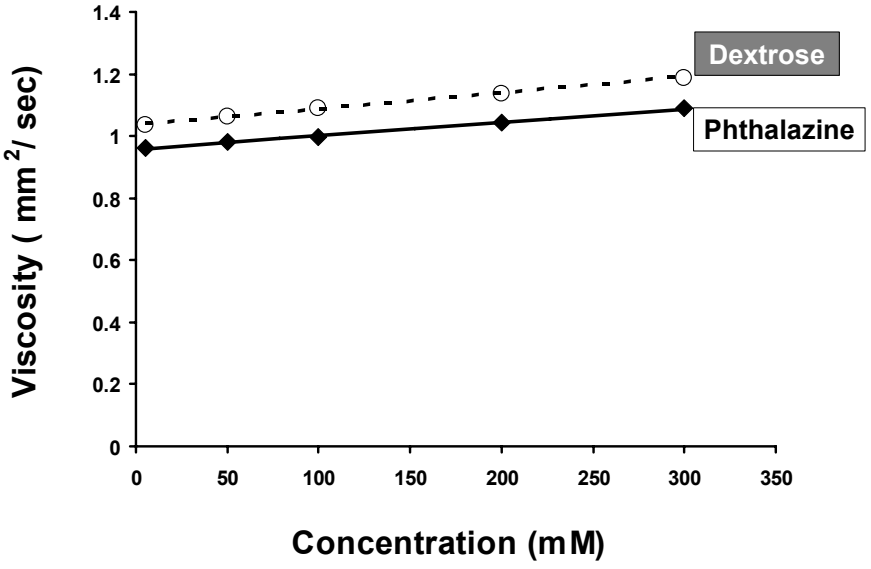

Figure 5-21. Viscosity of dextrose and phthalazine over the concentration range used

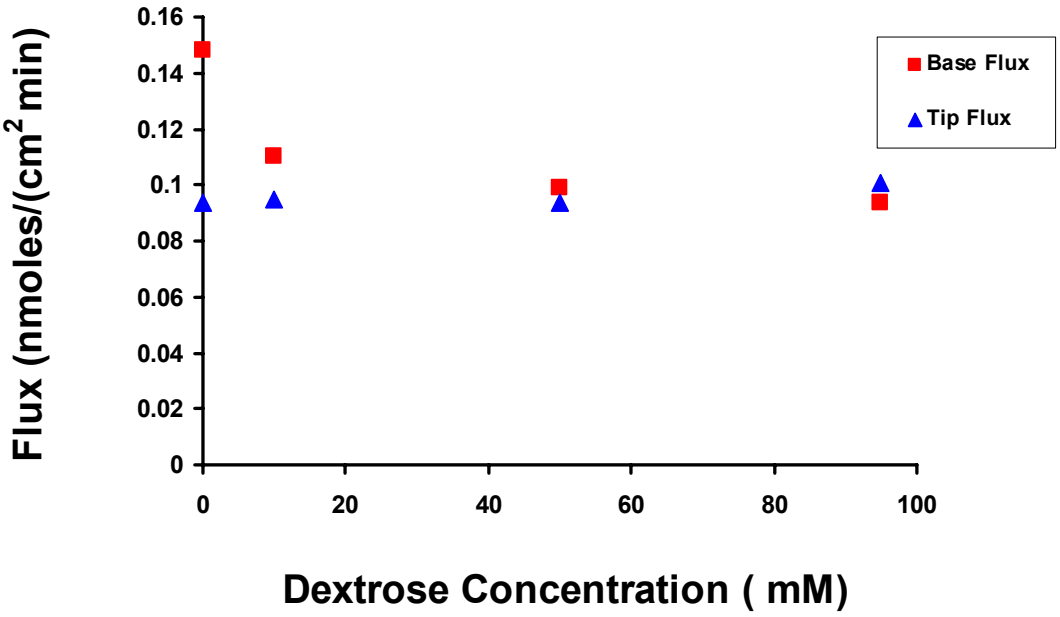

Figure 5-22. Influence of dextrose cosolute concentrations on the base and tip diffusion from 5 mM phthalazine

CHAPTER 6
CONCLUSION

The goals of this research were to develop conical nanopores and nanotube (single and multipore) in polymers and mica membranes by the track-etch method and extension of this technology for sensing and other applications, and to investigate the transport properties of these conical pores. Chapter 1 reviewed background information for this dissertation including the ion track-etch method, membrane based template synthesis, electroless metal deposition, chemical vapor deposition, resistive-pulse sensing, plasma based etching and asymmetric diffusion.

In Chapter 2, an extension of the track-etch method to make conical pores in a reproducible fashion was demonstrated. We have shown here that we can not only reproducibly prepare track-etched based conical nanopore sensor elements, but that we can predict from the experimental parameters used during the second etch, what the diameter of the all-important nanopore tip will be. For these reasons, we believe that the track-etch method will prove to be the technology of choice for taking artificial-nanopore resistive-pulse sensors from the bench top to the practical prototype-device stage of the R&D effort.

A method to make asymmetric pores in tracked muscovite mica films using an etch-refill-etch approach was the topic of Chapter 3. By controlling the concentration ratio of hydrofluoric acid to nitric acid, tapered pores with diamond shaped cross-section were obtained. Here, we see that a two dimensional control of the etch process was developed. Replicas of the asymmetric pores were accomplished by carbon vapor deposition, and scanning electron microscopy was used to give evidence of the resulting nanotubes. In this study, excellent control over cone angle was demonstrated. This control over cone angle has great potential to make the sensing zone of the conical pores limited to a very short distance from the tip. This is ideal for single molecule detection.

In Chapter 4, electroless gold plating properties on the surface and pore walls of track-etched Kapton polyimide nanoporous membranes were studied. SEM, AFM, and ion current measurements were used to characterize the surfaces and dimensions of the pores in the membrane. AFM images showed that after electroless gold plating, the gold surface layers are smooth compared to a similarly structured polycarbonate membrane. It is important that membranes remain relatively smooth after gold plating in order to have a well define pore area for transport and sensing. These properties suggest that Kapton might be a better candidate than PC for use in transport studies and molecular sensing.

Finally, asymmetric diffusional transport of neutral molecular species through Kapton conical pores was described in Chapter 5. Membranes containing conical nanopores from polyimide (Kapton HN Dupont) foils were prepared by the track-etching technique. We report the preferential direction of the flow of molecules through conical nanopores from the base side at low concentration. However, there is concentration dependence from the base side of the pores which causes the flux to approach that of the tip as concentration increases. Study of transport with a cosolute suggested that there may also be some sort of partial jamming effect with concentration from the base entry. It is hoped that further mathematical modeling of this system would shed some light on this interesting transport phenomenon

LIST OF REFERENCES

(1) Sotiropoulou, S.; Vamvakaki, V.; Chaniotakis, N. A. *Biosensors & Bioelectronics* **2007**, *22*, 1566.

(2) Heo, K.; Yoon, J.; Jin, K. S.; Jin, S.; Ree, M. *IEE Proceedings: Nanobiotechnology* **2006**, *153*, 121-128.

(3) Hinds, B. J.; Chopra, N.; Rantell, T.; Andrews, R.; Gavalas, V.; Bachas, L. G. *Science (Washington, DC, United States)* **2004**, *303*, 62-65.

(4) Lev, O.; Tsionsky, M.; Rabinovich, L.; Glezer, V.; Sampath, S.; Pankratov, I.; Gun, J. *Analytical Chemistry* **1995**, *67*, 22A-30A.

(5) Ree, M.; Yoon, J.; Heo, K. *Journal of Materials Chemistry* **2006**, *16*, 685-697.

(6) Apel, P. *Nuclear Instruments & Methods in Physics Research, Section B: Beam Interactions with Materials and Atoms* **2003**, *208*, 11-20.

(7) Choi, Y.; Baker, L. A.; Hillebrenner, H.; Martin, C. R. *Physical Chemistry Chemical Physics* **2006**, *8*, 4976-4988.

(8) Van der Bruggen, B.; Everaert, K.; Wilms, D.; Vandecasteele, C. *Journal of Membrane Science* **2001**, *193*, 239-248.

(9) Gilron, J.; Gara, N.; Kedem, O. *Journal of Membrane Science* **2001**, *185*, 223-236.

(10) Jirage, K. B.; Hulteen, J. C.; Martin, C. R. *Analytical Chemistry* **1999**, *71*, 4913-4918.

(11) Desai, T. A.; West, T.; Cohen, M.; Boiarski, T.; Rampersaud, A. *Advanced Drug Delivery Reviews* **2004**, *56*, 1661-1673.

(12) Cooper, G. M. In *The Cell- A Molecular Approach,* 2 ed.; Sinauer Associates, i., Ed., 2000, pp 81-84; 476-491.

(13) Fischer, B. E.; Spohr, R. *Interdisciplinary Science Reviews* **1984**, *9*, 329-335.

(14) Apel, P. *Radiation Measurements* **2001**, *34*, 559-566.

(15) Virk, H. S.; Kaur, S. A.; Randhawa, G. S. *Indian Journal of Environmental Protection* **2001**, *21*, 529-533.

(16) Fleischer, R. L.; Price, P. B.; Walker, R. M. *Nuclear Tracks in Solids: Principles and Applications*, 1975.

(17) Engels, O.; Schempp, A.; Pelzer, W.; Homeyer, H. *Proceedings of the Particle Accelerator Conference, 17th, Vancouver, B. C., May 12-16, 1997* **1998**, *1*, 1078-1080.

(18) Scopece, P.; Baker, L. A.; Ugo, P.; Martin, C. R. *Nanotechnology* **2006**, *17*, 3951-3956.

(19) Spohr, R. *Radiation Measurements* **2005**, *40*, 191-202.

(20) Toerber, G.; Enge, W.; Beaujean, R.; Siegmon, G. *Solid State Nucl. Track Detect., Proc. Int. Conf., 11th* **1982**, 307-310.

(21) Apel, P. Y.; Blonskaya, I. V.; Didyk, A. Y.; Dmitriev, S. N.; Orelovitch, O. L.; Root, D.; Samoilova, L. I.; Vutsadakis, V. A. *Nuclear Instruments & Methods in Physics Research, Section B: Beam Interactions with Materials and Atoms* **2001**, *179*, 55-62.

(22) Chien, C. L.; Sun, L.; Tanase, M.; Bauer, L. A.; Hultgren, A.; Silevitch, D. M.; Meyer, G. J.; Searson, P. C.; Reich, D. H. *Journal of Magnetism and Magnetic Materials* **2002**, *249*, 146-155.

(23) Martin, C. R. *Science (Washington, D. C.)* **1994**, *266*, 1961-1966.

(24) Martin, C. R.; Mitchell, D. T. *Analytical Chemistry* **1998**, *70*, 322A-327A.

(25) Hulteen, J. C.; Martin, C. R. *Nanoparticles and Nanostructured Films* **1998**, 235-262.

(26) Possin, G. E. *Review of Scientific Instruments* **1970**, *41*, 772-774.

(27) Nishizawa, M.; Menon, V. P.; Martin, C. R. *Science (Washington, D. C.)* **1995**, *268*, 700-702.

(28) Jirage, K. B.; Hulteen, J. C.; Martin, C. R. *Science (Washington, D. C.)* **1997**, *278*, 655-658.

(29) Hornyak, G. L.; Patrissi, C. J.; Martin, C. R. *Journal of Physical Chemistry B* **1997**, *101*, 1548-1555.

(30) Williams, W. D.; Giordano, N. *Review of Scientific Instruments* **1984**, *55*, 410-412.

(31) Hulteen, J. C.; Jirage, K. B.; Martin, C. R. *Journal of the American Chemical Society* **1998**, *120*, 6603-6604.

(32) Hou, Z.; Abbott, N. L.; Stroeve, P. *Langmuir* **2000**, *16*, 2401-2404.

(33) In *Handbook of Conducting Polymers,* 2 ed.; Skotheim, T. A., Elsenbaumer, R. L., Reynols, J. R., Eds., 1997; Vol. p, pp 1112.

(34) Duchet, J.; Legras, R.; Demoustier-Champagne, S. *Synthetic Metals* **1998**, *98*, 113-122.

(35) Demoustier-Champagne, S.; Stavaux, P.-Y. *Chemistry of Materials* **1999**, *11*, 829-834.

(36) Sukeerthi, S.; Contractor, A. Q. *Analytical Chemistry* **1999**, *71*, 2231-2236.

(37) Che, G.; Lakshmi, B. B.; Martin, C. R.; Fisher, E. R. *Langmuir* **1999**, *15*, 750-758.

(38) Che, G.; Lakshmi, B. B.; Fisher, E. R.; Martin, C. R. *Nature (London)* **1998**, *393*, 346-349.

(39) Kyotani, T.; Tsai, L.-f.; Tomita, A. *Chemical Communications (Cambridge)* **1997**, 701-702.

(40) Lakshmi, B. B.; Dorhout, P. K.; Martin, C. R. *Chemistry of Materials* **1997**, *9*, 857-862.

(41) Lakshmi, B. B.; Patrissi, C. J.; Martin, C. R. *Chemistry of Materials* **1997**, *9*, 2544-2550.

(42) Cepak, V. M.; Hulteen, J. C.; Che, G.; Jirage, K. B.; Lakshmi, B. B.; Fisher, E. R.; Martin, C. R. *Journal of Materials Research* **1998**, *13*, 3070-3080.

(43) Cepak, V. M.; Hulteen, J. C.; Che, G.; Jirage, K. B.; Lakshmi, B. B.; Fisher, E. R.; Martin, C. R.; Yoneyama, H. *Chemistry of Materials* **1997**, *9*, 1065-1067.

(44) Martin, B. R.; Dermody, D. J.; Reiss, B. D.; Fang, M.; Lyon, L. A.; Natan, M. J.; Mallouk, T. E. *Advanced Materials (Weinheim, Germany)* **1999**, *11*, 1021-1025.

(45) Bowes, C. L.; Malek, A.; Ozin, G. A. *Chemical Vapor Deposition* **1996**, *2*, 97-103.

(46) Shelimov, K. B.; Moskovits, M. *Chemistry of Materials* **2000**, *12*, 250-254.

(47) Foss, C. A., Jr.; Hornyak, G. L.; Stockert, J. A.; Martin, C. R. *Journal of Physical Chemistry* **1994**, *98*, 2963-2971.

(48) Blondel, A.; Meier, J. P.; Doudin, B.; Ansermet, J. P. *Applied Physics Letters* **1994**, *65*, 3019-3021.

(49) Schwarzacher, W. *Electrochemical Society Interface* **1999**, *8*, 20-24.

(50) Ang, L.-M.; Hor, T. S. A.; Xu, G.-Q.; Tung, C.-h.; Zhao, S.; Wang, J. L. S. *Chemistry of Materials* **1999**, *11*, 2115-2118.

(51) Menon, V. P.; Martin, C. R. *Analytical Chemistry* **1995**, *67*, 1920-1928.

(52) Parthasarathy, R. V.; Phani, K. L. N.; Martin, C. R. *Advanced Materials (Weinheim, Germany)* **1995**, *7*, 896-897.

(53) Cepak, V. M.; Martin, C. R. *Chemistry of Materials* **1999**, *11*, 1363-1367.

(54) Patrissi, C. J.; Martin, C. R. *Journal of the Electrochemical Society* **1999**, *146*, 3176-3180.

(55) Lee, S. B.; Martin, C. R. *Anal Chem FIELD Full Journal Title:Analytical chemistry* **2001**, *73*, 768-775.

(56) Miller, S. A.; Martin, C. R. *Journal of Electroanalytical Chemistry* **2002**, *522*, 66-69.

(57) Kyotani, T.; Tsai, L.-f.; Tomita, A. *Chemistry of Materials* **1996**, *8*, 2109-2113.

(58) Yuan, Z. h.; Huang, H.; Liu, L.; Fan, S. s. *Chemical Physics Letters* **2001**, *345*, 39-43.

(59) Kyotani, T.; Ma, Z.; Tomita, A. *Carbon* **2003**, *41*, 1451-1459.

(60) Bayley, H.; Martin, C. R. *Chemical Reviews (Washington, D. C.)* **2000**, *100*, 2575-2594.

(61) Gu, L. Q.; Braha, O.; Conlan, S.; Cheley, S.; Bayley, H. *Nature* **1999**, *398*, 686-690.

(62) Movileanu, L.; Cheley, S.; Bayley, H. *Biophysical journal* **2003**, *85*, 897-910.

(63) Gu, L. Q.; Bayley, H. *Biophysical journal* **2000**, *79*, 1967-1975.

(64) Kasianowicz, J. J.; Burden, D. L.; Han, L. C.; Cheley, S.; Bayley, H. *Biophysical journal* **1999**, *76*, 837-845.

(65) Astier, Y.; Braha, O.; Bayley, H. *Journal of the American Chemical Society* **2006**, *128*, 1705-1710.

(66) Mathe, J.; Aksimentiev, A.; Nelson, D. R.; Schulten, K.; Meller, A. *Proceedings of the National Academy of Sciences of the United States of America* **2005**, *102*, 12377-12382.

(67) Howorka, S.; Nam, J.; Bayley, H.; Kahne, D. *Angewandte Chemie, International Edition* **2004**, *43*, 842-846.

(68) Gu, L. Q.; Cheley, S.; Bayley, H. *Science* **2001**, *291*, 636-640.

(69) Schmidt, J. *Journal of Materials Chemistry* **2005**, *15*, 831-840.

(70) Heins Elizabeth, A.; Siwy Zuzanna, S.; Baker Lane, A.; Martin Charles, R. *Nano letters* **2005**, *5*, 1824-1829.

(71) Li, J.; Stein, D.; McMullan, C.; Branton, D.; Aziz, M. J.; Golovchenko, J. A. *Nature (London, United Kingdom)* **2001**, *412*, 166-169.

(72) Storm, A. J.; Chen, J. H.; Ling, X. S.; Zandbergen, H. W.; Dekker, C. *Nature Materials* **2003**, *2*, 537-540.

(73) Li, J.; Gershow, M.; Stein, D.; Brandin, E.; Golovchenko, J. A. *Nature Materials* **2003**, *2*, 611-615.

(74) Han, A.; Schurmann, G.; Mondin, G.; Bitterli, R. A.; Hegelbach, N. G.; de Rooij, N. F.; Staufer, U. *Applied Physics Letters* **2006**, *88*, 093901/093901-093901/093903.

(75) Mara, A.; Siwy, Z.; Trautmann, C.; Wan, J.; Kamme, F. *Nano Letters* **2004**, *4*, 497-501.

(76) Harrell, C. C.; Choi, Y.; Horne, L. P.; Baker, L. A.; Siwy, Z. S.; Martin, C. R. *Langmuir*, ACS ASAP.

(77) Siwy, Z.; Trofin, L.; Kohli, P.; Baker, L. A.; Trautmann, C.; Martin, C. R. *Journal of the American Chemical Society* **2005**, *127*, 5000-5001.

(78) Patolsky, F.; Zheng, G.; Lieber, C. M. *Analytical Chemistry* **2006**, *78*, 4260-4269.

(79) Lee, S.; Zhang, Y.; White, H. S.; Harrell, C. C.; Martin, C. R. *Analytical Chemistry* **2004**, *76*, 6108-6115.

(80) DeBlois, R. W.; Wesley, R. K. *Journal of virology* **1977**, *23*, 227-233.

(81) Apel, P. Y.; Korchev, Y. E.; Siwy, Z.; Spohr, R.; Yoshida, M. *Nuclear Instruments & Methods in Physics Research, Section B: Beam Interactions with Materials and Atoms* **2001**, *184*, 337-346.

(82) Fleischer, R. L.; Viertl, J. R. M.; Price, P. B. *Review of Scientific Instruments* **1972**, *43*, 1708-1709.

(83) Shul, R. J.; Pearton, S. J. *Handbook of Advanced Plasma Processing Techniques*; Sringer: Berlin Heidelberg: New York, 2000.

(84) Kuo, C.-W.; Shiu, J.-Y.; Cho, Y.-H.; Chen, P. *Advanced Materials (Weinheim, Germany)* **2003**, *15*, 1065-1068.

(85) Kuo, C.-W.; Shiu, J.-Y.; Chen, P. *Chemistry of Materials* **2003**, *15*, 2917-2920.

(86) Hegemann, D.; Brunner, H.; Oehr, C. *Nuclear Instruments & Methods in Physics Research, Section B: Beam Interactions with Materials and Atoms* **2003**, *208*, 281-286.

(87) Hille, B. *Ion Channels of Excitable Membranes*; Sinauer Associates, 2001.

(88) Siwy, Z.; Fulinski, A. *Physical Review Letters* **2002**, *89*, 198103/198101-198103/198104.

(89) Siwy, Z.; Kosinska, I. D.; Fulinski, A.; Martin, C. R. *Physical Review Letters* **2005**, *94*, 048102/048101-048102/048104.

(90) Chou, T. *Journal of Chemical Physics* **1999**, *110*, 606-615.

(91) Kim, K. S.; Davis, I. S.; Macpherson, P. A.; Pedley, T. J.; Hill, A. E. *Proceedings of the Royal Society A: Mathematical, Physical and Engineering Sciences* **2005**, *461*, 273-296.

(92) Harrell, C. C.; Siwy, Z. S.; Martin, C. R. *Small* **2006**, *2*, 194-198.

(93) Li, N.; Yu, S.; Harrell, C. C.; Martin, C. R. *Analytical Chemistry* **2004**, *76*, 2025-2030.

(94) Yu, S.; Lee, S. B.; Kang, M.; Martin, C. R. *Nano Letters* **2001**, *1*, 495-498.

(95) Harrell, C. C.; Lee, S. B.; Martin, C. R. *Analytical Chemistry* **2003**, *75*, 6861-6867.

(96) Martin, C. R.; Nishizawa, M.; Jirage, K.; Kang, M. *Journal of Physical Chemistry B* **2001**, *105*, 1925-1934.

(97) Siwy, Z.; Heins, E.; Harrell, C. C.; Kohli, P.; Martin, C. R. *Journal of the American Chemical Society* **2004**, *126*, 10850-10851.

(98) Harrell, C. C.; Kohli, P.; Siwy, Z.; Martin, C. R. *Journal of the American Chemical Society* **2004**, *126*, 15646-15647.

(99) Kovtyukhova, N. I.; Mallouk, T. E. *Chemistry--A European Journal* **2002**, *8*, 4354-4363.

(100) Harrell, C. C.; Choi, Y.; Horne, L. P.; Baker, L. A.; Siwy, Z. S.; Martin, C. R. *Langmuir* **2006**, *22*, 10837-10843.

(101) Schiedt, B.; Healy, K.; Morrison, A. P.; Neumann, R.; Siwy, Z. *Nuclear Instruments & Methods in Physics Research, Section B: Beam Interactions with Materials and Atoms* **2005**, *236*, 109-116.

(102) Siwy, Z. S. *Advanced Functional Materials* **2006**, *16*, 735-746.

(103) Merkulov, V. I.; Guillorn, M. A.; Lowndes, D. H.; Simpson, M. L.; Voelkl, E. *Applied Physics Letters* **2001**, *79*, 1178-1180.

(104) Heins, E. A.; Baker, L. A.; Siwy, Z. S.; Mota, M. O.; Martin, C. R. *Journal of Physical Chemistry B* **2005**, *109*, 18400-18407.

(105) Siwy, Z.; Apel, P.; Baur, D.; Dobrev, D. D.; Korchev, Y. E.; Neumann, R.; Spohr, R.; Trautmann, C.; Voss, K.-O. *Surface Science* **2003**, *532-535*, 1061-1066.

(106) Sasou, M.; Sugiyama, S.; Yoshino, T.; Ohtani, T. *Langmuir* **2003**, *19*, 9845-9849.

(107) Heim, M.; Cevc, G.; Guckenberger, R.; Knapp, H. F.; Wiegrabe, W. *Biophys J FIELD Full Journal Title:Biophysical journal* **1995**, *69*, 489-497.

(108) Sun, L.; Searson, P. C.; Chien, C. L. *Applied Physics Letters* **1999**, *74*, 2803-2805.

(109) Chen, L. H.; AuBuchon, J. F.; Gapin, A.; Daraio, C.; Bandaru, P.; Jin, S.; Kim, D. W.; Yoo, I. K.; Wang, C. M. *Applied Physics Letters* **2004**, *85*, 5373-5375.

(110) Che, G.; Lakshmi, B. B.; Martin, C. R.; Fisher, E. R.; Ruoff, R. S. *Chemistry of Materials* **1998**, *10*, 260-267.

(111) Miller, S. A.; Young, V. Y.; Martin, C. R. *Journal of the American Chemical Society* **2001**, *123*, 12335-12342.

(112) Siwy, Z.; Apel, P.; Dobrev, D.; Neumann, R.; Spohr, R.; Trautmann, C.; Voss, K. *Nuclear Instruments & Methods in Physics Research, Section B: Beam Interactions with Materials and Atoms* **2003**, *208*, 143-148.

(113) Schmidt-Rohr, K.; Hu, W.; Zumbulyadis, N. *Science (Washington, D. C.)* **1998**, *280*, 714-717.

(114) Ganz, M.; Feige, G.; Edelstein, N.; Bucher, J.; Zhu, T. C.; Vater, P.; Brandt, R.; Vetter, J. *Nuclear Tracks and Radiation Measurements* **1988**, *15*, 799-802.

(115) Vater, P. *Nuclear Tracks and Radiation Measurements* **1988**, *15*, 743-749.

(116) Trautmann, C.; Bruechle, W.; Spohr, R.; Vetter, J.; Angert, N. *Nuclear Instruments & Methods in Physics Research, Section B: Beam Interactions with Materials and Atoms* **1996**, *111*, 70-74.

(117) Hille, B. *Ionic Channels of Excitable Membranes*, 2nd ed.; Sinauer Associates, Inc: Sunderland, MA, 1992.

(118) Sakmann, B.; Neher, E. *Single-Channel Recording*, 2nd ed.; Plenum Press: New York, 1995.

(119) Sperelakis, N. *Cell Physiology*; Academic Press: San Diego, Califonia, 1998.

(120) Siwy, Z.; Gu, Y.; Spohr, H. A.; Baur, D.; Wolf-Reber, A.; Spohr, R.; Apel, P.; Korchev, Y. E. *Europhysics Letters* **2002**, *60*, 349-355.

(121) Siwy, Z.; Fulinski, A. *American Journal of Physics* **2004**, *72*, 567-574.

(122) Soltys, P. J.; Ofsthun, N. J.; Zydney, A. L. *Journal of Membrane Science* **1996**, *118*, 199-212.

(123) Patlak, C. S.; Goldstein, D. A.; Hoffmann, J. F. *J. Theoret. Biol.* **1963**, *5*, 426-442.

(124) Crank, J. *The Mathematics of Diffusion. 2d Ed*, 1975.

(125) Crank, J.; Park, G. S.; Editors *Diffusion in Polymers*, 1968.

(126) Renkin, E. M. *J Gen Physiol FIELD Full Journal Title:The Journal of general physiology* **1954**, *38*, 225-243.

(127) Davidson, M. G.; Deen, W. M. *Macromolecules* **1988**, *21*, 3474-3481.

(128) Ferry, J. D. *Journal of General Physiology* **1936**, *20*, 95-104.

(129) Vlassiouk, I.; Siwy, Z. S. *Nano Letters* **2007**, *7*, 552-556.

(130) Siwy, Z.; Dobrev, D.; Neumann, R.; Trautmann, C.; Voss, K. *Applied Physics A: Materials Science & Processing* **2003**, *76*, 781-785.

(131) Packard, N.; Shaw, R. *Los Alamos National Laboratory, Preprint Archive, Condensed Matter* **2004**, 1-17, arXiv:cond-mat/0412626.

BIOGRAPHICAL SKETCH

John Edwardson Wharton was born in St. Kitts, West Indies. He spent two years at the St. Kitts-Nevis Teachers College, earning a diploma in education in 1985. After graduation, he taught for two and a half years, before taking up employment at the St. Kitts Biomedical Research Foundation, where he worked for a few years. He later went on to pursue a B.S. in chemistry with physics at the University of the Virgin Island from 1992 to 1996. In August, 1999, John began his graduate work in analytical chemistry under the guidance of Prof. Dr. Charles R. Martin. He earned his M.S. in 2003 and continued in the Martin group in pursuit of his Ph.D. He completed his research in the spring of 2007, obtaining a Doctor of Philosophy in analytical chemistry in the area of nanostructured asymmetric pore design and fabrication for biosensor applications.